AD_____

Award Number: W81XWH-13-1-0129

TITLE: MAXIMIZING PTH ANABOLIC OSTEOPOROSIS THERAPY

PRINCIPAL INVESTIGATOR: JOSEPH BIDWELL

CONTRACTING ORGANIZATION:

INDIANA UNIVERSITY, INDIANAPOLIS
INDIANAPOLIS IN 46202-5130

REPORT DATE: September 2014

TYPE OF REPORT: Annual

PREPARED FOR: U.S. Army Medical Research and Materiel Command
Fort Detrick, Maryland 21702-5012

REPORT DOCUMENTATION PAGE

Form Approved
OMB No. 0704-0188

1. REPORT DATE	**2. REPORT TYPE**	**3. DATES COVERED**
September 2014	Annual	15 August 2013-14 August 2014

4. TITLE AND SUBTITLE
MAXIMIZING PTH ANABOLIC OSTEOPOROSIS THERAPY

5a. CONTRACT NUMBER
W81XWH-13-1-0129

5b. GRANT NUMBER
W81XWH-13-1-0129

5c. PROGRAM ELEMENT NUMBER

6. AUTHOR(S)

Joseph Bidwell

E-Mail: jbidwell@iupui.edu

5d. PROJECT NUMBER

5e. TASK NUMBER

5f. WORK UNIT NUMBER

7. PERFORMING ORGANIZATION NAME(S) AND ADDRESS(ES)

INDIANA UNIVERSITY, INDIANAPOLIS
980 INDIANA AVE RM 2232
INDIANAPOLIS IN 46202-5130

8. PERFORMING ORGANIZATION REPORT NUMBER

9. SPONSORING / MONITORING AGENCY NAME(S) AND ADDRESS(ES)
U.S. Army Medical Research and Materiel Command
Fort Detrick, Maryland 21702-5012

10. SPONSOR/MONITOR'S ACRONYM(S)

11. SPONSOR/MONITOR'S REPORT NUMBER(S)

12. DISTRIBUTION / AVAILABILITY STATEMENT
Approved for Public Release; Distribution Unlimited

13. SUPPLEMENTARY NOTES

14. ABSTRACT

The purpose of this study is to test the efficacy of parathyroid hormone (PTH) mono-therapy and PTH+ anti-resportive combination therapies on *Nmp4*-knockout (KO) and wild type (WT) mice. **The scope of** the research comprises the following specific aims: (i & ii) to determine the impact of Nmp4 on the efficacy of PTH mono- and combination therapies with various anti-resorptives in ovariectomized (ovx) mice; (iii) to determine the cell type-specific contributions to the enhanced response of the *Nmp4*-KO mouse to these osteoporosis therapies. In **YEAR 1** we completed experiments comparing ovx-induced bone loss in WT and *Nmp4*-knockout (KO) mice. We completed the evaluation of bone restoration by PTH mono-therapy in these ovx mice. **The most significant findings during this period include the following**:

1. *Nmp4*-KO mice are not protected from ovx-induced bone loss
2. *Nmp4*-KO mice exhibit an enhanced PTH-induced restoration of bone lost to ovx
3. Ovx does not deplete the expanded *Nmp4*-KO bone marrow osteogenic reserve
4. *Nmp4*-KO mesenchymal stem/progenitor cells exhibit an enhanced proliferation and precocious mineralization in culture
5. *Nmp4*-KO & WT mice under therapy exhibit similar histomorphometry and serum profiles

Our key discovery is that the enhanced response to PTH therapy in our *Nmp4*-KO mouse is preserved in a pre-clinical osteoporosis model.

15. SUBJECT TERMS
Nmp4-knockout (KO) mice, osteoporosis, ovariectomy, PTH combination therapies

16. SECURITY CLASSIFICATION OF:			**17. LIMITATION OF ABSTRACT**	**18. NUMBER OF PAGES**	**19a. NAME OF RESPONSIBLE PERSON**
a. REPORT	**b. ABSTRACT**	**c. THIS PAGE**			USAMRMC
U	U	U	UU	43	**19b. TELEPHONE NUMBER** *(include area code)*

Table of Contents

INTRODUCTION: The **subject of this research** is the need for improved osteoporosis therapies. The **purpose of this study** is to test the efficacy of parathyroid hormone (PTH) mono-therapy and PTH+ anti-resportive combination therapies on *Nmp4*-knockout (KO) and wild type (WT) mice. The **scope of the research** comprises the following specific aims: (i & ii) to determine the impact of Nmp4 on the efficacy of PTH mono- and combination therapies with bisphosphonates and the selective estrogen receptor modulator (SERM) raloxifene in ovariectomized (ovx) mice; (iii) to determine the cell type-specific contributions to the enhanced response of the *Nmp4*-KO mouse to these osteoporosis therapies.

BODY:

During Year 1 we successfully accomplished a number of objectives in the following Subtasks:

i. Subtasks 2.1, 2.2, 3.1-3.5: Compared impact of ovariectomy (ovx) on WT and *Nmp4*-KO bone loss. Evaluated the response of the ovx WT and ovx *Nmp4*-KO mice to PTH mono-therapy and initiated combination therapies.

ii. Subtasks 4.2.a and 4.3.a: Initiated breeding of the conditional knockout mice for production of *Nmp4*$^{fl/fl}$ *3.6Col-Cre+*, *Nmp4*$^{fl/fl}$ *Cathepsin K-Cre+*, and *Nmp4*$^{fl/fl}$*-Cre–* mice.

iii. Subtask 6.2: Initiated culture evaluation of WT and *Nmp4*-KO mesenchymal stem progenitor cells

KEY FINDING: *Nmp4-KO mice <u>are not</u> protected from ovx-induced bone loss*

Figure 1 outlines the treatment regimen used to evaluate the impact of Nmp4 on an osteoporosis pre-clinical mouse model. To determine whether disabling Nmp4 activity protects mice from ovx-induced bone loss, we removed the ovaries or performed sham operations on WT and *Nmp4*-KO mice as described in detail in our ACURO-approved protocol. Briefly, through a small skin incision, the muscle wall was incised 1cm lateral to the midline 1-2cm below the last rib to enter the abdominal cavity. The periovarian fat pad was grasped and exteriorized. The fallopian tube between the fat pad and uterus was clamped, crushed, and the ovary removed. The procedure was repeated on the contralateral side. The sham procedure included all steps except removing the ovaries. Both ovx genotypes experienced significant weight gain and decreased uterine weight. There was no genotype x treatment interaction (Table 1).

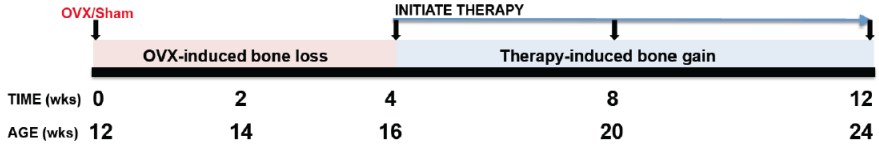

Figure 1: Schematic showing the treatment regimen of WT and Nmp4-KO mice

Table 1: Bone loss data. The % change body weight, uterine weight, microCT (distal femur and L5 vertebra) and serum formation/resorption markers from WT and *Nmp4*-KO mice after ovx or sham operation 4wks post-op. Abbreviations: trabecular bone volume per total volume (BV/TV), connectivity density (Conn.D, mm^{-3}), structure model index (SMI), trabecular number (Tb.N, mm^{-1}), trabecular thickness (Tb.Th, mm), and spacing (Tb.Sp, mm), pro-collagen type-1 amino-terminal pro-peptide (P1NP) and c-terminal telopeptide (CTX). Data are average ± SD, number of mice/experimental group=8-14 [4 mice in WT SHAM uterine weight]). Statistical significance was set at p≤0.05 and differences were determined using a 2-way ANOVA.

	WT		KO		2-WAY ANOVA p-values		
	SHAM	OVX	SHAM	OVX	Genotype	Treatment	Gene x Treat
%Δ Body weight	2.48±7.73	8.65±5.48	4.14±4.70	5.66±2.94	0.69	0.03	0.17
Uterine weight (g)	0.10±0.05	0.04±0.02	0.10±0.02	0.05±0.02	0.30	<0.0001	0.34
Distal Femur							
BV/TV	0.019±0.004	0.012±0.004	0.038±0.011	0.021±0.010	<0.0001	<0.0001	0.06
SMI	3.818±0.250	4.055±0.357	3.387±0.263	3.810±0.294	0.0008	0.0011	0.32
Tb.N (mm^{-1})	2.554±0.239	2.165±0.385	3.128±0.218	2.797±0.276	<0.0001	0.0004	0.76
Tb.Th (mm)	0.040±0.005	0.041±0.005	0.039±0.003	0.037±0.004	0.08	0.87	0.23
Tb.Sp (mm)	0.393±0.036	0.477±0.097	0.317±0.026	0.359±0.037	<0.0001	0.0012	0.25
L5 Vertebra							
BV/TV	0.189±0.028	0.177±0.013	0.253±0.019	0.212±0.019	<0.0001	0.0004	0.05
Tb.N (mm^{-1})	3.797±0.513	3.580±0.285	4.491±0.345	4.022±0.254	<0.0001	0.0091	0.32
Tb.Th (mm)	0.050±0.003	049±0.002	0.056±0.002	0.053±0.002	<0.0001	0.0032	0.02
Tb.Sp (mm)	0.227±0.023	0.229±0.013	0.202±0.020	0.214±0.012	0.0013	0.25	0.44
Serum	WT		KO		2-WAY ANOVA p-values		
	Pre-op	Post-op^{4wks}	Pre-op	Post-op^{4wks}	Genotype	Treatment	Gene x Treat
P1NP (ng/ml)	6.018±1.794	5.830±1.349	6.017±1.412	4.769±1.223	0.19	0.08	0.19
CTX (ng/ml)	13.498±2.423	12.932±2.910	13.372±1.878	12.898±2.717	0.92	0.46	0.96

WT and *Nmp4*-KO mice showed significant trabecular bone loss of the distal femur and L5 vertebra 4wks after ovx as measured by µCT (Table 1, references describing methods[1, 2] in appendix). The KO mice exhibited a modest enhanced bone loss (BV/TV) that was near significant in the femur and only just significant in the L5 vertebra (Table 1, BV/TV, gene x treat). This may be due to the elevated number of osteoclast progenitors in the null mice[1]. We observed no change in the serum bone formation (P1NP) or the resorption (CTX) markers 4wks post-op (Table 1).

KEY FINDING: *Nmp4-KO mice exhibit an enhanced PTH-induced restoration of bone lost to ovx*

We initiated treatment of both WT and *Nmp4*-null ovx animals with PTH (30µg/kg/day) or vehicle control 4wks after surgery. The duration of hormone therapy lasted 4wks (8wks post-op) and 8wks (12wks post-op). The ovx *Nmp4*-KO mice showed a significantly enhanced PTH-induced gain in femoral BV/TV at 4wks and 8wks of therapy compared to their ovx WT littermates (Figure 2A). The KO mice also showed an enhanced PTH response at the L5 vertebra at 8wks of treatment (Figure 2B). There was no difference in bone parameters between the vehicle-treated genotypes suggesting that bone loss was equivalent between the genotypes at 8wks and 12wks post-ovx (Figure 2). Table 2 provides additional architectural parameters of the distal femur and L5 vertebra from these treatment groups.

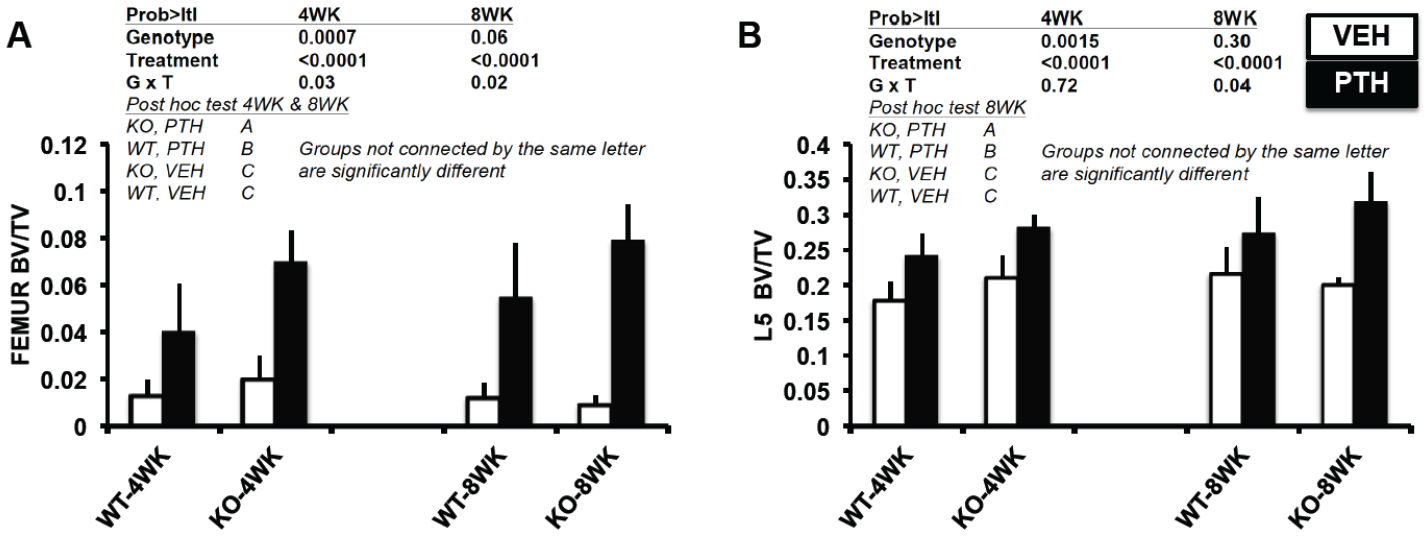

Figure 2: Trabecular bone volume/total volume (BV/TV) of ovx WT and ovx Nmp4-KO mice as determined by microCT analysis [A] distal femur and [B] L5 vertebra. Trabecular bone architecture was analyzed as previously described[1, 2]. Briefly, femurs/L5 were excised from mice after euthanasia, the muscle and connective tissue removed, and the bones transferred to 10% buffered formalin, 4°C for 48 hr, after which the bones were placed in 70% ethanol (4°C) until analyzed. Data are average ± SD, number of mice/experimental group = 8-9). Statistical differences were determined using a 2-way ANOVA. The Tukey's HSD (femur) or LS Means Student t (L5) post hoc tests were used to determine differences between the treatment groups if a significant genotype x treatment interaction was indicated.

Table 2: PTH-induced bone gain data. MicroCT (distal femur and L5 vertebra) from ovx WT and ovx *Nmp4*-KO mice after 4 wks and 8wks PTH/VEH therapy. Abbreviations: connectivity density (Conn.D, mm^{-3}), structure model index (SMI), trabecular number (Tb.N, mm^{-1}), trabecular thickness (Tb.Th, mm), and spacing (Tb.Sp, mm). Data are average ± SD, number of mice/experimental group = 8-9. Statistical significance was set at p≤0.05 and differences were determined using a 2-way ANOVA.

	WT		KO		2-WAY ANOVA p-values		
Distal Femur							
4wks	VEH	PTH	VEH	PTH	Genotype	Treatment	Gene x Treat
Conn D (mm^{-3})	3.180±3.870	33.230±26.730	9.681±15.979	67.533±14.111	0.0018	<0.0001	0.03
SMI	3.752±0.437	3.013±0.384	3.472±0.327	2.514±0.113	0.0025	<0.0001	0.36
Tb.N (mm^{-1})	2.100±0.519	2.441±0.281	2.712±0.241	2.833±0.224	0.0002	0.06	0.36
Tb.Th (mm)	0.039±0.010	0.042±0.007	0.033±0.003	0.044±0.003	0.54	0.004	0.09
Tb.Sp (mm)	0.510±0.157	0.409±0.051	0.370±0.036	0.342±0.032	0.0019	0.04	0.24
8wks							
Conn D (mm^{-3})	3.123±5.307	38.658±14.910	0.982±1.103	58.128±13.570	0.03	<0.0001	0.0064
SMI	3.808±0.479	2.470±0.284	3.589±0.218	2.262±0.141	0.05	<0.0001	0.96
Tb.N (mm^{-1})	2.132±0.297	2.164±0.431	2.286±0.145	2.552±0.277	0.02	0.17	0.28
Tb.Th (mm)	0.037±0.006	0.048±0.005	0.030±0.004	0.049±0.003	0.12	<0.0001	0.02
Tb.Sp (mm)	0.476±0.072	0.471±0.109	0.438±0.033	0.378±0.045	0.01	0.20	0.27
L5 Vertebra							
4wks	VEH	PTH	VEH	PTH	Genotype	Treatment	Gene x Treat
Tb.N (mm^{-1})	3.453±0.451	4.875±0.587	3.891±0.504	5.518±0.381	0.0049	<0.0001	0.56
Tb.Th (mm)	0.051±0.002	0.049±0.002	0.054±0.004	0.051±0.001	0.04	0.03	0.60
Tb.Sp (mm)	0.246±0.021	0.224±0.030	0.229±0.021	0.197±0.021	0.02	0.0036	0.52
8wks							
Tb.N (mm^{-1})	4.046±0.917	5.648±1.191	3.627±0.235	5.906±0.754	0.79	<0.0001	0.26
Tb.Th (mm)	0.053±0.003	0.049±0.004	0.055±0.001	0.054±0.001	0.0018	0.0044	0.09
Tb.Sp (mm)	0.239±0.021	0.206±0.037	0.256±0.020	0.186±0.023	0.86	<0.0001	0.05

KEY FINDING: *Ovx does not deplete the expanded Nmp4-KO osteogenic reserve*

Null bone marrow (BM) showed a significant elevation in CD45-/CD105+/CD146+/nestin+ osteoprogenitors at the end of 4wk therapy, irrespective of treatment (Figure 2A). By the end of 8wks treatment (12wks post-op) there was no difference in the number of these BM cells between the genotypes. However, there was a significant elevation in the number of these cells in the peripheral blood (PBL) of the untreated KO mice (Figure 2D). The KO mice showed a significant elevation in CD8+ T cells in both the BM and the PBL throughout the entire therapy regimen (Figure 2B and 2E). PTH significantly decreased the numbers of these cells in the BM at 8wks therapy in both genotypes (Figure 3B) but had no impact on the number of these cells in the PBL (Figure 2E). Disabling Nmp4 had little to no effect on CD4+ T cells, nor did treatment with PTH (Figure 2C and 2F), as we previously observed in the healthy mice[1].

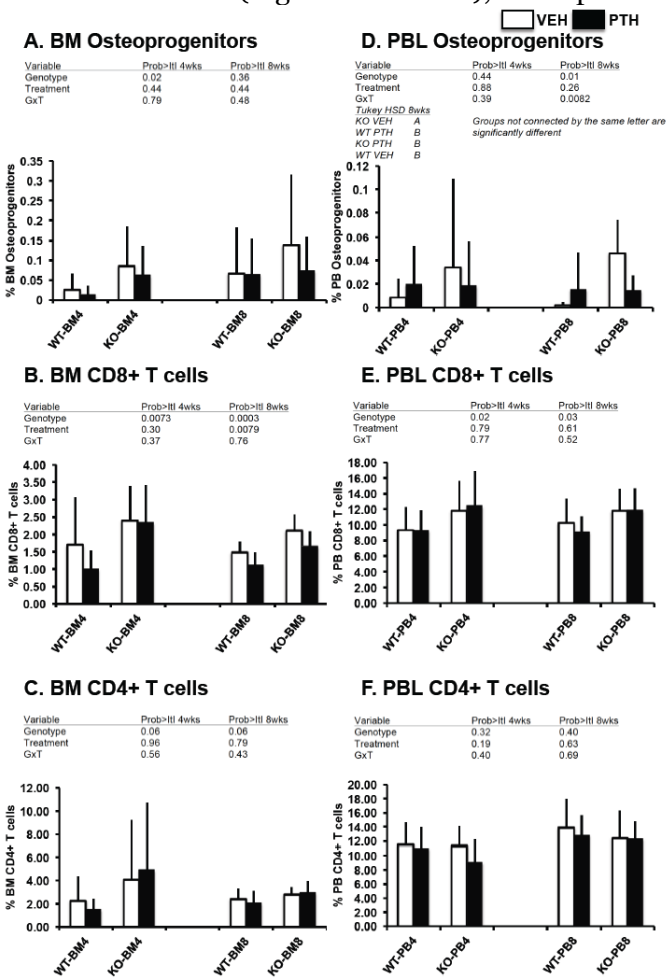

Figure 3: Flow cytometry analysis (FACs) of the femoral bone marrow (BM) and the peripheral blood (PBL) from ovx WT and ovx *Nmp4*-KO mice treated with human PTH (1-34) [30μg/kg/day] or vehicle control for 4wks or 8wks (treatments initiated 4wks post-op). These samples were analyzed as previously described[1] (reference in appendix). Briefly, whole BM was isolated by flushing the femurs of experimental mice with α-MEM supplemented with 10% FBS. PBL was collected from the mice by cardiac puncture. The red blood cells (RBCs) were lysed with an RBC lysis buffer (Qiagen) before the PBL and BM were processed for flow cytometric analysis. All antibodies for flow cytometry were purchased from BD Biosciences. Stained samples were analyzed on an FACS Caliber (BD Biosciences), and results were quantified using FlowJo Version 8.8.6 software (Tree Star, Inc.). (Average ± SD, number of mice/experimental group = 8-9). Statistical differences were determined using a 2-way ANOVA. A Tukey's HSD post hoc test was used to determine differences between the treatment groups if a significant genotype x treatment interaction was indicated.

KEY FINDING: *Nmp4-KO mesenchymal stem/progenitor cells (MSPCs) exhibit an enhanced proliferation in culture and precocious mineralization*

Expanded MSPC cultures were established using a standard protocol (reference [3] in appendix). Briefly, long BM was isolated from euthanized WT and KO mice 6-8wks of age and the mononuclear cells were isolated using a Ficoll gradient. These cells were plated in Mesencult™ Media + Mesencult™ Stimulatory Supplement (StemCell™ Technologies, Vancouver BC, Canada) and maintained in culture for 3-4wks without passage and fed every 5-7 days by removing 50% of the old media and adding 50% fresh media. At approximately 80% confluence, the cells were passaged at 1:3 dilution for two more passages before use or were frozen for storage. Cells were used for experiments between passages 5-10. For comparing cell proliferation rates between WT and *Nmp4*-KO MSPCs, the cells were transferred to α-MEM medium. To evaluate mineralization ascorbic acid and beta-glycerophosphate was added.

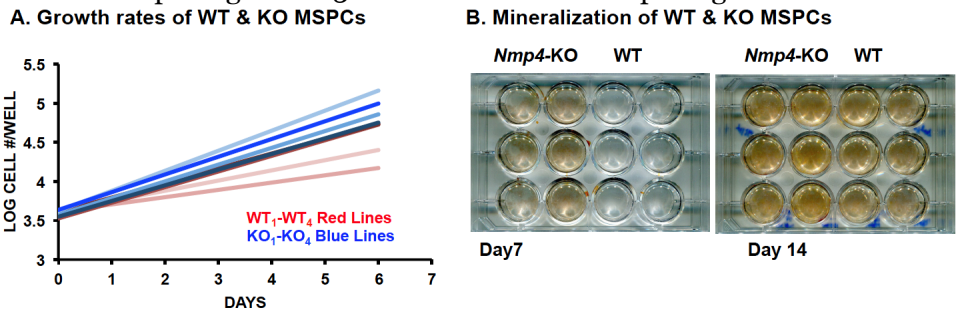

Figure 4: [A] Comparative growth rates of expanded WT and *Nmp4*-KO MSPCs. Cell counts/day (n=4 lines per genotype $\log_{10}$ cells/well, 3 wells/sample, average ± SD, t test, $t<0.05$). Note: each 'line' is derived from a single mouse [B] WT and KO MSPCs maintained in osteogenic medium for 7 and 14 days and then stained with alizarin red.

KO MSPCs from healthy mice exhibited modest but significantly enhanced proliferation (Figure 4A). and precocious mineralization (Figure 4B), consistent with our in vivo observations.

KEY FINDING: *Nmp4-KO and WT mice undergoing therapy exhibit similar bone histomorphometry and serum profiles*

We performed dynamic bone histomorphometry on WT and *Nmp4*-KO mice as previously described[2] at the end of 4wks PTH/VEH therapy (Table 3). Additionally, we evaluated the serum bone formation (P1NP) and resorption (CTX) markers, as described[2], at the end of the 8wk treatment regimen (Table 3). There was a strong treatment effect for all of these parameters, as expected. However, no significant differences were observed in any of these parameters between the genotypes. This was surprising considering the significant increase in PTH-induced bone formation observed in the *null* mice as compared to the WT animals. A plausible explanation for these results is that we missed the time point where significant differences in bone formation activity were transpiring. We are presently finishing static bone histomorphometry analysis for osteoblast and osteoclast numbers.

Table 3: Histomorphometry. Dynamic bone histomorphometry data of the distal femur from WT and *Nmp4*-KO mice treated with intermittent PTH or vehicle for 4wks (8wks post-op). Sera data were collected at the end of 8wks treatment (12wks post-op). The parameters include mineral apposition rate (MAR), mineralizing surface/bone surface (MS/BS), bone formation rate (BFR), pro-collagen type-1 amino-terminal pro-peptide (P1NP) and c-terminal telopeptide (CTX). Data are average ± SD, number of mice/experimental group = 4-7. A 2-way ANOVA was used to determine statistical differences and significance was set at p≤0.05.

	WT		KO		2-WAY ANOVA p-values		
	VEH	PTH	VEH	PTH	Genotype	Treatment	Gene x Treat
Dynamic histo							
MAR (μm/day)	2.28±0.37	3.80±0.73	2.29±0.37	3.61±0.40	0.70	<0.0001	0.66
MS/BS (%)	0.41±0.09	0.55±0.05	0.44±0.10	0.52±0.06	0.98	0.01	0.45
BFR (μm^2/μm/day)	0.95±0.28	2.09±0.52	1.01±0.25	1.86±0.22	0.60	<0.0001	0.37
Serum							
	WT		KO		2-WAY ANOVA p-values		
	VEH^{8wks}	PTH^{8wks}	VEH^{8wks}	PTH^{8wks}	Genotype	Treatment	Gene x Treat
P1NP (ng/ml)	3.147±0.653	10.066±2.659	2.806±0.760	8.042±3.304	0.19	<0.0001	0.34
CTX (ng/ml)	11.466±2.239	15.147±3.518	9.361±1.222	14.157±1.532	0.12	0.0002	0.56

ADDITIONAL RESEARCH ACTIVITIES:

Breeding of conditional knockout (KO) mice

The objectives for subtasks 4.2.a and 4.3.a are the breeding of *Nmp4$^{fl/fl}$ 3.6Col-Cre+*, *Nmp4$^{fl/fl}$ Cathepsin K-Cre+*, and *Nmp4$^{fl/fl}$-Cre–* mice. There are a number of crosses required to produce these mice and the entire breeding scheme is shown in Figure 5.

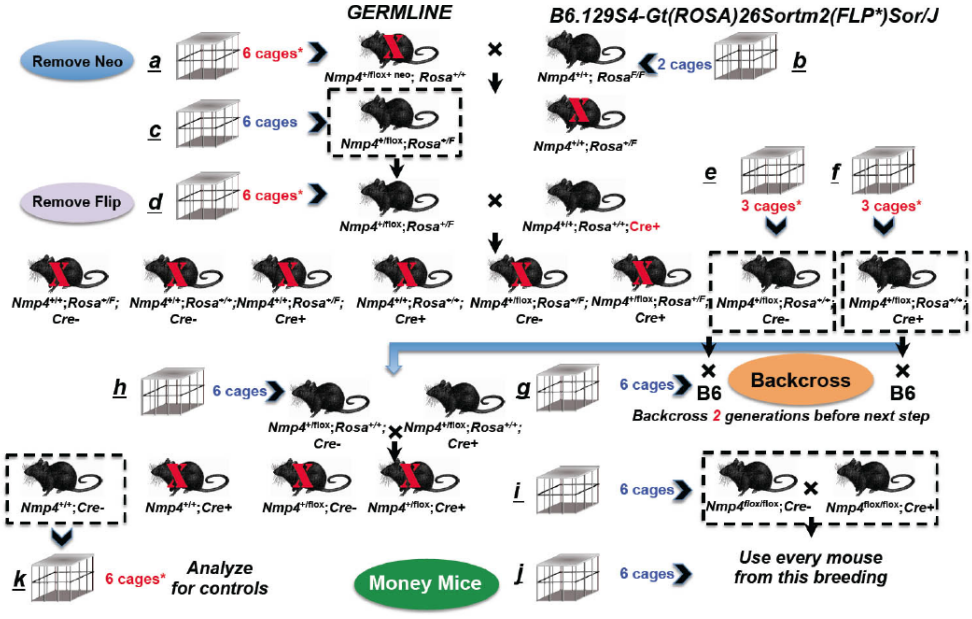

Figure 5: Breeding scheme for Nmp4 conditional KO mice. The Neo gene is removed from the flox construct by crossing ***a*** our confirmed flox germline transmission mice with ***b*** B6 (FLP*)Sor/J mouse. Select progeny ***c*** are bred with ***d*** Cre+ mice to remove the FLP (Flip) and to introduce the specific Cre. These mice are backcrossed further onto a C57B6/J strain [***e*** & ***f***]. This will produce ***g*** heterozygous Nmp4 flox mice lacking Cre- and ***h*** heterozygous Nmp4 flox mice containing Cre+. Breeding these mice will produce ***i*** homozygous Nmp4 flox mice with or without Cre. These are bred and all offspring ***j*** are used for the study. Nmp4+/+;Cre- mice ***k*** generated from the ***h*** x ***g*** crosses are used to test for the effects of non-recombined Nmp4 floxed. Red cages designate mice kept temporarily; blue cages are mice maintained as a source of breeders/experimental mice.

We are presently breeding our germline transmission mice (***a***) with the B6.129S4-Gt(ROSA)26Sortum2(FLP)Sor/J mice (***b***) obtained from Jackson labs.

ADDITIONAL RESEARCH ACTIVITIES [continued]:

Tally of mice completing combination treatments:

During this first year we initiated the PTH combination studies using the bisphosphonates alendronate (ALN) and zolendronate (ZOL) and the SERM raloxifene (RALOX). The experiments are progressing without any significant difficulties. The mice are not exhibiting any adverse reactions to the therapeutic regimens. Table 4 shows the running tally of the mice for these treatments at the writing of this progress report.

Table 4: Number of mice that have completed combination treatments, are currently in combination treatment, or have undergone ovx surgery and are waiting for treatment assignment. Abbreviations PTH (parathyroid hormone), ALN (alendronate), ZOL (zolendronic acid), RALOX (raloxifene) [8-10 mice/group required].

Genotype	**WT**			**KO**		
Treatment	PTH/ALN	PTH/ZOL	PTH/RALOX	PTH/ALN	PTH/ZOL	PTH/RALOX
# of mice completed	4	3	4	4	5	5
# of mice in treatment	2	2	1	4	3	3

# of WT mice completed surgery waiting for assignment: 22
# of KO mice completed surgery waiting for assignment: 8

KEY RESEARCH ACCOMPLISHMENTS:

- **KEY FINDING:** *Nmp4-KO mice are not protected from ovx-induced bone loss*
- **KEY FINDING:** *Nmp4-KO mice exhibit an enhanced PTH-induced restoration of bone lost to ovariectomy*
- **KEY FINDING:** *Ovx does not deplete the expanded Nmp4-KO osteogenic reserve*
- **KEY FINDING**: *Nmp4-KO MSPCs exhibit an enhanced proliferation and precocious mineralization in culture*
- **KEY FINDING:** *Nmp4-KO & WT mice under therapy exhibit similar histomorphometry and serum profiles*
- *Initiated breeding of conditional KO mice*
- *Initiated PTH combination treatments*

REPORTABLE OUTCOMES:

Abstract presentations in which the DOD support was acknowledged:

1. American Society for Bone & Mineral Research:
a. Date/location: October 4-7 2013, Baltimore, MD
b. Title: Nmp4/CIZ-knockout mice are hyper-responsive to anabolic agonists but susceptible to ovariectomy-induced bone loss
c. Authors: Paul Childress, Marta Alvarez, Joseph P Bidwell
2. American Society for Bone & Mineral Research:
a. Date/location: September 12-15 2014, Houston, TX
b. Title: Improving parathyroid hormone (PTH) therapy in an osteoporotic mouse model
c. Authors: Paul Childress, Yu Shao, Selene Hernandez-Buquer, Yongzheng He, Daniel Horan3 Alexander G. Robling, Stuart Warden, Feng-chun Yang, Matthew R Allen, Joseph P Bidwell
3. 4th annual National Clinical and Translational Science Predoctoral Programs Meeting
a. Date/location: May 5-7, 2013, Mayo Clinic, Rochester MN
b. Title: Enhancing Parathyroid Hormone (PTH) Osteoporosis Therapy
c. Authors: Paul Childress, Joseph P. Bidwell
4. 5th annual National Clinical and Translational Science Predoctoral Programs Meeting
a. Date/location: April 9-11, 2014, Omni Shoreham Hotel, Washington, DC
b. Title: Developing Nmp4 as a drug target to enhance parathyroid hormone therapy for osteoporosis
c. Authors: Paul Childress, Joseph P. Bidwell

Funding applied for based on work supported by this award:
Agency: The Indiana Clinical and Translational Sciences Institute
Program: Collaboration in Translational Research Pilot Grant Program
Title: Boosting bone anabolism
Date submitted: 05/09/2014
Total costs & dates if funding awarded: $75,000 [09/01/2014-08/31/2016]

Employment received based on experience/training supported by this award:
Paul Childress: PhD graduate student in the Bidwell lab has accepted a post-doctoral position with Dr. Melissa Kacena, Department of Orthopaedic Surgery, Indiana University School of Medicine

CONCLUSION: Key experimental discovery for 1st year of DOD study
Our key discovery is that ovariectomy does not abrogate the enhanced response to PTH therapy in our Nmp4-KO mouse pre-clinical model. The deficiency in estrogen, the leading cause of osteoporosis, does not attenuate the number or responsiveness of the null osteoprogenitors or their supporting CD8+ T cells.
"So what?"
This pre-clinical breakthrough is important because it suggests that disabling Nmp4 or some component of its pathway will *enhance and extend* PTH-induced regeneration of osteoporotic bone in post-menopausal female veterans. PTH is the only FDA-approved anabolic osteoporosis therapy and adds significant amounts of bone to the osteoporotic skeleton. Therefore, this drug has the potential to restore the bone lost in a variety of VA clinical settings. However, a drawback to PTH use is that potency declines within 2 years and thus it is not suitable as a long-term therapy, which is problematic in treating a chronic degenerative disease. Women comprise the fastest growing group of the US veterans contributing to the looming osteoporosis epidemic within the veteran population. The Veterans Affairs (VA) health care system will be in high demand by female veterans of Operation Enduring Freedom and Operation Iraqi Freedom.

REFERENCES:

1. He Y, Childress P, Hood M Jr, Alvarez M, Kacena MA, Hanlon M, McKee B, Bidwell JP, Yang FC. 2013 Nmp4/CIZ suppresses the parathyroid hormone anabolic window by restricting mesenchymal stem cell and osteoprogenitor frequency. Stem Cells Dev. 22(3):492-500
2. Childress P, Philip BK, Robling AG, Bruzzaniti A, Kacena MA, Bivi N, Plotkin LI, Heller A, Bidwell JP. 2011 Nmp4/CIZ suppresses the response of bone to anabolic parathyroid hormone by regulating both osteoblasts and osteoclasts. Calcif Tissue Int. 89(1):74-89.
3. Wu X, Estwick SA, Chen S, Yu M, Ming W, Nebesio TD, Li Y, Yuan J, Kapur R, Ingram D, Yoder MC, Yang FC. 2006 Neurofibromin plays a critical role in modulating osteoblast differentiation of mesenchymal stem/progenitor cells. Hum Mol Genet. 15(19):2837-45.

APPENDIX:
Note: Full copies of cited references [1-3, see above] that include details for materials and methods are included below.

STEM CELLS AND DEVELOPMENT
Volume 00, Number 00, 2012

DOI: 10.1089/scd.2012.0308

ORIGINAL RESEARCH REPORT

Nmp4/CIZ Suppresses the Parathyroid Hormone Anabolic Window by Restricting Mesenchymal Stem Cell and Osteoprogenitor Frequency

Yongzheng He,[1,2,*] Paul Childress,[3,*] Mark Hood, Jr.,[3] Marta Alvarez,[3] Melissa A. Kacena,[4] Michael Hanlon,[3,†] Bryce McKee,[3] Joseph P. Bidwell,[3] and Feng-Chun Yang[1–3]

Parathyroid hormone (PTH) anabolic osteoporosis therapy is intrinsically limited by unknown mechanisms. We previously showed that disabling the transcription factor Nmp4/CIZ in mice expanded this anabolic window while modestly elevating bone resorption. This enhanced bone formation requires a lag period to materialize. Wild-type (WT) and *Nmp4*-knockout (KO) mice exhibited equivalent PTH-induced increases in bone at 2 weeks of treatment, but by 7 weeks, the null mice showed more new bone. At 3-week treatment, serum osteocalcin, a bone formation marker, peaked in WT mice, but continued to increase in null mice. To determine if 3 weeks is the time when the addition of new bone diverges and to investigate its cellular basis, we treated 10-week-old null and WT animals with human PTH (1–34) (30 μg/kg/day) or vehicle before analyzing femoral trabecular architecture and bone marrow (BM) and peripheral blood phenotypic cell profiles. PTH-treated *Nmp4*-KO mice gained over 2-fold more femoral trabecular bone than WT by 3 weeks. There was no difference between genotypes in BM cellularity or profiles of several blood elements. However, the KO mice exhibited a significant elevation in CFU-F cells, CFU-$F^{AlkPhos+}$ cells (osteoprogenitors), and a higher percentage of CFU-$F^{AlkPhos+}$ cells/CFU-F cells consistent with an increase in CD45−/CD146+/CD105+/nestin+ mesenchymal stem cell frequency. Null BM exhibited a 2-fold enhancement in CD8+ T cells known to support osteoprogenitor differentiation and a 1.6-fold increase in CFU-GM colonies (osteoclast progenitors). We propose that Nmp4/CIZ limits the PTH anabolic window by restricting the number of BM stem, progenitor, and blood cells that support anabolic bone remodeling.

Introduction

Anabolic therapy is the preferred pharmacological intervention for osteoporosis [1], and parathyroid hormone (PTH) is the only FDA-approved drug that adds bone to the osteoporotic skeleton; however, its bone-forming activity, or anabolic window is intrinsically limited to about 2 years, thereafter falling to baseline [2–5]. Therefore, PTH is not approved as a long-term osteoporosis therapy, and its use is indicated only for those patients who are at a high risk of fractures or who are unresponsive to other available therapies [6].

While the mechanisms regulating the extent of the PTH anabolic window are unknown, we demonstrated that disabling the transcription factor nuclear matrix protein 4/cas-interacting zinc-finger protein (Nmp4/CIZ) in mice significantly extends and augments PTH bone-forming capacity; treatment of wild-type (WT) and *Nmp4*- knockout (KO) mice with intermittent PTH for 7 weeks resulted in significant increases in serum osteocalcin, a marker for bone formation, but these serum profiles as a function of time were strikingly different [7,8]. In the WT mice, serum osteocalcin peaked at 3 weeks of treatment and returned to baseline by 7 weeks of hormone administration [7]. However, in the null mice, this PTH-induced surge in serum osteocalcin exceeded that observed in the WT mice and was still climbing at the end of the 7-week treatment regimen [7]. Consistent with this sustained serum osteocalcin surge, at the end of the 7-week treatment period, the null mice had gained significantly more femoral, vertebral, and tibial trabecular bone than WT mice while maintaining robust increases in cortical bone [7,8]. These enhanced increases in cancellous bone in the *Nmp4*-KO skeleton all showed significant treatment × genotype

[1]Department of Pediatrics, Indiana University School of Medicine, Indianapolis, Indiana.
[2]Herman B Wells Center for Pediatric Research, Indianapolis, Indiana.
Departments of [3]Anatomy & Cell Biology and [4]Orthopaedic Surgery, Indiana University School of Medicine, Indianapolis, Indiana.
*These authors contributed equally to this work.
†Present affiliation: Iowa State University College of Veterinary Medicine, Ames, Iowa.

interactions, thus demonstrating that Nmp4/CIZ suppresses PTH-stimulated anabolism [7,8].

When in the PTH treatment regimen does bone formation in the *Nmp4*-KO mice eclipse WT growth, and what sustains this extended and enhanced anabolic activity? The WT and *Nmp4*-KO mice exhibited equivalent PTH-induced increases in trabecular bone during the first 2 weeks of treatment; however, at this treatment point, femoral mRNA profiles revealed a transient enhanced increase in PTH-stimulated *c-fos* and *Fra-2* expression in the null mice as well as an elevated expression of *Nfatc1* in these animals [7]. Although these transcription factors mediate numerous functions within the context of bone, this is consistent with an enhanced PTH-induced increase in mesenchymal stem cell self-renewal and/or recruitment of null osteoblasts and osteoclasts into the anabolic window [9–13]. Interestingly, the untreated *Nmp4*-KO mice had a modest, but significantly elevated, bone mineral density and bone mineral content as compared to WT animals [8] despite modestly elevated levels of serum C-terminal telopeptides of type I collagen (CTX), a marker for bone resorption [7]. The *Nmp4*-KO bone marrow (BM) yielded ~1.8-fold more osteoclasts in vitro as compared to WT marrow, and the null osteoclasts were significantly more active than their WT counterparts [7]. Therefore, bone formation was exceeding resorption, but how this occurred was not clear (eg, osteoblast–osteoclast coupling [14] and/or intrinsic differences in stem and progenitor pools that support bone formation or resorption).

To address whether the enhanced PTH-stimulated addition of trabecular bone in the *Nmp4*-KO mice is coincident with the initial surge in the serum osteocalcin, and to determine the cellular basis of this sustained enhanced anabolic activity, we treated WT and *Nmp4*-KO female mice with intermittent PTH for 3 weeks before harvesting femurs, femoral BM, and peripheral blood (PBL). Our data reveal that the *Nmp4*-KO mice show significantly enhanced PTH-stimulated addition of trabecular bone at 3 weeks of hormone treatment, and that Nmp4 has a profound regulatory role in BM population dynamics. Disabling this transcription factor results in alterations in stem, progenitor, and blood cell populations that accommodate the prolongation of the PTH anabolic window while maintaining bone remodeling. These data reveal novel aspects of how the PTH anabolic window is regulated and have implications for a novel adjuvant osteoporosis therapy.

Materials and Methods

Mice

Nmp4-KO mice, backcrossed onto a C57BL/6J background for 6–7 generations, [7,8], and their WT littermates were used for these studies. Our local Institutional Animal Care and Use Committee approved all experiments and procedures involving the production and use of the mice described in this investigation.

PTH treatment

Before initiating hormone treatment, 8-week-old female WT and *Nmp4*-KO mice were given 100 μL sterile saline by subcutaneous (sc) injection, once daily to habituate them to handling. At 10 weeks of age, animals were sorted into 4 treatment groups based on equivalent mean-group–body weight. These 4 groups included (1) vehicle-treated WT; (2) PTH-treated WT; (3) vehicle-treated *Nmp4*-KO, and (4) PTH-treated *Nmp4*-KO mice. Experimental animals were injected sc with human PTH 1–34 [hPTH(1–34), Bachem Bioscience, Inc.] at 30 μg/kg/day, daily or vehicle control (0.2% BSA/0.1% 1.0 mN HCl in saline; Abbott Laboratory) for 3 weeks. There was no significant difference in initial and final mean-group-body weights between genotypes. In a separate experiment, the BM of untreated female WT and *Nmp4*-KO mice (13 weeks of age) was harvested to compare the multipotent mesenchymal stem cell (CD45−/CD146+/CD105+/nestin+) frequency.

CFU-$F^{AlkPhos+}$ assay [15]

BM was flushed from femurs; single-cell suspensions were prepared, and cells were seeded into 6-well plates at an initial density of 1×10^6 cells/well. Each culture well contained 2 mL of complete α-MEM supplemented with 100 IU/mL penicillin, 100 μg/mL streptomycin, 25 μg/mL amphotericin, 2 mM L-glutamine (Hyclone Laboratories, Inc.), ascorbic acid (50 μg/mL, Sigma), and 10% fetal bovine serum (FBS; Atlanta Biologicals). The medium was changed every 2 days for 14 days. Subsequently, cells were fixed and stained for alkaline phosphatase using a Sigma-Aldrich Alkaline Phosphatase Staining Kit and then counted for colony-forming units—fibroblastic/alkaline phosphatase+ (CFU-$F^{AlkPhos+}$). Colonies were defined as positive staining with 25 or more cells per colony. After counting CFU-$F^{AlkPhos+}$ colonies, the cells were stained with crystal violet, and all colonies were counted for total CFU-F.

Flow cytometry

Whole BM was isolated by flushing the femurs of experimental mice with α-MEM supplemented with 10% FBS. PBL was collected from the mice by cardiac puncture. The red blood cells (RBCs) were lysed with an RBC lysis buffer (Qiagen) before the PBL and BM were processed for flow cytometric analysis. All antibodies for flow cytometry were purchased from BD Biosciences. Stained samples were analyzed on an FACS Caliber (BD Biosciences), and results were quantified using FlowJo Version 8.8.6 software (Tree Star, Inc.).

Clonogenic assays

Colony-forming units (CFU-Cs) were assayed as previously described [16]. Briefly, 2.5×10^4 BM mononucleated cells or 25 μL PBL was seeded onto a 35-mm gridded dish containing methylcellulose and murine stem cell factor (100 ng/mL), murine granulocyte–macrophage colony-stimulating factor (10 ng/mL), murine interleukin 3 (IL3, 5 ng/mL), murine recombinant macrophage–colony stimulating factor (10 ng/mL), and human erythropoietin (4 U/mL) for 7 days at 37°C in a 5% CO_2 incubator. Colonies were scored using an inverted light microscope. All cytokines were purchased from PeproTech.

Hemavet analysis

PBL was collected from the WT and *Nmp4-KO* mice and processed for blood cell enumeration using the Hemavet 950

FS according to the manufacturer's instructions (Drew Scientific).

Micro computed tomography

We previously reported no differences in the femur length between *Nmp4*-KO and WT mice at 8 and 17 weeks of age [8]. Therefore, after euthanasia, a 2.6-mm span ($\sim 5\,mm^3$ of medullary space) of the distal femoral metaphysis was scanned in 70% ethanol on a desktop microcomputed tomography (μCT) (μCT 35; Scanco Medical AG) at 10-μm resolution using 55-kVp tube potential and 400-ms integration time to measure trabecular three-dimensional (3D) morphometric properties as previously described [17]. From the 3D constructs, trabecular bone volume per total volume (BV/TV, %), connectivity density (Conn.D, mm^{-3}), structure model index (SMI), trabecular number (Tb.N, mm^{-1}), trabecular thickness (Tb.Th, mm), and spacing (Tb.Sp, mm) were calculated using Scanco software.

Statistical analysis

The program JMP version 7.0.1 (SAS Institute) was used to process all statistical evaluations. We employed a 2-way analysis of variance (ANOVA) for the PTH studies using genotype and treatment as the independent variables. If a genotype × treatment interaction was indicated, the data were analyzed by a Tukey honestly significant difference (HSD) post hoc test to determine significant differences between the experimental groups. Statistical significance was set at $P \leq 0.01$ to guard against type I errors. A separate experiment was conducted using a distinct group of our experimental mice for the purpose of comparing the frequency of multipotent mesenchymal stem cells (CD45−/CD146+/CD105+/nestin+) in untreated female WT and *Nmp4*-KO mice. These data were analyzed with a 2-sample *t*-test, assuming unequal variances and statistical significance was set at $P \leq 0.05$. The numbers of mice per treatment group are indicated in the appropriate Figures and Tables.

Results

Nmp4-KO mice exhibited an enhanced increase in femoral trabecular bone after 3 weeks of treatment

To determine if the divergence between the WT and *Nmp4*-KO mice in serum osteocalcin levels at 3 weeks is coincident with the beginning of the enhanced addition of trabecular bone in the null animals observed at 7 weeks [7], we sorted WT and *Nmp4*-KO mice into 4 treatment groups and harvested the femurs for μCT analysis as described in the Materials and Methods section. Although the WT and null mice had previously shown equivalent PTH-induced increases in trabecular bone at 2 weeks of treatment [7], in the present study, the null mice exhibited significantly augmented PTH-stimulated increase in femoral trabecular bone as compared to their WT littermates at 3 weeks (Fig. 1). The *Nmp4*-null mice showed a more robust PTH-stimulated increase in BV/TV compared to the WT animals during the first 3 weeks of treatment (Fig. 1A). The KO mice added ~2.3-fold more bone than their WT littermates in response to PTH (Fig. 1A). The 2-way ANOVA indicated a strong genotype × treatment interaction, and the Tukey HSD post hoc determined that there was no difference in BV/TV between the vehicle-treated WT and KO animals (Fig. 1A). While PTH treatment increased connectivity parameters (Conn.D, mm^{-3}) for both genotypes, a significantly greater enhancement was observed in *Nmp4*-KO mice compared to WT mice (Fig. 1B). Again, there was no difference between the vehicle-treated WT and null mice. The SMI was used to evaluate the PTH-induced alteration in femoral trabecular morphology. This parameter measures changes from a rod-like to a plate-like form, and the lower the value, the more plate-like the shape, which is indicative of an increase in bone strength [18]. PTH treatment of both WT and *Nmp4*-KO mice resulted in a significant transition to a more plate-like morphology, which was more pronounced in the null mice with a significant genotype × treatment effect (Fig. 1C). Interestingly, the SMI value for the femoral bone of the KO mice treated with vehicle was statistically equivalent to that of the WT mice treated with PTH (Fig. 1C). While PTH treatment significantly increased trabecular thickness (Tb.Th, mm, Fig. 1D) in null mice, treatment did not alter trabecular thickness in WT mice. Finally, PTH equivalently increased the trabecular number (Tb.N, mm^{-1}, Fig. 1E) and decreased spacing (Tb.Sp, mm, Fig. 1F) in both genotypes.

BM cellularity, spleen weight, and the profiles of most blood elements did not differ between the WT and Nmp4-KO mice

To address whether there are differences between the *Nmp4*-null and WT mice in the BM or PBL cellular profiles supportive of the observed enhanced PTH-induced addition of trabecular bone, we obtained immunophenotypic, clonogenic, and hematological profiles at 3 weeks of treatment (Tables 1–3). The spleen weight measured, as a% of total body weight, did not differ with the genotype, but did modestly increase with PTH treatment in both WT and null mice (Table 1). The profiles of blood elements between the *Nmp4*-KO and WT mice were unremarkable. We observed no differences between any of the treatment groups in the BM and PBL profiles of the RBCs, WBCs, platelets, neutrophils, lymphocytes, eosinophils, monocytes, B-cell lineages, CD4+ T cells, or the Lin(-)Sca-1(+)c-Kit(+) (LSK) cells (Tables 1 and 2). Finally, there were no differences between WT and *Nmp4*-KO mice in CFU-C, CFU-G, CFU-GEMM, and CFU-M cells (Table 3). PTH treatment had no impact on any of these parameters (Tables 1–3).

Nmp4-KO BM yielded more multipotent MSCs (CD146+/nestin+), CFU-$F^{AlkPhos+}$, CFU-GM, and CD8+ T cells than WT BM

To determine if the source of this augmented bone formation in *Nmp4*-null mice is derived, in part, from an expanded pool of osteoprogenitors, we obtained BM from our experimental groups for analysis of CFU-$F^{AlkPhos+}$ colonies as described in the Materials and Methods section. We recovered ~4-fold more CFU-$F^{AlkPhos+}$ colonies from the null mice than the WT animals (Fig. 2A). The total number of CFU-F colonies was significantly elevated in the *Nmp4*-KO cultures (Fig. 2B), and the percentage of CFU-$F^{AlkPhos+}$/total CFU-F colonies was significantly increased in the cultures

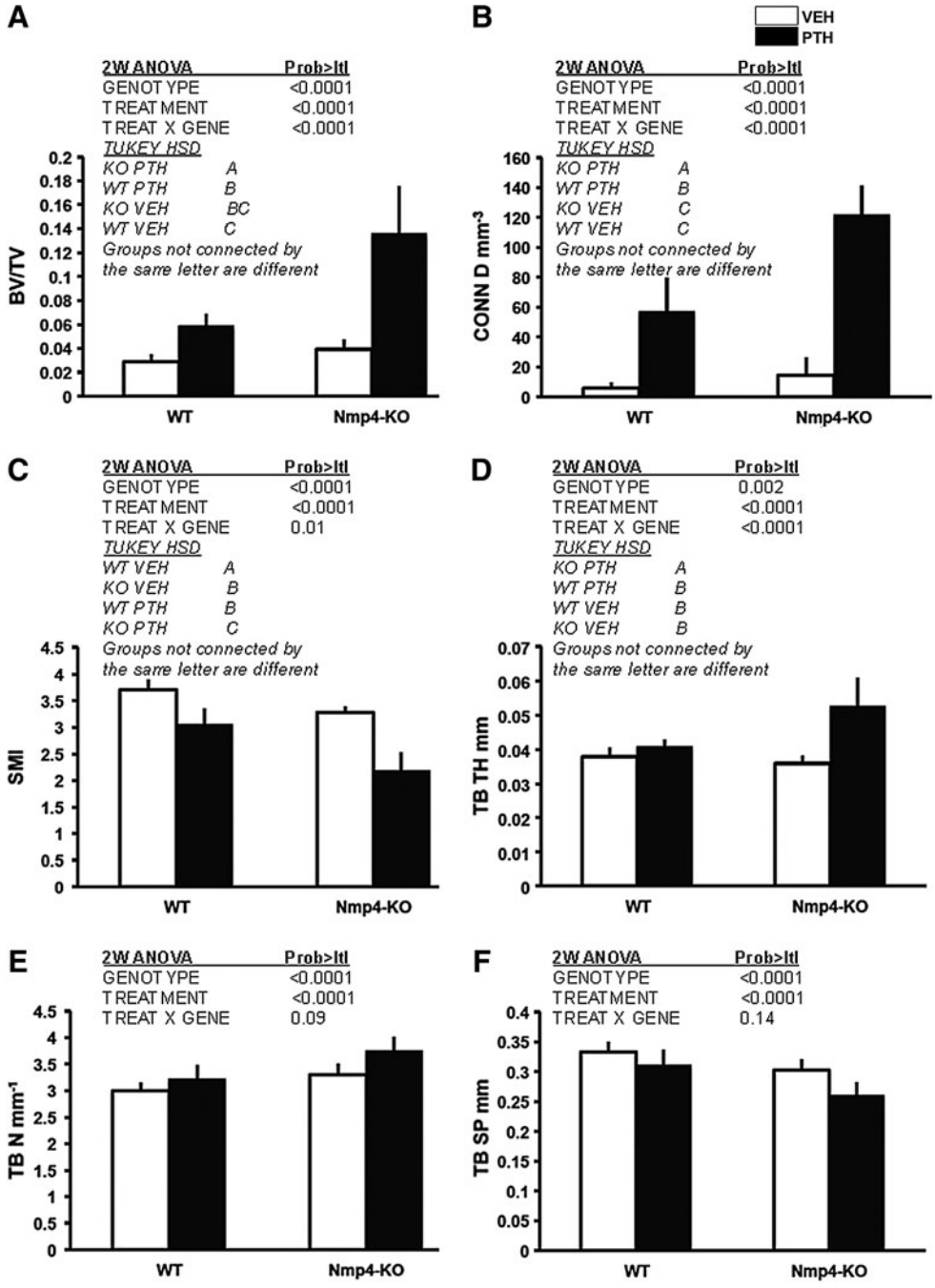

FIG. 1. Disabling Nmp4 enhanced PTH-induced increases in femoral cancellous bone after 3 weeks of treatment. Microcomputed tomography-acquired femoral trabecular architecture, including **(A)** BV/TV%; **(B)** Conn D mm^{-3}; **(C)** SMI; **(D)** Tb.Th mm: **(E)** Tb.N mm^{-1}: **(F)** Tb.Sp mm was compared between WT and *Nmp4*-KO mice that had been treated with intermittent hPTH (1–34) 30 μg/kg/day or vehicle for 3 weeks (average ± SD, number of mice/experimental group = 10). Statistical differences were determined using a 2-way ANOVA. A Tukey's HSD post hoc test was used to determine differences between the treatment groups if a significant genotype × treatment interaction was indicated, and there was such an interaction for BV/TV, Conn D, SMI, and Tb.Th. HSD, honestly significant difference; PTH, parathyroid hormone; VEH, vehicle; SMI, structure model index; Tb.N, trabecular number; Tb.Th, trabecular thickness; Tb.Sp, trabecular spacing; WT, wild type; KO, knockout.

from the *Nmp4*-null BM as compared to the WT BM (Fig. 2C). There was a trend toward increased yield of CFU-F and CFU-$F^{AlkPhos+}$ cells with PTH treatment in both genotypes, but this was not significant. Therefore, we next addressed whether the frequency of the self-renewing multipotent mesenchymal stem cell (CD45−/CD146+/CD105+/nestin+), the precursor of CFU-F-derived lineages, including osteoprogenitors, is elevated in untreated *Nmp4*-KO mice. Indeed, we observed a nearly 4-fold increase in this cell phenotype in the null BM (Fig. 2D).

Nmp4 has no significant influence on the percentage of CD4+ T cells in the BM or PBL (Table 2), but recent studies have demonstrated that CD8+ T cells play an obligatory role in the PTH anabolic response via their release of the glycoprotein Wnt10b, a potent agonist for osteoprogenitors [19,20]. Indeed, the present data show that the percentage of CD8+ T cells in the null BM was 2-fold greater than that observed in the WT BM (Fig. 3A), but there was no difference in the percent CD8+ T cells in the PBL between the genotypes (Fig. 3B). Additionally, PTH treatment had no effect on the size of this population of cells in either the BM or PBL.

Next, to address whether the observed modest elevation in bone resorption in the null mice and the enhanced number of osteoclasts derived from their BM [7] is due, in part, to an increase in osteoclast progenitors, we evaluated the number of CFU-GM cells from our treatment groups. Indeed, the *Nmp4*-null mice exhibited a modest (~1.6-fold), but significant, increase in CFU-GM cells as compared to their WT

Table 1. Peripheral Blood of the WT and *Nmp4*-KO Mice Was Analyzed Using the Hemavet 950 as Described in the Materials and Method Section

	WT		*KO*		*2-Way ANOVA* P *values*		
	VEH	*PTH*	*VEH*	*PTH*	*Genotype*	*Treatment*	*Gene×Treat*
Cellularity (10^6/femur)	9.1±6.2	8.1±5.6	14.3±7.1	11.5±6.6	0.04	0.33	0.64
% Spleen weight	0.40±0.03	0.47±0.06	0.42±0.08	0.46±0.07	0.84	0.01	0.49
WBC (K/μL)	4.8±1.1	4.9±1.4	4.5±1.6	5.6±1.6	0.70	0.16	0.24
NE (K/μL)	0.70±0.28	0.62±0.40	0.56±0.32	0.73±0.33	0.86	0.67	0.22
NE%	14.2±3.3	12.6±6.1	12.7±5.7	12.8±4.7	0.88	0.33	0.82
LY (K/μL)	1.0±0.78	4.1±1.1	3.7±1.4	4.8±1.3	0.62	0.11	0.26
LY%	82.4±4.3	83.8±5.9	82.2±8.1	84.4±4.8	0.88	0.33	0.82
MO (K/μL)	0.13±0.05	0.14±0.06	0.16±0.09	0.12±0.03	0.89	0.53	0.21
MO%	2.7±0.87	2.9±1.0	3.6±2.1	2.2±0.53	0.69	0.15	0.06
EO (IC/μL)	0.03±0.05	0.03±0.04	0.04±0.05	0.02±0.03	0.92	0.49	0.54
EO%	0.54±0.88	0.56±0.53	1.17±1.57	0.43±0.52	0.42	0.24	0.23
RBC (M/μL)	9.6±0.46	9.1±1.5	8.6±1.2	8.8±1.4	0.09	0.67	0.38
PLT (K/μL)	493.8±124.7	486.6±167.4	378.9±207.9	487.5±142.8	0.27	0.32	0.26

WT and null mice were treated with intermittent PTH or vehicle for 3 weeks (number of mice/experimental group = 9–14). A 2-factor ANOVA was used to evaluate the impact of genotype and treatment on the individual parameters. Statistical significance was set at $P < 0.01$ to guard against type I errors. Percent (%) spleen weight is the weight of the organ divided by the total body weight.

WT, wild type; VEH, vehicle; PTH, parathyroid hormone; KO, knockout; ANOVA, analysis of variance; EO, eosinophils; LY, lymphocytes; MO, monocytes; NE, neutrophils; PLT, platelets; RBC, red blood cell; WBC, white blood cells.

littermates (Fig. 4). PTH had no effect on the number of these cells (Fig. 4).

Discussion

A significant drawback to the use of PTH as an osteoporosis drug is that its anabolic potency declines within a relatively short period of time, which is particularly problematic in treating a chronic degenerative disease [21]. The cellular and molecular mechanisms underlying this closing of the PTH anabolic window are unknown. We have recently determined that deleting the transcription factor Nmp4/CIZ from mice significantly extends the PTH anabolic window and results in enhanced trabecular bone formation without compromising hormone-stimulated gains in cortical bone [7,8].

An intriguing aspect of the *Nmp4*-KO mouse response to anabolic doses of PTH is that the enhanced addition of trabecular bone requires a lag period to materialize [7]. Previously, we reported that both WT and null mice exhibited equivalent PTH-stimulated increases in trabecular bone during the first 2 weeks of a 7-week treatment. In this study, we compared hormone-induced increases in femoral cancellous bone after 3 weeks of treatment and indeed observed that the *Nmp4*-KO mice exhibited a >2-fold increase in PTH-induced accrual of femoral trabecular bone formation as compared to their WT littermates. This enhanced response to PTH was manifested in an augmented increase in BV/TV, trabecular connectivity (Conn D), and trabecular thickness (Tb.Th). Additionally, PTH had a greater impact on the SMI in the null mice. A decrease in SMI indicates a change in cancellous architecture from a rod-like to a plate-like

Table 2. Immunophenotypic Evaluation of BM and PBL Cell Types in WT and *Nmp4*-KO Mice Using Fluorescence Activated Cell Sorting Analysis as Described in the Materials and Method Section

	WT		*KO*		*2-Way ANOVA* P *values*		
Units (%)	*VEH*	*PTH*	*VEH*	*PTH*	*Genotype*	*Treatment*	*Gene×Treat*
Pre-B (BM)	11.6±7.2	12.1±7.0	7.6±4.7	9.7±5.7	0.08	0.45	0.65
Pre-B (PBL)	17.5±6.5	20.0±7.8	11.7±6.5	16.9±7.6	0.04	0.06	0.52
Immature B (BM)	5.9±1.3	6.3±2.7	6.8±3.5	6.3±4.4	0.64	0.95	0.65
Immature B (PBL)	20.7±10.9	22.3±8.5	25.1±11.3	22.8±11.6	0.43	0.90	0.54
Mature B (BM)	3.5±3.5	3.5±3.7	3.0±3.0	3.5±3.4	0.81	0.75	0.79
Mature B (PBL)	5.7±3.8	5.5±4.8	7.2±6.7	8.3±6.7	0.20	0.79	0.68
CD4+T (BM)	1.6±0.39	1.4±0.40	1.9±0.74	2.0±1.0	0.03	0.73	0.36
CD4+ T (PBL)	15.8±2.5	15.6±4.3	16.3±5.5	17.1±3.7	0.41	0.79	0.68
Myeloid (BM)	34.5±5.7	36.4±4.8	32.0±7.6	34.1±11.2	0.30	0.38	0.97
Myeloid (PBL)	6.0±2.5	5.3±1.3	5.9±2.9	7.4±4.4	0.24	0.65	0.22
LSK (BM)	0.11±0.06	0.11±0.06	0.12±0.14	0.26±0.22	0.05	0.07	0.09
L5K (PBL)	0.03±0.03	0.03±0.03	0.03±0.04	0.02±0.03	0.60	0.95	0.92

Mice were treated with PTH or vehicle for 3 weeks (number of mice/experimental group = 11–14). Statistical significance was set at $P < 0.0$l.
LSK, lin-/Scal+/c-Kit+; BM, bone marrow; PBL, peripheral blood.

Table 3. Clonogenic Assays of WT and *Nmp4*-KO Mice as Described in the Materials and Method Section

	WT		*KO*		*2-Way ANOVA* P *values*		
Units: colony/femur	*VEH*	*PTH*	*VEH*	*PTH*	*Genotype*	*Treatment*	*Gene × Treat*
CFU-C	27307 ± 13080	31311 ± 17107	44898 ± 22460	40573 ± 27265	0.04	0.98	0.52
CFU-G	1145 ± 2204	936 ± 1402	560 ± 998	284 ± 460	0.12	0.54	0.93
CFU-GEMM	941 ± 1219	762 ± 830	1065 ± 1817	847 ± 987	0.78	0.61	0.96
CFU-M	7409 ± 4316	9405 ± 7227	11229 ± 6172	9629 ± 6478	0.27	0.91	0.33

WT and null mice were treated with intermittent PTH or vehicle for 3 weeks (number of mice/experimental group = 10–14). A 2-factor ANOVA was used to evaluate the impact of genotype and treatment on the individual parameters. Statistical significance was set at $P < 0.01$ to guard against type I errors.

morphology and is a result of alterations in modeling and remodeling [18,22,23]. This suggests that PTH-stimulated increases in bone strength are enhanced in the *Nmp4*-KO mice, although this must be confirmed by biomechanical testing.

Our data indicate that deleting Nmp4/CIZ establishes a BM microenvironment that is primed for anabolic signals. We observed no differences in femur cellularity, % spleen weight, or in the profiles of the vast majority of blood elements; however, there was a striking difference in the number of osteoprogenitor cells as evaluated by the clonogenic CFU-$F^{Alkphos+}$ assay. The *Nmp4*-null BM yielded 4-fold more of these colonies than did the WT BM. In an earlier study, Noda and colleagues observed that BM cultures from null mice yielded about 3-fold more mineralized nodules than WT mice [24], which is equivalent to measuring CFU–osteoblast colonies [25]. In the present study, we also determined that the total number of CFU-F colonies obtained from the null mice was significantly elevated as was the% CFU-$F^{Alkphos+}$/total CFU-F. These data together suggest that Nmp4 suppresses the frequency of CFU-F cells and impedes commitment to the osteogenic lineage. This is consistent with the elevated number of CD45−/CD146+/CD105+/nestin+ cells obtained in the *Nmp4*-KO mice. These cells are self-renewing multipotent mesenchymal stem cells and contain all the bone marrow colony-forming-unit fibroblastic colony activity [26,27]. PTH did not significantly impact the number of CFU-$F^{AlkPhos+}$ colonies recovered from the BM of either genotype, although there was a trend toward modestly elevating the frequency of these cells. A variety of studies have shown conflicting stimulatory and inhibitory effects of PTH on osteoprogenitor proliferation [28–30]; however, the

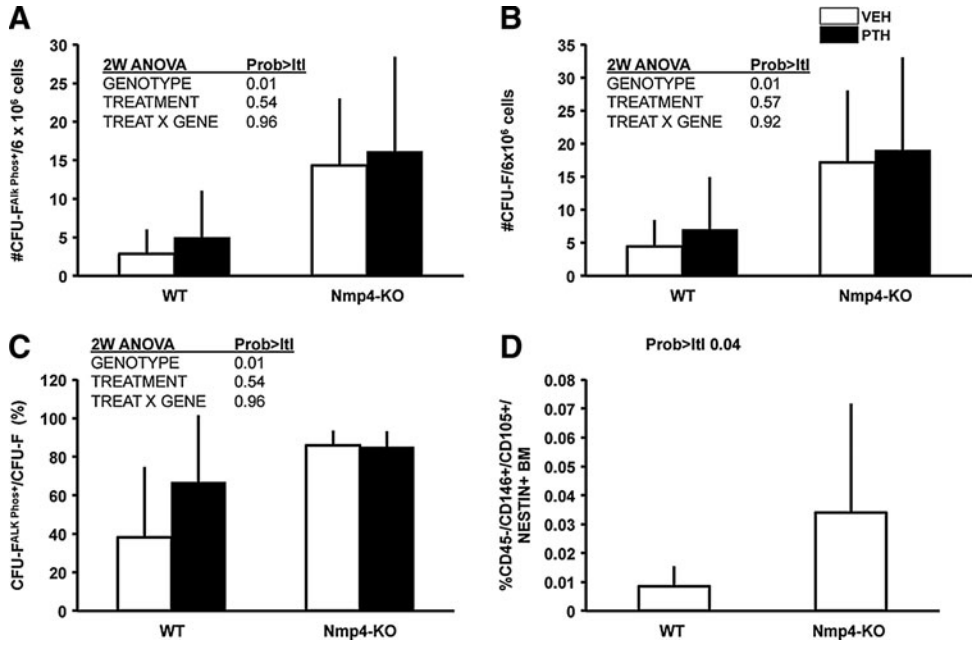

FIG. 2. *Nmp4*-KO BM yielded more osteogenic stem and progenitor cells irrespective of treatment. **(A)** Total number of CFU-$F^{AlkPhos+}$ colonies in BM cultures derived from WT and *Nmp4*-KO mice treated with intermittent hPTH (1–34) 30 μg/kg/day or vehicle for 3 weeks. **(B)** Total number of CFU-F colonies. **(C)** The percent CFU-$F^{AlkPhos+}$ colonies/total CFU-F colonies (average ± SD, number of mice/experimental group = 6–8; statistical differences determined by a 2-way ANOVA). **(D)** The frequency of femoral CD45−/CD146+/CD105+/nestin+ multipotent mesenchymal stem cells in untreated WT and *Nmp4*-KO mice; FACS was used to evaluate the BM from each mouse as described in the Materials and Methods section (average ± SD, number of mice/experimental group = 12–20; statistical difference was determined using a 2-sample *t*-test assuming unequal variances). BM, bone marrow; FACS, fluorescence activated cell sorting.

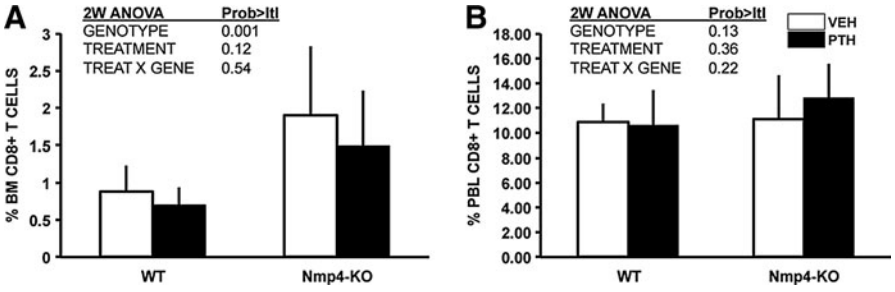

FIG. 3. *Nmp4*-KO BM harbored more CD8+ T cells than WT BM irrespective of treatment. **(A)** FACS analysis showed that there were significantly more CD8+ T cells in the BM of *Nmp4*-KO mice as compared to that observed in WT mice. **(B)** No differences between WT and *Nmp4*-KO mice in CD8+ T cells were detected in the PBL (average ± SD, number of mice/experimental group 11–14; statistical differences were determined using a 2-way ANOVA). PBL, peripheral blood.

prevailing view is that intermittent PTH recruits osteoprogenitors into the osteoblast differentiation pathway and enhances their survival instead of increasing the size of this progenitor pool [31, and references therein]. It is the accumulation of repeated new waves of osteoprogenitors with enhanced osteogenic potential that mediates the PTH-stimulated increase in bone mass [28,32]. This may also explain that the observed lag period before the enhanced PTH-induced bone formation phase is initiated in the *Nmp4*-null mice. If indeed the anabolic effect of intermittent PTH is the result of consecutive waves of committed osteoblast differentiation accumulated from each PTH exposure, in which hormone only acts on the BM early osteoprogenitor cells [28], then the rate of PTH osteoprogenitor recruitment would be equivalent in both the WT and KO mice, but the WT osteoprogenitor pool would be depleted before the KO population. This is consistent with the observed equivalent addition of bone during the first 2 weeks of treatment, but the divergence in both serum osteocalcin and bone formation in the null mice at 3 weeks [7 and the present work]. Finally, the *Nmp4/CIZ*-KO osteoblast exhibits a modest, but significant, enhanced response to numerous anabolic stimuli, including PTH, BMP2, and mechanical loading [24,33–35]; therefore, an expanded population of such cells is certainly consistent with the augmented skeletal bone mineral density and bone mineral content of the null animals.

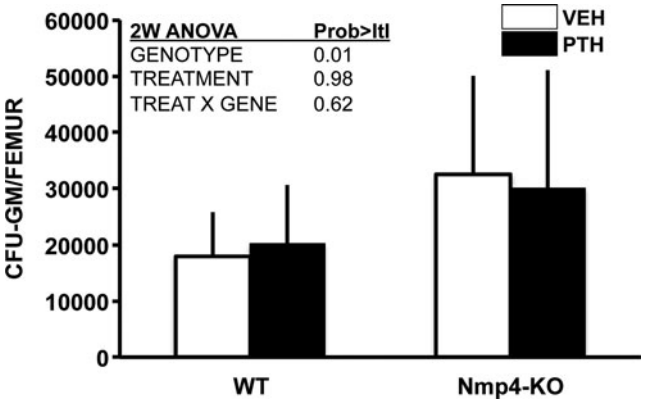

FIG. 4. More CFU-GM cells were obtained from *Nmp4*-KO mice than WT mice, irrespective of treatment. Intermittent hPTH (1–34) 30 μg/kg/day or vehicle was administered for 3 weeks as described in the Materials and Methods section (average ± SD, number of mice/experimental group = 10–14; statistical differences were determined using a 2-way ANOVA).

The expanded *Nmp4*-KO osteoprogenitor pool may be supported by the 2-fold increase in BM CD8+ T cells as compared to the WT mice. CD8+ T cells express the PTH receptor PTHR1 and support intermittent hormone anabolic activity via their secretion of the glycoprotein Wnt10b, a potent agonist of osteoblast activity [19,20]. PTH-induced bone formation was significantly reduced in T-cell-deficient mice and in these mice reconstituted with *Wnt10b*$^{-/-}$ T cells [20]. Interestingly, we observed no difference in the level of CD8+ T cells in the PBL, suggesting that the recruitment and/or the retention of these cells is enhanced in the null BM microenvironment. BM CD8+ T cells consist chiefly (~50%) of CCR7+ L-selectin+central memory cells [36], and the mechanisms underlying this concentration in the marrow involve PSGL-1-mediated rolling and VCAM-1-VLA-4-mediated arrest in BM venules [36]. The retention of these cells may be enhanced by CXCL12 (a ligand for CXCR4 on central memory T cells) [36]. Finally, IL15-dependent homeostatic proliferation of memory T cells contributes to their disproportionate presence in the BM [37,38]. Whether the null BM microenvironment is enriched in these various cytokines and/or selectin ligands and adhesion molecules remains to be determined.

A second provocative aspect of the *Nmp4*-KO skeletal phenotype is that the baseline bone mineral density and bone mineral content are slightly increased despite a modest elevation of bone resorption [7]. While the increase in osteoclast number may be attributed to coupling (eg, increased osteoblast support of an increase in osteoclastogenesis [14 and references therein]), the present data suggest that this reflects intrinsic differences in osteoclast progenitor populations. We observed a modest (1.6-fold), but statistically significant, increase in CFU-GM cells in the null mice as compared to their WT counterparts. Although CFU-C cells were elevated in the *Nmp4*-KO mice, this only approached significance, and there was no difference in the levels of CFU-M cells between the genotypes. The precise lineage of the osteoclast and its relationship to other hematopoietic cells is controversial; however, there are a number of studies supporting the hypothesis that the osteoclast lineage branches to terminal differentiation via the CFU-GM cells before further passage toward the monocyte/macrophage lineage [39,40].

The present data suggest that the heightened bone anabolism and modestly elevated bone resorption in the global *Nmp4*-KO mouse are derived, in part, from a unique confluence of BM stem, progenitor, and blood cells. The null BM harbors an expanded pool of MSCs (CD146+/nestin+), osteoprogenitors, and CD8+ T cells, which together supply the osteoblasts necessary for the observed augmented bone-forming activity, even in the presence of elevated bone resorption driven by the modestly enlarged CFU-GM pool (1.6-fold) that contributes to the osteoclasts. This may support an environment of enhanced anabolic remodeling.

Our data do not directly relate the differences in cellular composition observed in the *Nmp4*-KO mice to enhanced PTH-stimulated increases in trabecular architecture. To address this issue, a combination of genetic-, drug-, and transplantation-based approaches will be required, because all of these methods have strengths and drawbacks, yet their intersection reveals complementary aspects of the phenomenon under study. However, the previously observed heightened PTH-responsiveness and osteogenic capacity of *Nmp4*-KO BMSCs and osteoblasts in culture [24,33,35] and the enhanced number of the progenitors of these cells (present study) likely make a substantial contribution to the extended anabolic window. Additionally, Nmp4/CIZ deficiency augmented newly formed trabecular bone mass after femoral BM ablation as compared to WT mice [24], confirming the enhanced osteogenic capacity of the reconstituted KO BM. It is certainly tenable that multiple stem/progenitor types are necessary for maintaining an open PTH anabolic window, and that one transcription factor has significant direct and/or indirect control over these populations was unexpected despite the fact that Nmp4/CIZ is expressed in multiple cell and tissue types [41]. Nmp4/CIZ has been proposed as a potential target for osteoporosis therapy, [42] and the present data further develop this idea, suggesting that disabling Nmp4/CIZ may provide an adjuvant therapy for extending PTH clinical efficacy by expanding the stem/progenitor populations sustaining its anabolic action.

Acknowledgments

This work was supported by grants from the Leukemia & Lymphoma Society (6234-12, FCY), Department of Defense (NF100087, FCY), and from NIH National Institute of Diabetes and Digestive and Kidney Diseases (NIDDK), contract grant number DK053796 (JPB).

Author Disclosure Statement

No competing financial interests exist.

References

1. Trivedi R, R Goswami and N Chattopadhyay. (2010). Investigational anabolic therapies for osteoporosis. Expert Opin Investig Drugs 19:995–1005.
2. Cusano NE and JP Bilezikian. (2011). Combination antiresorptive and osteoanabolic therapy for osteoporosis: we are not there yet. Curr Med Res Opin 27:1705–1707.
3. Cusano NE and JP Bilezikian. (2010). Teriparatide: variations on the theme of a 2-year therapeutic course. IBMS Bone Key 7:84–87.
4. Bilezikian JP. (2008). Combination anabolic and antiresorptive therapy for osteoporosis: opening the anabolic window. Curr Osteoporos Rep 6:24–30.
5. Cosman F, J Nieves, M Zion, L Woelfert, M Luckey and R Lindsay. (2005). Daily and cyclic parathyroid hormone in women receiving alendronate. N Engl J Med 353: 566–575.
6. Silverman S and C Christiansen. (2012). Individualizing osteoporosis therapy. Osteoporos Int 23:797–809.
7. Childress P, BK Philip, AG Robling, A Bruzzaniti, MA Kacena, N Bivi, LI Plotkin, A Heller and JP Bidwell. (2011). Nmp4/CIZ suppresses the response of bone to anabolic parathyroid hormone by regulating both osteoblasts and osteoclasts. Calcif Tissue Int 89:74–89.
8. Robling AG, P Childress, J Yu, J Cotte, A Heller, BK Philip and JP Bidwell. (2009). Nmp4/CIZ suppresses parathyroid hormone-induced increases in trabecular bone. J Cell Physiol 219:734–743.
9. Satija NK, GU Gurudutta, S Sharma, F Afrin, P Gupta, YK Verma, VK Singh and RP Tripathi. (2007). Mesenchymal stem cells: molecular targets for tissue engineering. Stem Cells Dev 16:7–23.
10. Qin L, J Tamasi, L Raggatt, X Li, JH Feyen, DC Lee, E Dicicco-Bloom and NC Partridge. (2005). Amphiregulin is a novel growth factor involved in normal bone development and in the cellular response to parathyroid hormone stimulation. J Biol Chem 280:3974–3981.
11. Bozec A, L Bakiri, A Hoebertz, R Eferl, AF Schilling, V Komnenovic, H Scheuch, M Priemel, CL Stewart, M Amling, and EF Wagner. (2008). Osteoclast size is controlled by Fra-2 through LIF/LIFreceptorsignalling and hypoxia. Nature 454:221–225.
12. Karreth F, A Hoebertz, H Scheuch, R Eferl and EF Wagner. (2004). The AP1 transcription factor Fra2 is required for efficient cartilage development. Development 131:5717–5725.
13. Qin L, LJ Raggatt, and Partridge. (2004). Parathyroid hormone: a double-edged sword for bone metabolism. Trends Endocrinol Metab 15:60–65.
14. Kular J, J Tickner, SM Chim and J Xu. (2012). An overview of the regulation of bone remodelling at the cellular level. Clin Biochem 45:863–873.
15. Nishida S, A Yamaguchi, T Tanizawa, N Endo, T Mashiba, Y Uchiyama, T Suda, S Yoshiki and HE Takahashi. (1994). Increased bone formation by intermittent parathyroid hormone administration is due to the stimulation of proliferation and differentiation of osteoprogenitor cells in BM. Bone 15:717–723.
16. Yang FC, S Watanabe, K Tsuji, MJ Xu, A Kaneko, Y Ebihara and T Nakahata. (1998). Human granulocyte colony-stimulating factor (G-CSF) stimulates the in vitro and in vivo development but not commitment of primitive multipotential progenitors from transgenic mice expressing the human G-CSF receptor. Blood 92:4632–4640.
17. Niziolek PJ, S Murthy, SN Ellis, KB Sukhija, TA Hornberger, CH Turner and AG Robling. (2009). Rapamycin impairs trabecular bone acquisition from high-dose but not low-dose intermittent parathyroid hormone treatment. J Cell Physiol 221:579–585.
18. Ding M and I Hvid. (2000). Quantification of age-related changes in the structure model type and trabecular thickness of human tibial cancellous bone. Bone 26:291–295.
19. Bedi B, JY Li, H Tawfeek, KH Baek, J Adams, SS Vangara, MK Chang, M Kneissel, MN Weitzmann and R Pacifici. (2012). Silencing of parathyroid hormone (PTH) receptor 1 in

T cells blunts the bone anabolic activity of PTH. Proc Natl Acad Sci U S A 109:E725–E733.
20. Terauchi M, JY Li, B Bedi, KH Baek, H Tawfeek, S Galley, L Gilbert, MS Nanes, M Zayzafoon, et al. (2009). T lymphocytes amplify the anabolic activity of parathyroid hormone through Wnt10b signaling. Cell Metab 10:229–240.
21. Baron R and H Hesse. (2012). Update on bone anabolics in osteoporosis treatment: rationale, current status, and perspectives. J Clin Endocrinol Metab 97:311–325.
22. Allen MR and DB Burr. (2006). Parathyroid hormone and bone biomechanics. Clin Rev Bone Miner Metab 4:259–268.
23. Riggs BL and AM Parfitt. (2005). Drugs used to treat osteoporosis: the critical need for a uniform nomenclature based on their action on bone remodeling. J Bone Miner Res 20:177–184.
24. Morinobu M, T Nakamoto, K Hino, K Tsuji, ZJ Shen, K Nakashima, A Nifuji, H Yamamoto, H Hirai and M Noda. (2005). The nucleocytoplasmic shuttling protein CIZ reduces adult bone mass by inhibiting bone morphogenetic protein-induced bone formation. J Exp Med 201:961–970.
25. Owen M and AJ Friedenstein. (1988). Stromal stem cells: marrow-derived osteogenic precursors. Ciba Found Symp 136:42–60.
26. Méndez-Ferrer S, TV Michurina, F Ferraro, AR Mazloom, BD Macarthur, SA Lira, DT Scadden, A Ma'ayan, GN Enikolopov and PS Frenette. (2010). Mesenchymal and haematopoietic stem cells form a unique bone marrow niche. Nature 466:829–834.
27. Sacchetti B, A Funari, S Michienzi, S Di Cesare, S Piersanti, I Saggio, E Tagliafico, S Ferrari, PG Robey, M Riminucci and P Bianco. (2007). Self-renewing osteoprogenitors in bone marrow sinusoids can organize a hematopoietic microenvironment. Cell 131:324–336.
28. Wang YH, Y Liu and DW Rowe. (2007). Effects of transient PTH on early proliferation, apoptosis, and subsequent differentiation of osteoblast in primary osteoblast cultures. Am J Physiol Endocrinol Metab 292:E594–E603.
29. Onyia JE, B Miller, J Hulman, J Liang, R Galvin, C Frolik, S Chandrasekhar, AK Harvey, J Bidwell, J Herring and JM Hock. (1997). Proliferating cells in the primary spongiosa express osteoblastic phenotype in vitro. Bone 20:93–100.
30. Isogai Y, T Akatsu, T Ishizuya, A Yamaguchi, M Hori, N Takahashi and T Suda. (1996). Parathyroid hormone regulates osteoblast differentiation positively or negatively depending on the differentiation stages. J Bone Miner Res 11:1384–1393.
31. Jilka RL. (2007). Molecular and cellular mechanisms of the anabolic effect of intermittent PTH. Bone 40:1434–1446.
32. Wang YH, Y Liu, K Buhl and DW Rowe. (2005). Comparison of the action of transient and continuous PTH on primary osteoblast cultures expressing differentiation stage-specific GFP. J Bone Miner Res 20:5–14.
33. Alvarez MB, P Childress, BK Philip, R Gerard-O'Riley, M Hanlon, BS Herbert, AG Robling, FM Pavalko and JP Bidwell. (2012). Immortalization and characterization of osteoblast cell lines generated from wild-type and Nmp4-null mouse BM stromal cells using murine telomerase reverse transcriptase (mTERT). J Cell Physiol 227:1873–1882.
34. Yang Z, JP Bidwell, SR Young, R Gerard-O'Riley, H Wang and FM Pavalko. (2010). Nmp4/CIZ inhibits mechanically induced beta-catenin signaling activity in osteoblasts. J Cell Physiol 223:435–441.
35. Shen ZJ, T Nakamoto, K Tsuji, A Nifuji, K Miyazono, T Komori, H Hirai and M Noda. (2002). Negative regulation of bone morphogenetic protein/Smad signaling by Cas-interacting zinc finger protein in osteoblasts. J Biol Chem 277:29840–29846.
36. Mazo IB, M Honczarenko, H Leung, LL Cavanagh, R Bonasio, W Weninger, K Engelke, L Xia, RP McEver, PA Koni, LE Silberstein, UH von Andrian. (2005). BM is a major reservoir and site of recruitment for central memory CD8+ T cells. Immunity 22:259–270.
37. Herndler-Brandstetter D, K Landgraf, B Jenewein, A Tzankov, R Brunauer, S Brunner, W Parson, F Kloss, R Gassner, G Lepperdinger and B Grubeck-Loebenstein. (2011). Human BM hosts polyfunctional memory CD4+ and CD8+ T cells with close contact to IL-15-producing cells. J Immunol 186:6965–6971.
38. Becker TC, SM Coley, EJ Wherry and R Ahmed. (2005). BM is a preferred site for homeostatic proliferation of memory CD8 T cells. J Immunol 174:1269–1273.
39. Hodge JM, MA Kirkland, CJ Aitken, CM Waugh, DE Myers, CM Lopez, BE Adams and GC Nicholson. (2004). Osteoclastic potential of human CFU-GM: biphasic effect of GM-CSF. J Bone Miner Res 19:190–199.
40. Menaa C, N Kurihara and GD Roodman. (2000). CFU-GM-derived cells form osteoclasts at a very high efficiency. Biochem Biophys Res Commun 267:943–946.
41. Thunyakitpisal P, M Alvarez, K Tokunaga, JE Onyia, J Hock, N Ohashi, H Feister, SJ Rhodes and JP Bidwell. (2001). Cloning and functional analysis of a family of nuclear matrix transcription factors (NP/NMP4) that regulate type I collagen expression in osteoblasts. J Bone Miner Res 16:10–23.
42. Krane SM. (2005). Identifying genes that regulate bone remodeling as potential therapeutic targets. J Exp Med 201:841–843.

Address correspondence to:
Dr. Feng-Chun Yang
Department of Pediatrics
Indiana University School of Medicine
R4-427, 1044 West Walnut Street
Indianapolis, IN 46202

E-mail: fyang@iupui.edu

Dr. Joseph P. Bidwell
Department of Anatomy & Cell Biology
Indiana University School of Medicine
Medical Science Building 5035
635 Barnhill Drive
Indianapolis, IN 46202

E-mail: jbidwell@iupui.edu

Received for publication June 11, 2012
Accepted after revision August 5, 2012
Prepublished on Liebert Instant Online XXXX XX, XXXX

Calcif Tissue Int
DOI 10.1007/s00223-011-9496-y

ORIGINAL RESEARCH

Nmp4/CIZ Suppresses the Response of Bone to Anabolic Parathyroid Hormone by Regulating Both Osteoblasts and Osteoclasts

Paul Childress · Binu K. Philip · Alexander G. Robling · Angela Bruzzaniti · Melissa A. Kacena · Nicoletta Bivi · Lilian I. Plotkin · Aaron Heller · Joseph P. Bidwell

Received: 22 November 2010 / Accepted: 27 April 2011

Abstract How parathyroid hormone (PTH) increases bone mass is unclear, but understanding this phenomenon is significant to the improvement of osteoporosis therapy. Nmp4/CIZ is a nucleocytoplasmic shuttling transcriptional repressor that suppresses PTH-induced osteoblast gene expression and hormone-stimulated gains in murine femoral trabecular bone. To further characterize Nmp4/CIZ suppression of hormone-mediated bone growth, we treated 10-week-old *Nmp4*-knockout (KO) and wild-type (WT) mice with intermittent human PTH(1–34) at 30 μg/kg daily or vehicle, 7 days/week, for 2, 3, or 7 weeks. Null mice treated with hormone (7 weeks) gained more vertebral and tibial cancellous bone than WT animals, paralleling the exaggerated response in the femur. Interestingly, Nmp4/CIZ suppression of this hormone-stimulated bone formation was not apparent during the first 2 weeks of treatment. Consistent with the null mice enhanced PTH-stimulated addition of trabecular bone, these animals exhibited an augmented hormone-induced increase in serum osteocalcin 3 weeks into treatment. Unexpectedly, the *Nmp4*-KO mice displayed an osteoclast phenotype. Serum C-terminal telopeptide, a marker for bone resorption, was elevated in the null mice, irrespective of treatment. *Nmp4*-KO bone marrow cultures produced more osteoclasts, which exhibited elevated resorbing activity, compared to WT cultures. The expression of several genes critical to the development of both osteoblasts and osteoclasts was elevated in *Nmp4*-KO mice at 2 weeks, but not 3 weeks, of hormone exposure. We propose that Nmp4/CIZ dampens PTH-induced improvement of trabecular bone throughout the skeleton by transiently suppressing hormone-stimulated increases in the expression of proteins key to the required enhanced activity and number of both osteoblasts and osteoclasts.

Keywords c-fos · Fra-2 · Ephrin · Osteoclastogenesis · Osteocalcin · Osteoporosis

Parathyroid hormone (PTH) therapy is the only osteoporosis treatment that restores bone to the aged skeleton; however, its expense makes it the least cost-effective [1, 2]. The development of shorter PTH-based treatments yielding similar efficacy as the longer-term therapy will improve its cost–benefit ratio [2], but this requires a better understanding of the mechanisms underlying the PTH anabolic response.

The authors have stated that they have no conflict of interest.

P. Childress · B. K. Philip · A. G. Robling · M. A. Kacena · N. Bivi · L. I. Plotkin · A. Heller · J. P. Bidwell (✉)
Department of Anatomy and Cell Biology, Indiana University School of Medicine (IUSM), Medical Science Bldg. 5035, 635 Barnhill Drive, Indianapolis, IN 46202, USA
e-mail: jbidwell@iupui.edu

A. G. Robling · M. A. Kacena
Department of Biomedical Engineering, Indiana University-Purdue University at Indianapolis, Indianapolis, IN 46202, USA

A. Bruzzaniti
Department of Oral Biology, Indiana University School of Dentistry, Indianapolis, IN, USA

M. A. Kacena
Department of Orthopaedic Surgery, Indiana University School of Medicine, Indianapolis, IN, USA

Present Address:
B. K. Philip
Bristol-Myers Squibb, Mt. Vernon, IN 47620, USA

Present Address:
A. Heller
Kansas City University of Medicine and Biosciences, Kansas City, MO 64106-1453, USA

Published online: 24 May 2011

Data on the self-limiting pathways to PTH action, inherent to all endocrine response loops, are lacking; and it is these molecules that may provide the best pharmaceutical targets for improving hormone efficacy and cost-effectiveness [3]. For example, as PTH activates the osteoblast generation of cAMP and the enhanced expression of RUNX2, it simultaneously stimulates phosphodiesterase activity [4] and Smurf1-mediated RUNX2 proteasomal degradation [5].

We recently demonstrated that disabling the nucleocytoplasmic shuttling transcription factor Nmp4/CIZ (nuclear matrix protein 4/cas interacting zinc finger protein) in mice enhances the skeletal response to anabolic PTH [6], suggestive of a significant role in the hormone's self-limiting pathways. Ten-week-old *Nmp4*-knockout (KO) mice treated with intermittent PTH for 7 weeks exhibited an augmented increase in femoral trabecular bone compared to wild-type (WT) mice without compromising the hormone-stimulated increases in bone mineral density (BMD) and content throughout the skeleton [6].

The ubiquitously expressed Nmp4/CIZ appears to act as a general repressor of anabolic bone growth, in part, by suppressing the transcription of genes that support the development of the osteoblast phenotype, including the pro-alpha1(I) chain (*Col1a1*) and the *Mmp-13* promoters [3, 7, 8]. This *trans*-acting protein suppressed the PTH induction of rat *Mmp-13* transcription in UMR-106-01 osteoblast-like cells via its binding to a PTH-responsive element in the 5′ regulatory region of the gene [8], but whether Nmp4 represses the hormone responsiveness of other tissues has not been reported.

In the present study we determined that Nmp4/CIZ suppressed the PTH-stimulated improvement of trabecular bone throughout the mouse skeleton and was not site-specific, as is common in other mouse models [9, 10]. Most surprisingly, we discovered that the null mice have an osteoclast phenotype. Analysis of serum biochemistry, bone histomorphometry, bone mRNA expression profiles, and osteoclast cell culture suggested that the numbers and activities of both osteoblasts and osteoclasts are enhanced in *Nmp4*-KO mice due, in part, to a transient derepression of key transcription factors and signaling proteins common to pathways critical for the development and hormone responsiveness of both cell types.

Materials and Methods

Mice

Construction of the *Nmp4*-KO mouse, its backcrossing six generations onto a C57BL/6J background, and the baseline phenotype have been described [6]. As in our previous study, WT C57BL/6J mice from Jackson Laboratories (Bar Harbor, ME) were used as controls [6]. Experiments designed to compare the response of WT and *Nmp4*-KO mice to PTH compensated for any differences in genetic and environmental factors (see Statistical Analyses). Our local Institutional Animal Care and Use Committee approved all experiments and procedures involving the production and use of the experimental mice described in this study.

PTH Treatment Regimen

Prior to the start of an experiment, 8-week-old female WT and *Nmp4*-KO mice were given 100 µl sterile saline by subcutaneous (sc) injection once daily to acclimatize them to handling. At 10 weeks of age, mice were sorted into four groups based on equivalent mean group body weight. The four treatment groups were (1) vehicle-treated WT, (2) PTH-treated WT, (3) vehicle-treated *Nmp4*-KO, and (4) PTH-treated *Nmp4*-KO. Mice were injected sc with human PTH(1–34) (Bachem Bioscience, Torrance, CA) at 30 µg/kg daily or vehicle control (0.2% BSA/0.1% 1.0 mN HCl in saline; Abbott Laboratory, North Chicago, IL) for the times specified (see Results). Additionally, animals were administered intraperitoneal injections of calcein green (20 mg/kg; Sigma-Aldrich, St. Louis, MO) and alizarin red (25 mg/kg, Sigma-Aldrich) 6 and 3 days before being killed, respectively.

Dual-Energy X-Ray Absorptiometry

Bone mineral content (BMC, g), areal bone mineral density (aBMD, mg/cm^2), and body weight were measured weekly (8–12 weeks of age). BMC and aBMD were obtained for the postcranial skeleton by dual-energy X-ray absorptiometry (DEXA) using an X-ray PIXImus mouse densitometer (PIXImus II; GE-Lunar, Madison, WI) as previously described [6]. We report whole-body (WB), femur, tibia, and spine BMD and BMC.

Micro-Computed Tomography

Vertebrae, femora, and tibiae were dissected from WT and *Nmp4*-KO animals after death; the connective tissue and muscle were removed; and the bones were stored in 10% buffered formalin at 4°C. After 48 h, the bones were transferred to 70% ethanol and stored at 4°C until analyzed. We previously described our methodology for assessing the trabecular microarchitecture at the distal femoral metaphysis and within the fifth lumbar vertebra using a desktop micro-computed tomographer (µCT 20; Scanco Medical, Bassersdorf, Switzerland) [6, 9]. Cancellous bone of the tibia was evaluated by scanning the

proximal 20% of each tibia at 9 μm resolution. A microfocus X-ray tube with a focal spot of 10 μm was used as a source. Precisely 90 μCT slices were acquired per bone beginning 1 mm from the epiphysis and extending distally 1.53 mm using a slice increment of 17 μm. For each slice, 600 projections were taken over 216° (180° plus half of the fan angle on either side). Proximal tibia stacks were reconstructed to the third dimension using a standard convolution–backprojection procedure with a Shepp-Logan filter using a threshold value of 275. The Scanco software permitted evaluation of tibial, femoral, and vertebral trabecular bone volume per total volume (BV/TV), connectivity density (Conn.D, mm^{-3}), structure model index (SMI), trabecular number (Tb.N, mm^{-1}), trabecular thickness (Tb.Th, mm), and trabecular spacing (Tb.Sp, mm) from the 3D constructs. To evaluate cortical architecture, a single slice was taken through the midshaft femur (simply by measuring the number of slices for the whole femur and dividing by 2), and the cortical area (CA, mm^2), marrow area (MA, mm^2), and total area (TA, mm^2) were calculated [6]. Additionally, the moment of inertia (the resistance of the bone to a bending load) was derived from these data. These parameters included the largest (I_{MAX}, mm^4) and smallest (I_{MIN}, mm^4) flexural rigidity as well as the polar moment of inertia (J, mm^4), which is the torsional and bending rigidity around the neutral axis of the bone and perpendicular to the *x* and *y* axes passing through the center of mass [11].

Quantitative Real-Time PCR Analysis

Femoral or tibial RNA from mice that had been treated with intermittent PTH or vehicle for 2 or 3 weeks was harvested either 1 or 24 h after the last injection. The harvesting, processing, and analysis protocols for quantitative real-time PCR analysis have been described [6, 9]. Real-time PCR primers and probes were obtained from Assays-on-Demand™ (Applied Biosystems, Foster City CA; see Table 1). The ΔΔCT method was used to evaluate gene expression between WT and KO animals using *Rplp2* as the normalizer after screening several housekeeping gene candidates. The coefficient of variation of *Rplp2* was

Table 1 Real-Time PCR Primers from Assays-on-Demand™

Gene (mRNA)	ABI Assay ID
Alpl (alkaline phosphatase)	Mm01187117_m1
Bcl2 (B-cell lymphoma 2)	Mm00477631_m1
Bmp2 (bone morphogenic protein 2)	Mm01340178_m1
c-fms (colony stimulating factor 1 receptor [CSF1R])	Mm01266652_m1
c-fos (FBJ murine osteosarcoma viral oncogene homolog)	Mm00487425_m1
Col1a1 (type I; pro-alpha1(I) chain)	Mm00801666_g1
EphB4 (ephrin type-B receptor 4)	Mm01201157_m1
EphrinB2 (EPH-related receptor tyrosine kinase ligand 5)	Mm00438670_m1
Fra-2 (fos-related antigen 2)	Mm00484442_m1
Igf-1 (insulin-like growth factor 1)	Mm0043559_m1
JunD (Jun proto-oncogene related gene d)	Mm00495088_s1
Lef1 (lymphoid enhancer-binding factor-1)	Mm00550265_m1
M-csf (macrophage colony stimulating factor 1)	Mm00432686_m1
Mcp-1 (monocyte chemotactic protein-1)	Mm00441242_m1
Mkp-1 (MAPK phosphatase 1)	Mm00457274_g1
Mmp-13 (matrix metalloproteinase 13)	Mm00439491_m1
Nfatc1 (nuclear factor of activated T-cells, cytoplasmic, calcineurin-dependent 1)	Mm012479445_m1
Nurr-1 (nuclear receptor-related factor 1)	Mm00443056_m1
Opg (osteoprotegerin)	Mm00435452_m1
Osterix (Sp7 transcription factor)	Mm00504574_m1
Pthr1 (parathyroid hormone receptor 1)	Mm00441046_m1
Pthrp (parathyroid hormone-related peptide)	Mm00436057_m1
Rage (Ager) (receptor for advanced glycation endproducts)	Mm00545815_m1
Rankl (receptor activator for nuclear factor κ B ligand)	Mm00441908_m1
Runx2 (runt-related transcription factor 2)	Mm00501578_m1
Smad3 (Sma- and Mad-related protein)	Mm01170760_m1
Sost (sclerostin)	Mm00470479_m1

typically 2–3% between all samples. Normalization against internal control genes is most frequently used because it can control all variables including cell number [12, 13]. The data represent the mean ± standard deviation from at least six mice per genotype.

Bone Histomorphometry

Femora were removed from WT and *Nmp4*-KO animals after death and fixed as described above. The anterior face of the epiphyseal plate was cut to expose the marrow cavity. Samples were then dehydrated with graded alcohols, embedded in methyl-methacrylate, sectioned (4 μm) with a microtome (RM2255; Leica Microsystems, Wetzlar, Germany), and mounted on standard microscope slides. All histomorphometric parameters were obtained following ASBMR guidelines [14]. Mineral apposition rate (MAR), mineralizing surface (MS/BS), and bone formation rate (BFR) were obtained from a 0.03-mm^2 metaphyseal region of interest 250–1,750 μm below the growth plate using ImagePro 3.1 software (Media Cybernetics, Bethesda, MD). Some sections were stained for tartrate-resistant acid phosphatase (TRAP). The number of $TRAP^+$ cells on the bone surface ($Trap^+$ N/BS) and the TRAP-stained surface to bone surface ($Trap^+$ S/BS) were determined.

Serum Biochemistry

Intact serum osteocalcin was measured using the sandwich ELISA BTI Mouse Osteocalcin EIA Kit (Biomedical Technologies, Stoughton MA) [15]. Serum C-terminal telopeptides (CTX) were determined using the RatLaps™ ELISA (Immunodiagnostic Systems, Scottsdale, AZ) [15].

Osteoclast Culture and Activity

To compare the number of osteoclasts derived from *Nmp4*-KO and WT mice, bone marrow was flushed from the long bones of animals 6–8 weeks old. Cells were seeded into 24-well culture dishes at an initial density of 2.1×10^5/mm^2 and cultured in alpha-MEM (Invitrogen, Carlsbad, CA) supplemented with 10% FBS (Hyclone, Logan, UT) and 20 ng/ml of recombinant human M-CSF (Peprotech, Rocky Hill, NJ) for 2 days and then supplemented with 20 ng/ml of recombinant human M-CSF and 80 ng/ml of recombinant human RANKL (Peprotech) for the duration of the experiment. The cell culture medium was changed every third day until osteoclasts were visible. Once osteoclasts had formed, the cells were fixed with 2.5% glutaraldehyde in phosphate-buffered saline for 30 min at room temperature and stained for TRAP (Sigma-Aldrich) and $TRAP^+$, multinucleated (≥3) cells were counted.

The osteoclast resorption activity of cells derived from KO and WT mice was evaluated using a standard pit assay [16]. Bone marrow was isolated as above and plated into six-well culture dishes at 2×10^6 cells/well (2.1×10^5 cells/mm^2). As detailed above, cells were incubated in alpha-MEM containing 10% FBS and 20 ng/ml M-CSF for 2 days. The medium was removed and replaced with fresh medium containing 20 ng/ml M-CSF and 80 ng/ml RANKL for an additional 2–3 days. Mature osteoclasts were detached by trypsinization, washed once, replated onto dentin slices (Immunodiagnostic Systems), and cultured for an additional 48 h in medium containing 20 ng/ml M-CSF and 80 ng/ml RANKL. Dentin slices were washed, incubated in 6% NaOCl for 5 min, and sonicated for 20 s to remove cells. Resorption pits were stained with a solution containing 1% toluidine blue and 1% sodium borate for 1 min, washed with water, and air-dried. Pit surface area was quantified using ImagePro 7.0 on a Leica DMI4000 with a 10× objective. Results were normalized for osteoclast number, as determined by counting $TRAP^+$ cells containing three or more nuclei. Experiments were performed in triplicate, and results represent average pit area per dentin slice/osteoclast number.

Statistical Analyses

Statistical analysis was processed using JMP version 7.0.1 (SAS Institute, Cary, NC). Experiments designed to compare the response of WT and *Nmp4*-KO mice to PTH compensated for any differences in genetic and environmental factors; i.e., the fact that WT mice were not bred in-house was accounted for by our analyses. For example, raw BMD and BMC data were converted to percent change (8–12 weeks of age). Comparing hormone-treated to vehicle-treated within each genotype for all end-point analyses removed baseline differences from those factors and permitted analysis for genotype × treatment interactions, i.e., whether WT and *Nmp4*-KO mice responded differently to hormone for the parameter under consideration. We employed a two-factor ANOVA for these analyses. If a genotype × treatment interaction was indicated, the data were analyzed by a Tukey HSD post hoc test to determine significant differences between the experimental groups. For the serum analysis experiment we used a repeated-measures multivariate analysis of variance (MANOVA) to evaluate the raw longitudinal serum osteoclast and CTX levels over the 7-week hormone treatment period. Additionally, we converted the serum data to percent change and analyzed with the two-factor ANOVA. The genotype × time term for the raw longitudinal serum data is equivalent to the genotype term for the percent change data; i.e., both terms indicate a difference in the rate of either osteocalcin/CTX increase or bone accrual (for the

BMD/BMC study) between WT and null mice. For some experiments, unpaired *t*-tests were employed as indicated. Data are presented as mean ± SD unless otherwise indicated. Statistical significance was taken at $P < 0.05$.

Results

Nmp4-KO Mice Exhibited Enhanced PTH-Induced Acquisition of Trabecular Bone Throughout the Skeleton Compared to WT Mice After 7 Weeks, but not 2 Weeks, of Treatment

We previously showed that *Nmp4*-KO mice exhibited a significantly exaggerated PTH-stimulated increase in femoral trabecular bone compared to WT mice after 7 weeks of hormone challenge [6]; here, we addressed whether Nmp4/CIZ represses PTH-induced improvement in other parts of the skeleton and if this suppression is evident from the start of the treatment regimen. Animals were treated with intermittent hPTH(1–34) 30 μg/kg daily or vehicle for 7 weeks from 10 weeks of age. Mice were sorted in the four treatment groups, and the cancellous architecture was characterized as described in "Materials and Methods" section. The *Nmp4*-KO L5 vertebra BV/TV exhibited a more robust increase in response to 7 weeks of PTH than the WT BV/TV as demonstrated by a strong treatment effect and significant genotype × treatment interaction (Fig. 1a). The PTH-induced change in vertebral morphology from a rod-like to a plate-like form was more pronounced in the null mice (SMI, Fig. 1c). Vertebral Tb.Th was significantly enhanced in response to 7 weeks of hormone in null mice but not in WT animals (Fig. 1e), whereas PTH had an equivalent impact on Tb.Sp (Fig. 1f), a consequence of the fact that these parameters do not have a simple reciprocal relationship [14]. PTH had an equivalent impact on Conn.D (Fig. 1b) in the genotypes. Finally, there was a strong genotype effect for all the measured vertebral parameters, consistent with the more robust trabecular architecture in the null mice (Fig. 1a–f). Typical μCT scans of L5 vertebra from mice treated with intermittent hormone or vehicle for 7 weeks are shown in Fig. 1g.

To evaluate the early hormone response of the L5 vertebra, we compared bones from WT and *Nmp4*-KO mice that had been treated with PTH or vehicle for 2 weeks. The L5 vertebra trabecular bone showed no improvement after 2 weeks of hormone in either WT or null animals (Fig. 1a–f). However, there was a genotype effect for BV/TV, Conn.D, SMI, and Tb.Th (Fig. 1a–c, e, respectively); thus, the enhanced vertebral trabecular architecture observed in the 17-week-old null mice irrespective of treatment was apparent in these mice at 12 weeks of age.

Nmp4/CIZ also repressed the hormone-induced increase in tibial cancellous bone (Fig. 2). The PTH-stimulated increase in tibial BV/TV after 7 weeks of hormone was greater in null than WT mice (Fig. 2a). PTH increased tibial Tb.N in both genotypes but significantly more so in null mice (Fig. 2d), and the hormone-stimulated change in tibial SMI was more pronounced in null mice (Fig. 2c). PTH had a comparable positive effect on Conn.D (Fig. 2b), Tb.Th (Fig. 2e), and Tb.Sp (Fig. 2f) in WT and null mice with 7 weeks of treatment. Typical μCT scans of tibiae from mice treated with hormone or vehicle for 7 weeks are shown in Fig. 2g.

To evaluate the early hormone response of the tibia, we compared bones from WT and *Nmp4*-KO mice that had been treated with PTH or vehicle for 2 weeks. Both genotypes showed equal hormone-induced improvement of tibial BV/TV, Conn.D, SMI, and Tb.Th during the initial 2 weeks of treatment (Fig. 2a–c, e). PTH failed to improve Tb.N and Tb.Sp in both WT and null mice during this period of the regimen; however, there was a genotype effect for these two parameters, indicating enhanced aspects of tibial architecture in the null mice at 12 weeks of age (Fig. 2d, f).

Disabling Nmp4 had no impact on any aspect of the skeletal response to PTH (no genotype × treatment interaction) during the first 2 weeks of treatment including femoral cancellous architecture (Table 2), midshaft cortical architecture (Table 3), and the percent change in skeletal BMD and BMC (Table 4). Consistent with Nmp4's repressive action on bone growth [6], genotype effects were observed for some of these parameters indicative of the modestly enhanced skeletal phenotype of the null animals. Interestingly, the genotype effects for WB BMC and femoral and tibial BMD and BMC (Table 4) indicated that the rate of bone accrual was lower in null mice over the 4-week period of measurement irrespective of treatment.

Enhanced PTH-Stimulated Increase in Femoral Trabecular Bone Observed in *Nmp4*-KO Mice Occurred After 2 Weeks and Before 7 Weeks of Hormone Exposure

Histological sections of the femoral spongiosa prepared for histomorphometry (Fig. 3a) confirmed our previous analysis using μCT [6] that *Nmp4*-KO mice added more cancellous bone in response to 7 weeks of hormone treatment than WT mice. However, BFR parameters were not different between the null and WT mice at the end of treatment and, in fact, were declining, suggesting that the PTH response was beginning to plateau in both genotypes. MS/BS (the proportion of bone surface undergoing mineralization) was significantly decreased in both genotype treatment groups, consistent with the declining PTH

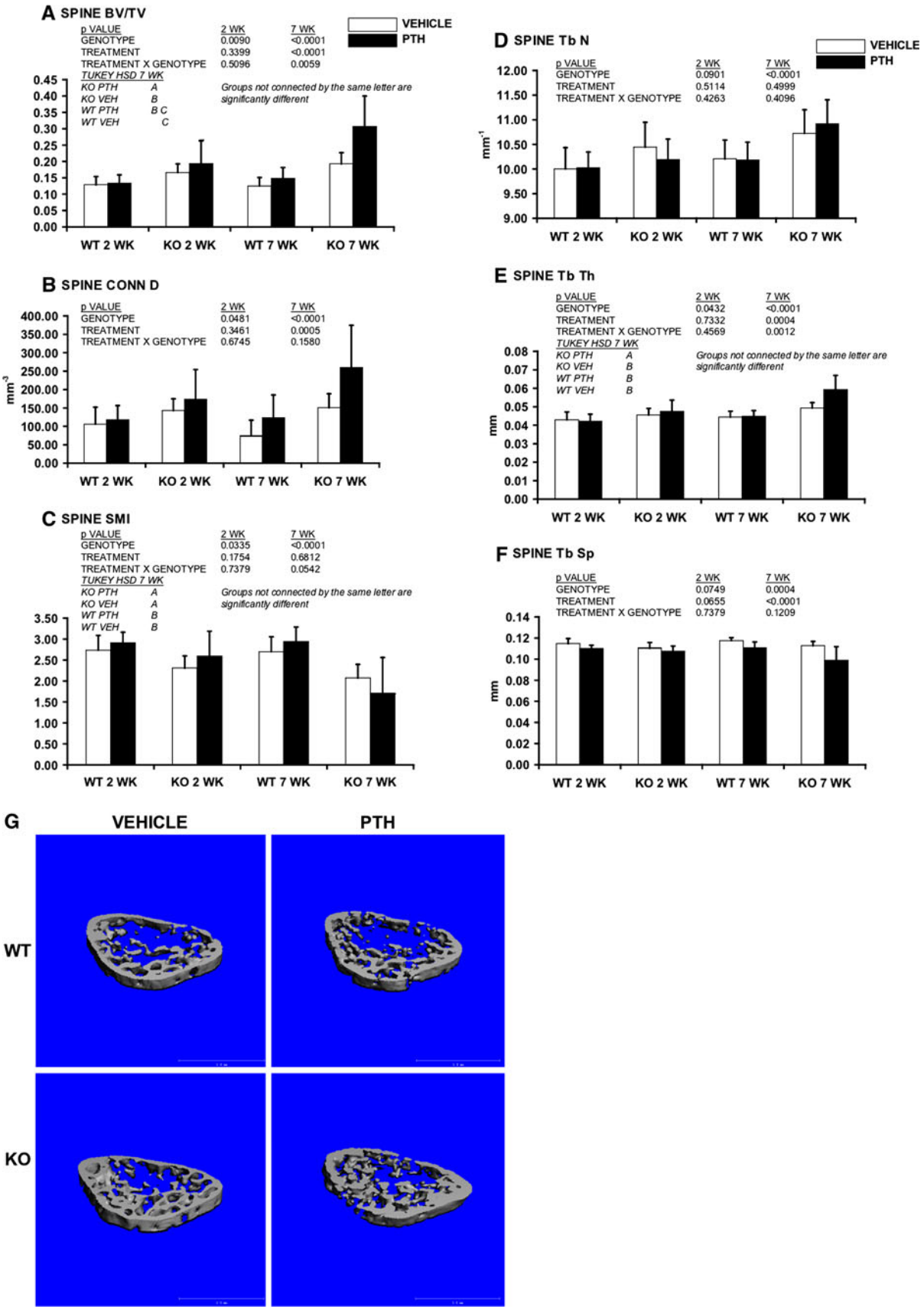
A SPINE BV/TV
p VALUE 2 WK 7 WK
GENOTYPE 0.0090 <0.0001
TREATMENT 0.3399 <0.0001
TREATMENT X GENOTYPE 0.5096 0.0059
TUKEY HSD 7 WK
KO PTH A
KO VEH B
WT PTH B C
WT VEH C
Groups not connected by the same letter are significantly different
VEHICLE
PTH
WT 2 WK
KO 2 WK
WT 7 WK
KO 7 WK
B SPINE CONN D
p VALUE 2 WK 7 WK
GENOTYPE 0.0481 <0.0001
TREATMENT 0.3461 0.0005
TREATMENT X GENOTYPE 0.6745 0.1580
mm-3
C SPINE SMI
p VALUE 2 WK 7 WK
GENOTYPE 0.0335 <0.0001
TREATMENT 0.1754 0.6812
TREATMENT X GENOTYPE 0.7379 0.0542
TUKEY HSD 7 WK
KO PTH A
KO VEH A
WT PTH B
WT VEH B
Groups not connected by the same letter are significantly different
D SPINE Tb N
p VALUE 2 WK 7 WK
GENOTYPE 0.0901 <0.0001
TREATMENT 0.5114 0.4999
TREATMENT X GENOTYPE 0.4263 0.4096
mm-1
E SPINE Tb Th
p VALUE 2 WK 7 WK
GENOTYPE 0.0432 <0.0001
TREATMENT 0.7332 0.0004
TREATMENT X GENOTYPE 0.4569 0.0012
TUKEY HSD 7 WK
KO PTH A
KO VEH B
WT PTH B
WT VEH B
Groups not connected by the same letter are significantly different
mm
F SPINE Tb Sp
p VALUE 2 WK 7 WK
GENOTYPE 0.0749 0.0004
TREATMENT 0.0655 <0.0001
TREATMENT X GENOTYPE 0.7379 0.1209
mm
G
VEHICLE
PTH
WT
KO

◀ **Fig. 1** Disabling Nmp4 enhanced PTH responsiveness of vertebral cancellous bone. μCT-acquired vertebral (L5) trabecular architecture including **a** BV/TV, **b** Conn.D (mm^{-3}), **c** SMI, **d** Tb.N (mm^{-1}), **e** Tb.Th (mm), and **f** Tb.Sp (mm) was compared between WT and *Nmp4*-KO mice that had been treated with intermittent hPTH(1–34) 30 μg/kg daily or vehicle for 7 weeks (number of mice/experimental group = 11–12). To evaluate the early hormone response, we compared bones from WT and *Nmp4*-KO mice that had been treated with intermittent PTH or vehicle for 2 weeks using the same experimental design (number of mice/experimental group = 5–7). No improvement was observed after 2 weeks of intermittent PTH treatment in either WT or null animals (**a**–**f**). There was a genotype effect for BV/TV, Conn.D, SMI, and Tb.Th (**a**–**c** and **e**, respectively) consistent with the enhanced trabecular architecture of the null mice, regardless of treatment. **g** μCT images of vertebral trabecular bone from WT and *Nmp4*-KO mice that had been treated with intermittent PTH or vehicle for 7 weeks. *Scale bar* 1 mm. Data presented as average ± SD. *P* values were determined with a two-factor ANOVA. Tukey's HSD post hoc test was used to determine differences between the treatment groups if a significant genotype × treatment interaction was indicated

responsiveness (Table 5). Additionally, we did not observe a significant hormone-induced increase in BFR in either of the genotypes at this point in treatment (Table 5). Nevertheless, PTH equally enhanced MAR in both genotypes at this time point (Table 5).

Our histomorphometric analysis of mice treated with PTH or vehicle for 7 weeks included the parameters of $TRAP^+$ S/BS and $TRAP^+$ *n*/BS, which provide an estimate of the size and number of osteoclast precursors and mature osteoclasts normalized to the bone surface. Clearly, anabolic hormone treatment enhanced the absolute number of osteoclasts and the total osteoclast surface over bone in both genotypes as evident from the histological sections (Fig. 3b); normalizing these parameters to the bone surface revealed that, although both parameters are elevated in null mice, the differences are not statistically significant (Table 5). However, there were strong treatment effects; i.e., PTH significantly attenuated the percent bone surface covered by $TRAP^+$ cells and their number/surface (Table 5). Interestingly, there was a genotype × treatment interaction for $TRAP^+$ S/BS, indicating that hormone had a larger impact on the reduction of bone surface covered by osteoclasts in null mice than in WT animals (Table 5).

Nmp4-KO Mice Exhibited Strikingly Different Serum Osteocalcin and CTX Profiles Compared to WT Animals

Whole blood was collected and the serum separated from the mice of the four treatment groups at 10 weeks of age (before initiation of treatment), 13 weeks of age (3 weeks of PTH/vehicle treatment), and 17 weeks of age (7 weeks of PTH/vehicle treatment). The raw longitudinal data and the percent change data for osteocalcin, a standard marker for bone formation and osteoblast number, revealed that null and WT mice had equivalent serum levels just prior to hormone treatment but that the *Nmp4*-KO mice exhibited a higher rate of increase over the hormone treatment period (genotype × time interaction, longitudinal data; genotype interaction, percent change data) and an enhanced response to hormone (genotype × treatment interaction, Fig. 4a, b). Specifically, null mice showed an enhanced and sustained increase in osteocalcin after 3 weeks of treatment, while WT animals showed a peak at 3 weeks of treatment, followed by a decline by 7 weeks of treatment (Fig. 4a, b).

CTX, a marker for bone resorption, was significantly elevated in *Nmp4*-KO mice compared to WT animals before and during the hormone treatment period. CTX was elevated with PTH treatment in both genotypes, but this increase was not statistically significant (Fig. 4c, d).

Bone Marrow from *Nmp4*-KO Mice Yields More Osteoclasts than Marrow from WT Mice and the Null Osteoclasts Exhibit Enhanced Resorbing Activity

To confirm our serum data indicating increased activity of osteoclasts in *Nmp4*-KO mice, we compared the number of these cells derived from bone marrow cultures of untreated null and WT animals at 7–8 weeks of age. Bone marrow preparations from three null mice and four WT mice were cultured in six-well plates and treated with M-CSF and RANKL as described in "Materials and Methods" section. On average, the *Nmp4*-KO bone marrow cultures produced twofold more osteoclasts than the WT marrow (null = 1,608 ± 87 osteoclasts/well, WT = 877 ± 243 osteoclasts/well; $P < 0.05$, data presented as average ± SD). This experiment was performed twice, yielding similar results.

Next, we compared the dentin-resorbing activities of *Nmp4*-KO and WT osteoclasts. Mature osteoclasts were obtained from the bone marrow of WT and null mice ($n = 2$–3 mice per group) as described in "Materials and Methods" section. Fully differentiated bone marrow-derived osteoclasts were replated on dentin slices for 48 h. The area resorbed was quantified and normalized for $TRAP^+$ osteoclasts. *Nmp4*-KO osteoclasts exhibited a 50% increase in the area resorbed on dentin compared to WT osteoclasts (null = 154 ± 4.6% area resorbed/$Trap^+$ cells, WT = 100 ± 13.3% area resorbed/$Trap^+$ cells; $P < 0.05$, data presented as average ± SD).

Nmp4-KO Mice Exhibit a Transiently Enhanced Basal or PTH-Stimulated Expression of Genes Common to Osteoblast and Osteoclast Development

To follow up on our observation that both osteoblast and osteoclast numbers were enhanced in null mice, we analyzed femoral RNA harvested during the early phase of PTH treatment to evaluate the expression of genes that

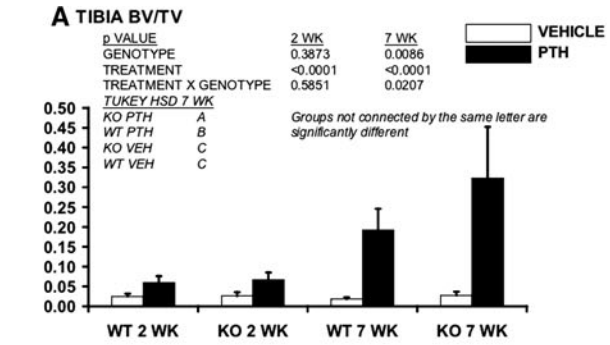
A TIBIA BV/TV
p VALUE 2 WK 7 WK
GENOTYPE 0.3873 0.0086
TREATMENT <0.0001 <0.0001
TREATMENT X GENOTYPE 0.5851 0.0207
TUKEY HSD 7 WK
KO PTH A
WT PTH B
KO VEH C
WT VEH C
Groups not connected by the same letter are significantly different
VEHICLE
PTH
0.50 0.45 0.40 0.35 0.30 0.25 0.20 0.15 0.10 0.05 0.00
WT 2 WK KO 2 WK WT 7 WK KO 7 WK

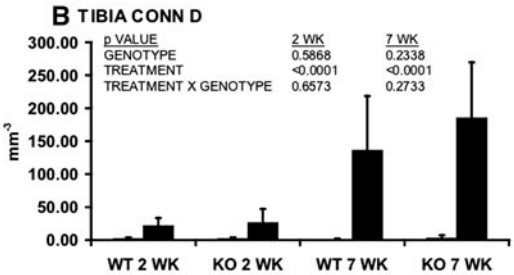
B TIBIA CONN D
p VALUE 2 WK 7 WK
GENOTYPE 0.5868 0.2338
TREATMENT <0.0001 <0.0001
TREATMENT X GENOTYPE 0.6573 0.2733
mm-3
300.00 250.00 200.00 150.00 100.00 50.00 0.00
WT 2 WK KO 2 WK WT 7 WK KO 7 WK

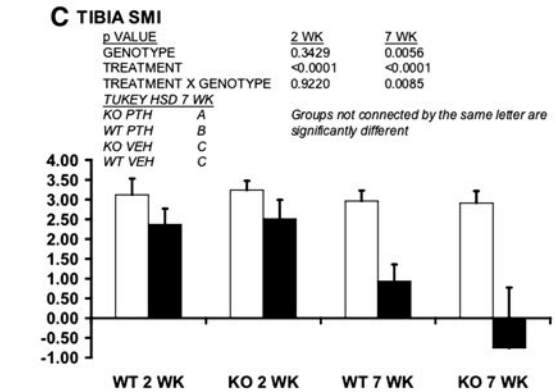
C TIBIA SMI
p VALUE 2 WK 7 WK
GENOTYPE 0.3429 0.0056
TREATMENT <0.0001 <0.0001
TREATMENT X GENOTYPE 0.9220 0.0085
TUKEY HSD 7 WK
KO PTH A
WT PTH B
KO VEH C
WT VEH C
Groups not connected by the same letter are significantly different
4.00 3.50 3.00 2.50 2.00 1.50 1.00 0.50 0.00 -0.50 -1.00
WT 2 WK KO 2 WK WT 7 WK KO 7 WK

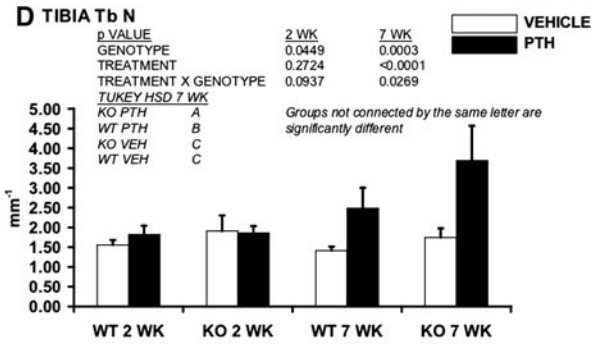
D TIBIA Tb N
p VALUE 2 WK 7 WK
GENOTYPE 0.0449 0.0003
TREATMENT 0.2724 <0.0001
TREATMENT X GENOTYPE 0.0937 0.0269
TUKEY HSD 7 WK
KO PTH A
WT PTH B
KO VEH C
WT VEH C
Groups not connected by the same letter are significantly different
VEHICLE
PTH
mm-1
5.00 4.50 4.00 3.50 3.00 2.50 2.00 1.50 1.00 0.50 0.00
WT 2 WK KO 2 WK WT 7 WK KO 7 WK

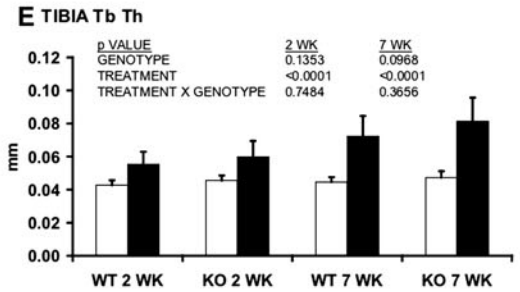
E TIBIA Tb Th
p VALUE 2 WK 7 WK
GENOTYPE 0.1353 0.0968
TREATMENT <0.0001 <0.0001
TREATMENT X GENOTYPE 0.7484 0.3656
mm
0.12 0.10 0.08 0.06 0.04 0.02 0.00
WT 2 WK KO 2 WK WT 7 WK KO 7 WK

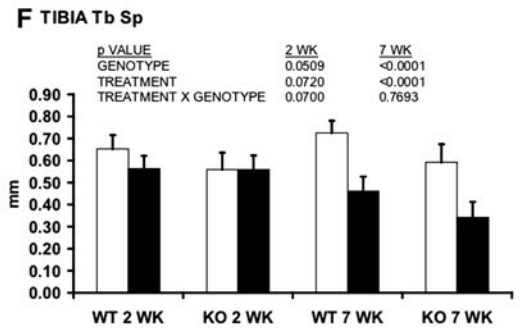
F TIBIA Tb Sp
p VALUE 2 WK 7 WK
GENOTYPE 0.0509 <0.0001
TREATMENT 0.0720 <0.0001
TREATMENT X GENOTYPE 0.0700 0.7693
mm
0.90 0.80 0.70 0.60 0.50 0.40 0.30 0.20 0.10 0.00
WT 2 WK KO 2 WK WT 7 WK KO 7 WK

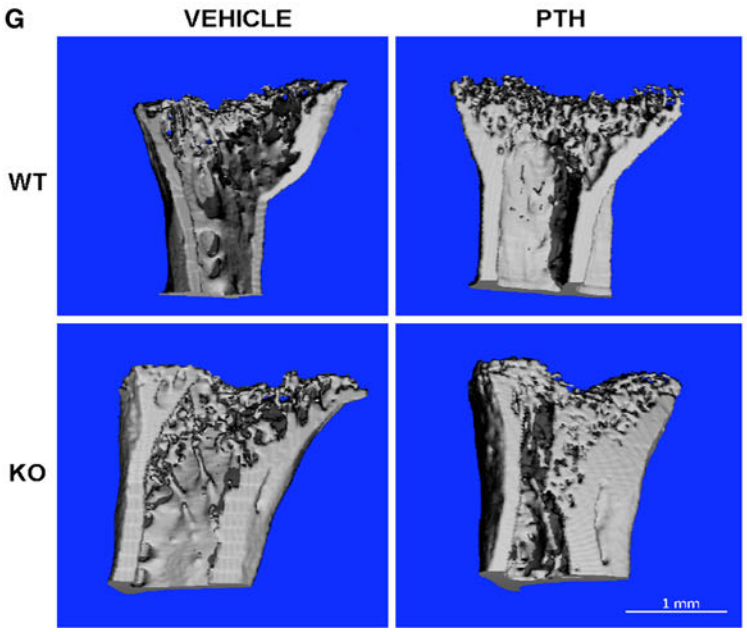
G
VEHICLE
PTH
WT
KO
1 mm

◀ **Fig. 2** *Nmp4*-KO mice exhibited an enhanced PTH-induced increase in tibial trabecular bone. μCT-acquired tibial trabecular architecture including **a** BV/TV, **b** Conn.D (mm^{-3}), **c** SMI, **d** Tb.N (mm^{-1}), **e** Tb.Th (mm), and **f** Tb.Sp (mm) was compared between WT and *Nmp4*-KO mice that had been treated with intermittent PTH or vehicle for 7 weeks (number of mice/experimental group = 8). To evaluate the early hormone response, we compared bones from WT and *Nmp4*-KO mice that had been treated with intermittent PTH or vehicle for 2 weeks (number of mice/experimental group = 7–9). Both genotypes showed equal hormone-induced improvement of tibial **a** BV/TV, **b** Conn.D, **c** SMI, and **e** Tb.Th during the initial 2 weeks of treatment. There was a genotype effect for **d** Tb.N and **f** Tb.Sp, indicating enhanced aspects of tibial architecture in null mice at 12 weeks of age irrespective of treatment. **g** μCT images of tibial trabecular bone from WT and *Nmp4*-KO mice that had been treated with intermittent PTH or vehicle for 7 weeks. *Scale bar* 1 mm. *P* values were determined with a two-factor ANOVA. Tukey's HSD post hoc test was used to determine differences between the treatment groups if a significant genotype × treatment interaction was indicated

support the development of both cells. Animals were treated with intermittent PTH or vehicle for 2 or 3 weeks and RNA was harvested 1 h after the last injection. The AP-1 transcription factors *c-fos* and *Fra-2* exhibited a significantly enhanced PTH-stimulated increase in *Nmp4*-KO mice (genotype × treatment interaction) after 2 weeks of treatment, but these differences were absent after 3 weeks of PTH (Table 6). Additionally, the transcription factor *Nfatc1* was significantly elevated in the femur of null mice (genotype effect) at the 2-week time point but equivalent to the WT expression at 3 weeks of treatment (Table 6). We also examined the expression of several genes that mediate osteoblast–osteoclast signaling. Interestingly, the *Nmp4*-KO mice showed a significant increase in the expression of *EphB4*, the receptor for *EphrinB2*, its transmembrane ligand, which also showed an elevation in expression that approached significance; but again, these differences between the genotypes disappeared at the 3-week time point (Table 6). Both EphB4 and EphrinB2 were responsive to PTH in the null and WT mice (Table 6). Interestingly, the *Rankl/Opg* ratio was diminished in the null mice compared to WT animals at 2 and 3 weeks of treatment, which was significant at the later time point (Table 6).

Further comparative analysis of femoral gene expression profiles between WT and null mice at the 2-week time period failed to show any significant differences between the two genotypes with one exception (Table 7). The expression of the prosurvival gene *Bcl2* was not different in WT and null mice and did not respond to hormone in either genotype at this point in the treatment regimen; however,

Table 2 PTH-induced improvements in femoral trabecular architecture were equivalent in WT and *Nmp4*-KO mice after the first 2 weeks of treatment

	WT		KO		2-Way ANOVA *P*-values		
	VEH	PTH	VEH	PTH	Genotype	Treatment	Genotype × treatment
BV/TV	0.016 ± 0.001	0.042 ± 0.012	0.019 ± 0.007	0.047 ± 0.017	0.3349	<0.0001	0.8654
Conn D, mm^{-3}	0.86 ± 0.81	22.11 ± 7.10	1.66 ± 1.09	14.14 ± 11.74	0.1904	<0.0001	0.1131
SMI	3.39 ± 0.21	2.72 ± 0.39	3.51 ± 0.25	3.24 ± 0.37	0.0170	0.0009	0.1197
Tb.N, mm^{-1}	1.61 ± 0.19	1.78 ± 0.19	1.98 ± 0.35	2.44 ± 0.39	0.0002	0.0131	0.2100
Tb.Th, mm	0.043 ± 0.002	0.056 ± 0.004	0.042 ± 0.003	0.052 ± 0.005	0.1232	<0.0001	0.4117
Tb.Sp, mm	0.629 ± 0.066	0.575 ± 0.058	0.523 ± 0.103	0.422 ± 0.080	0.3048	0.0004	0.4783

WT and *Nmp4*-KO mice were treated with intermittent PTH or vehicle (number of mice/experimental group = 6–7) for 2 weeks. A two-factor AVOVA was used to evaluate the individual parameters

Table 3 Cortical architecture at the midshaft femur from WT and *Nmp4*-KO mice treated with vehicle or intermittent PTH for 2 weeks

	WT		KO		2-Way ANOVA *P*-values		
	VEH	PTH	VEH	PTH	Genotype	Treatment	Genotype × treatment
MA	1.40 ± 0.08	1.34 ± 0.07	1.39 ± 0.09	1.39 ± 0.13	0.5363	0.4618	0.4141
CA	0.98 ± 0.03	1.04 ± 0.06	1.01 ± 0.07	1.08 ± 0.07	0.1073	0.0067	0.6478
TA	2.38 ± 0.09	2.38 ± 0.11	2.40 ± 0.13	2.47 ± 0.17	0.2392	0.4539	0.4223
I_{MAX}	0.41 ± 0.02	0.41 ± 0.05	0.40 ± 0.04	0.43 ± 0.06	0.9661	0.2440	0.2649
I_{MIN}	0.21 ± 0.02	0.23 ± 0.02	0.23 ± 0.02	0.26 ± 0.03	0.0084	0.0382	0.6726
J	0.63 ± 0.04	0.64 ± 0.07	0.63 ± 0.07	0.69 ± 0.09	0.3048	0.1254	0.3670

Number of mice/experimental group = 7–10. The parameters include cortical area (CA, mm^2), marrow area (MA, mm^2), total area (TA, mm^2), and the maximum, minimum, and polar moments of inertia (I_{MAX}, I_{MIN}, and *J*, respectively [mm^4]). A two-factor ANOVA was used to evaluate the individual parameters

Table 4 Values for percent change (%Δ) BMD and BMC between 8 and 12 weeks of age

	WT		KO		2-Way ANOVA *P*-values		
	VEH	PTH	VEH	PTH	Genotype	Treatment	Genotype × treatment
%ΔWB BMD	5.27 ± 3.02	10.28 ± 2.83	6.18 ± 3.61	9.04 ± 2.81	0.8895	0.0032	0.3791
%ΔWB BMC	15.94 ± 7.39	22.73 ± 8.79	6.73 ± 6.14	16.34 ± 8.56	0.0158	0.0116	0.6410
%ΔFm BMD	12.86 ± 4.81	18.49 ± 1.69	8.93 ± 4.98	13.84 ± 3.74	0.0113	0.0026	0.8220
%ΔFm BMC	29.71 ± 11.72	36.01 ± 11.61	11.74 ± 8.87	23.59 ± 8.69	0.0009	0.0332	0.4950
%ΔTb BMD	7.25 ± 3.48	14.43 ± 4.90	5.98 ± 4.73	8.64 ± 4.86	0.0545	0.0096	0.2086
%ΔTb BMC	9.70 ± 7.20	24.84 ± 6.07	6.67 ± 4.53	11.61 ± 8.68	0.0045	0.0007	0.0608
%ΔSp BMD	6.22 ± 7.26	12.93 ± 6.41	9.57 ± 11.24	10.99 ± 9.44	0.8366	0.2421	0.4423
%ΔSP BMD	7.60 ± 8.61	15.11 ± 11.39	6.59 ± 15.10	10.96 ± 8.96	0.5635	0.1903	0.7246

Mice were challenged with vehicle or intermittent PTH for 2 weeks (10–12 weeks of age, number of mice/experimental group = 6–7). *P* values were determined with a two-factor ANOVA

WB Whole body, *FM* femur, *Sp* spine

the expression of *Bax*, the proapoptotic gene, was significantly attenuated in *Nmp4*-KO mice (Table 7). *M-csf*, its receptor *c-fms*, and the osteoclast recruitment cytokine *Mcp-1* showed no difference in their expression or PTH responsiveness between WT and *Nmp4*-KO animals (Table 7). Hormone induced over a 25-fold increase in *Nurr1* expression in both WT and null mice (Table 7). The expression of *Mkp-1*, *JunD*, *Smad3*, and *Lef1* was modestly but equally elevated with PTH in both genotypes (Table 7). Conversely, the mRNA expression of the receptor for advanced glycation end products (*Rage*) was attenuated by hormone treatment in both WT and *Nmp4*-KO mice (Table 7).

Next, we characterized the expression of genes that support bone formation by analyzing femoral RNA obtained 24 h after the last injection of intermittent PTH or vehicle after 2 weeks of treatment. We observed a treatment effect but no genotype effect or genotype × treatment interaction for *Runx2*, *Osterix*, *Col1a1*, *Alpl*, *Mmp13*, *Sost*, *Bmp2*, and *Pthr1* mRNA profiles (Table 7). Intermittent hormone treatment did not impact the expression of PTH-related peptide (*Pthrp*) in either genotype (Table 7).

Our preliminary evaluation of gene expression in the tibia showed that the RNA profiles at 3 weeks of treatment were generally similar to those observed for the femur at the same time point with the exception of *Nfatc1*, which was still significantly elevated in the tibia of the null mice (Table 8). Additionally, the decrease in the *Rankl*/*Opg* ratio did not reach significance in the tibia as demonstrated for the femur (Table 8).

Discussion

The present data demonstrate that Nmp4/CIZ significantly blunts PTH-stimulated improvement in cancellous bone throughout the skeleton, that this repression of bone gain is apparent between 2 and 7 weeks of hormone treatment, and that Nmp4/CIZ suppresses osteoclast as well as osteoblast number and activity, likely by regulating key transcription factors critical to the development of both cells. The global impact of Nmp4 on the trabecular skeleton is in stark contrast to recent studies showing the site-specific effects of Rage [9] and connexin 43 [10] on PTH-induced cancellous bone improvement.

Nmp4/CIZ repression of the PTH-mediated increase in trabecular bone was not observed during the initial 2-week treatment period; WT and KO mice showed equivalent hormone-stimulated increases in BMD, BMC, trabecular improvement, and enhanced expression of numerous genes that support bone formation. At 7 weeks of hormone challenge the striking expansion of the null trabecular compartment had been added and bone histomorphometry indicated that both the KO and WT mice exhibited a diminished response to PTH, consistent with previous observations on C57BL/6 mice [17]. However, starting at 3 weeks of hormone challenge, the KO mice exhibited an enhanced and sustained PTH-induced increase in serum osteocalcin. The significance of the 2- to 3-week lag period required for distinguishing the difference in PTH-stimulated bone formation between the *Nmp4*-KO and WT mice remains to be elucidated. Does this delay represent the time necessary to dramatically expand the null bone-forming osteoblast population? Further histomorphometric analysis at various time points throughout the treatment regimen is required to address this question.

Of particular significance was our discovery of an osteoclast phenotype in the *Nmp4*-KO mouse. The null mice had significantly higher serum CTX; more osteoclasts were recovered from *Nmp4*-KO marrow cultures than from WT cultures, and the null osteoclasts were more active as determined by in vitro resorption of dentin. Interestingly,

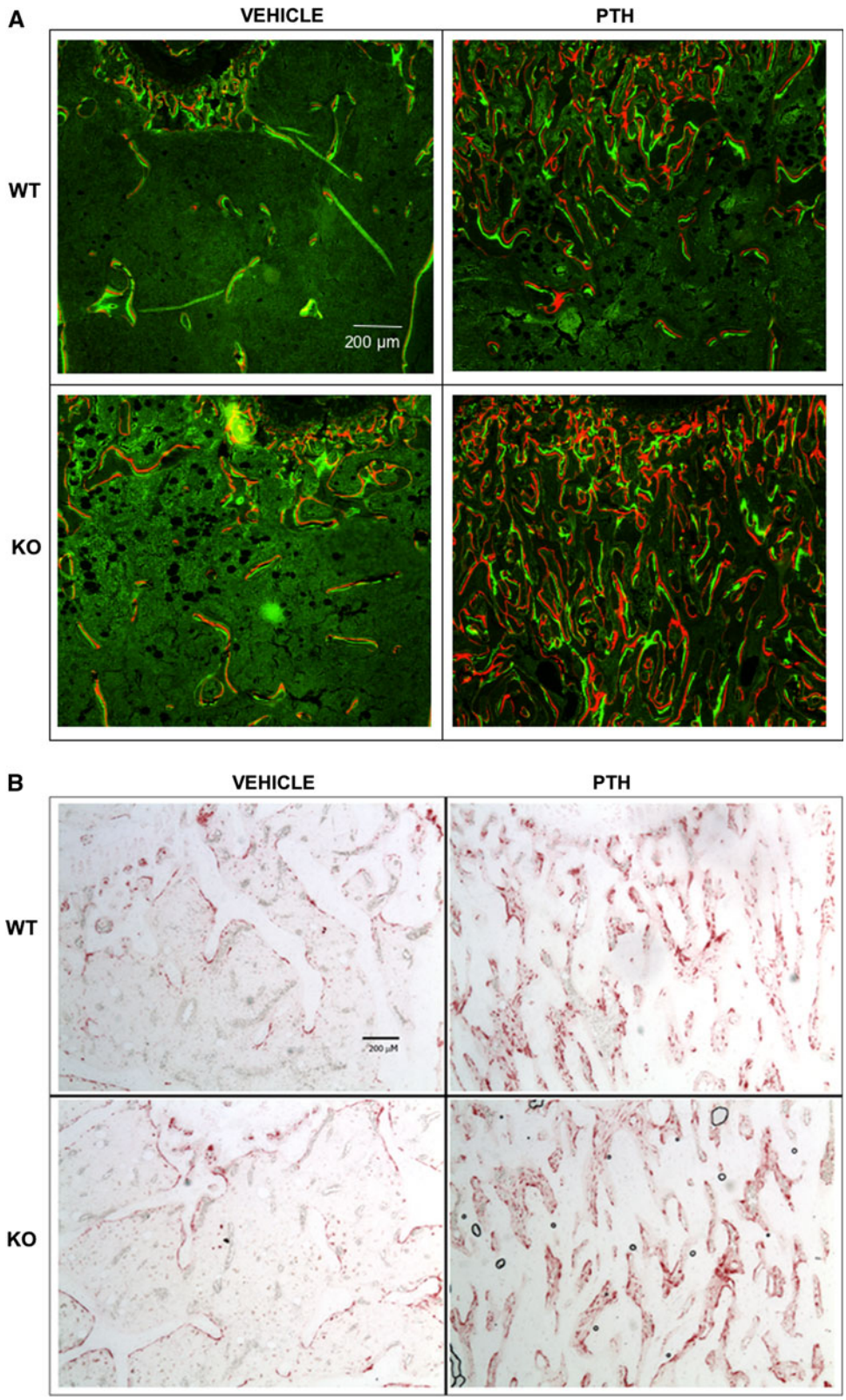

Fig. 3 **a** PTH-induced improvements in femoral trabecular architecture were enhanced in *Nmp4*-KO mice after 7 weeks of treatment. Femoral tissue sections were obtained from WT and *Nmp4*-KO mice treated with intermittent PTH or vehicle for 7 weeks (number of mice/experimental group = 5–6). Additionally, animals were administered intraperitoneal injections of calcein green (20 mg/kg) and alizarin red (25 mg/kg) 6 and 3 days before death, respectively. **b** Sections were stained for TRAP to evaluate osteoclast number and surface. Histological sections were prepared as described in "Materials and Methods" section. *Scale bar* 200 μm

PTH had a more significant impact on decreasing the osteoclast-covered bone surface in null mice without significantly lowering serum CTX, perhaps in part a consequence of the enhanced activity of the null osteoclasts. Despite the multiple lines of evidence suggesting higher bone resorption in the untreated nulls, these mice

Table 5 Bone histomorphometry of the distal femur from WT and *Nmp4*-KO mice treated with intermittent PTH or vehicle for 7 weeks

	WT		KO		2-Way ANOVA *P*-values		
	VEH	PTH	VEH	PTH	Genotype	Treatment	Gene × treat
MAR (μm/day)	2.80 ± 0.20	3.30 ± 0.21	2.88 ± 0.22	3.19 ± 0.16	0.8288	<0.0001	0.2628
MS/BS (%)	0.53 ± 0.08	0.49 ± 0.05	0.52 ± 0.03	0.50 ± 0.04	0.9331	0.0507	0.3275
BFR ($\mu m^2/\mu m$/day)	1.49 ± 0.08	1.61 ± 0.22	1.49 ± 0.16	1.59 ± 0.15	0.9135	0.0905	0.9175
Trap + S/BS (%)	0.37 ± 0.03	0.36 ± 0.09	0.48 ± 0.07	0.33 ± 0.12	0.2420	0.0383	0.0549
							Tukey's HSD
							KO VEH A
							WT VEH A B
							WT PTH A B
							KO PTH B
Trap + N/BS (mm^{-1})	0.45 ± 0.06	0.41 ± 0.11	0.60 ± 0.10	0.41 ± 0.10	0.0863	0.0110	0.0918

Number of mice/experimental group = 5–6). The parameters include mineral apposition rate (MAR), mineralizing surface/bone surface (MS/BS), bone formation rate (BFR), the TRAP-stained surface to bone surface ($TRAP^+$ S/BS), and the number of TRAP-stained cells on the bone surface ($TRAP^+$ N/BS). A two-factor ANOVA was used to evaluate the impact of genotype and treatment on the individual parameter. A Tukey's HSD post hoc test was used to determine differences between treatment groups if a significant genotype × treatment interaction was indicated ($TRAP^+$ S/BS). Groups not connected by the same letter are significantly different

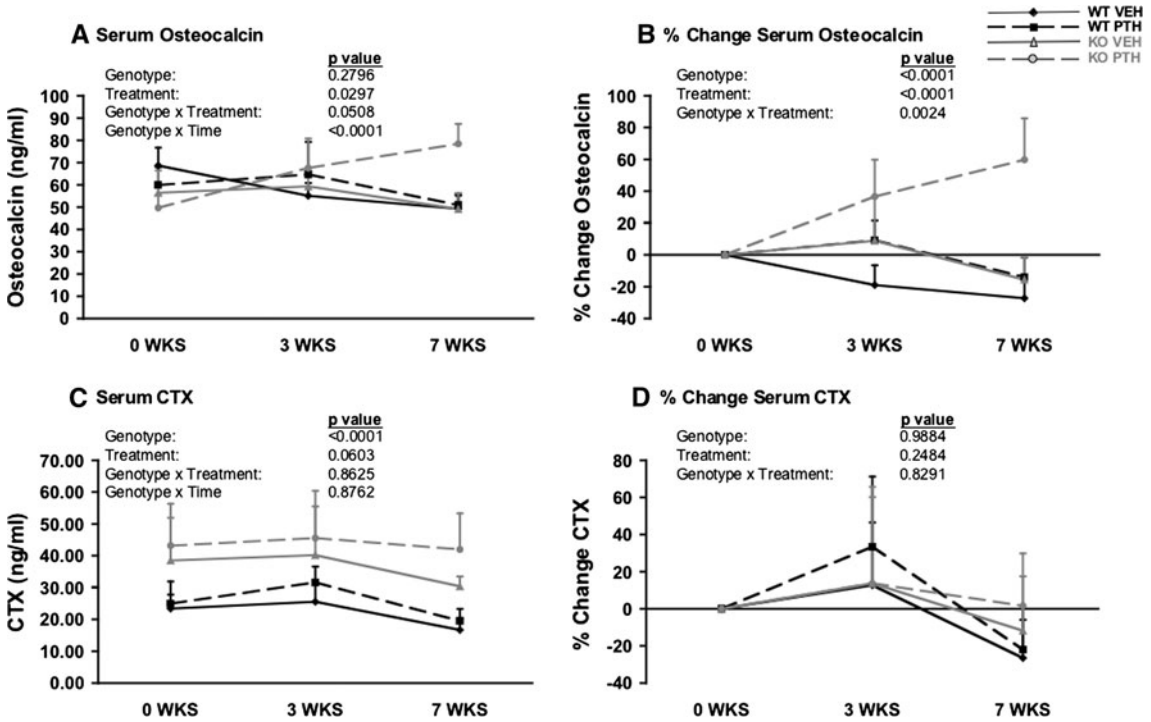

Fig. 4 PTH-treated *Nmp4*-KO mice exhibited strikingly distinct serum chemistries from WT animals. Whole blood was collected and serum separated from WT and *Nmp4*-KO mice treated with intermittent PTH or vehicle (number of mice/experimental group = 6–7) at baseline just prior to initiation of treatment, at 3 weeks of treatment, and at 7 weeks of treatment. **a** Raw longitudinal serum osteocalcin concentrations showed no genotype effect but revealed a significant treatment effect, a genotype × treatment interaction, and a genotype × time interaction, indicating that WT and null mice had equivalent baseline values but that *Nmp4*-KO had an enhanced response to hormone and a higher rate of increase over the experimental time period. **b** Percent change data confirmed the raw longitudinal data, revealing a significant genotype effect (higher rate of osteocalcin increase in nulls), a treatment effect, and a genotype × treatment interaction over the experimental period. **c** Raw longitudinal serum CTX concentrations showed a genotype effect but no significant treatment effect, no genotype × treatment interaction, and no genotype × time interaction. **d** Percent change CTX data showed no significant responsiveness to hormone treatment in WT and null mice. *P* values were determined with a repeated-measures MANOVA (longitudinal data) or a two-factor ANOVA

Table 6 Comparative femoral RNA expression of WT and *Nmp4*-KO mice treated with PTH or vehicle for 2 or 3 weeks

Gene	WT		KO		2-way ANOVA *P*-values		
	VEH	PTH	VEH	PTH	Genotype	Treatment	Gene × treat
c-fos (2 weeks)	0.73 ± 0.25	7.94 ± 1.00	1.87 ± 0.71	12.04 ± 2.31	<0.001	<0.0001	0.0121
							Tukey's HSD
							KO PTH A
							WT PTH B
							KO VEH C
							WT VEH C
c-fos (3 weeks)	1.04 ± 0.31	8.73 ± 2.07	1.05 ± 0.31	8.33 ± 1.85	0.7380	<0.0001	0.7235
Fra-2 (2 weeks)	0.72 ± 0.15	4.25 ± 0.50	0.96 ± 0.13	5.56 ± 0.97	0.0028	<0.0001	0.0301
							Tukey's HSD
							KO PTH A
							WT PTH B
							KO VEH C
							WT VEH C
Fra-2 (3 weeks)	1.01 ± 0.12	5.32 ± 1.23	1.03 ± 0.18	4.72 ± 0.98	0.3905	<0.0001	0.3441
Nfatc1 (2 weeks)	1.03 ± 0.43	1.46 ± .0.31	1.48 ± 0.43	1.96 ± 0.27	0.0051	0.0074	0.8659
Nfatc1 (3 weeks)	1.00 ± 0.11	1.76 ± 0.48	1.02 ± 0.27	1.41 ± 0.26	0.2008	0.0002	0.1699
EphB4 (2 weeks)	0.80 ± 0.16	1.27 ± .0.12	0.98 ± 0.22	1.41 ± 0.21	0.0466	<0.0001	0.7544
EphB4 (3 weeks)	1.01 ± 0.16	1.78 ± 0.39	0.95 ± 0.33	1.74 ± 0.40	0.7131	<0.0001	0.9257
EphrinB2 (2 weeks)	0.75 ± 0.18	5.16 ± .0.68	1.19 ± 0.27	5.87 ± 1.23	0.0658	<0.0001	0.6555
EphrinB2 (3 weeks)	1.02 ± 0.24	6.85 ± 2.82	1.01 ± 0.32	6.24 ± 1.05	0.6209	<0.0001	0.6355
Opg (2 weeks)	0.85 ± 0.14	0.82 ± 0.14	1.23 ± 0.41	0.97 ± 0.21	0.0150	0.1625	0.2862
Opg (3 weeks)	1.03 ± 0.29	1.19 ± 0.33	1.13 ± 0.26	1.34 ± 0.26	0.2943	0.1372	0.8389
Rankl (2 weeks)	0.96 ± 0.11	21.34 ± 6.20	1.19 ± 0.59	16.75 ± 3.43	0.1492	<0.0001	0.1124
Rankl (3 weeks)	1.04 ± 0.34	13.72 ± 4.58	0.82 ± 0.26	11.04 ± 1.79	0.1663	<0.0001	0.2367
Rankl/Opg (2 weeks)	1.14 ± 0.18	27.39 ± 12.45	0.94 ± 0.23	17.84 ± 5.60	0.0954	<0.0001	0.1092
Rankl/Opg (3 weeks)	1.04 ± 0.18	11.53 ± 2.04	0.73 ± 0.22	8.60 ± 2.38	0.0207	<0.0001	0.0558

Number of mice/experimental group = 6–9 for 2 weeks or 6 for 3 weeks, harvested 1 h after the last injection. *P* values were determined with a two-factor ANOVA. A Tukey's HSD post hoc test was used to determine differences between treatment groups if a significant genotype × treatment interaction was indicated. Groups not connected by the same letter are significantly different

are not osteopenic and in fact have a modestly enhanced skeleton, although the rate of bone accrual from 8 to 12 weeks is marginally slower in the null animals. Femoral bone marrow-derived osteoblasts from Nmp4/CIZ-deficient mice exhibited enhanced alkaline phosphatase expression and formed more mineralized nodules than WT osteoblasts [18], suggesting in vivo that the null osteoblast outpaces the null osteoclast. Further study is required to determine if there is an increased rate of remodeling (activation frequency) with a positive bone balance in the untreated mice and if so, how this is achieved.

Although the in vivo mRNA expression profiles represent a composite of multiple marrow and bone cell types, the transiently enhanced expression of *c-fos*, *Fra-2*, and *Nfatc1* in the null mice may be part of the molecular mechanism contributing to the apparent increased number of osteoblasts and osteoclasts. Fra-2 plays a significant role in chondrocyte differentiation and matrix production in embryonic and newborn mice [19] and in regulating the size of osteoclasts [20].

The contribution of c-Fos to the PTH anabolic response involves both osteoblasts and osteoclasts; in the former it is part of the immediate-early gene response [21] and, as such, is critical for subsequent induction of select target genes. As a key regulator of bone cell growth and differentiation, c-Fos often interacts with RUNX2 [22]. PTH stimulation of *Mmp-13* transcription in osteoblast-like cells requires the cooperative interaction between the c-Fos·c-Jun AP-1 complex and RUNX2 [23], and Nmp4/CIZ dampens this induction [8]. Consequently, the heightened PTH-stimulated increase in osteoblast c-Fos activity in *Nmp4*-KO mice may boost hormone transcriptional induction of some genes supporting the anabolic response. The impact of Nmp4/CIZ on *c-fos* and *Fra-2* was specific within the context of the PTH-induced immediate-early response because we did not observe differences in other

Table 7 Comparative femoral RNA expression of WT and *Nmp4*-KO mice treated with PTH or vehicle for 2 weeks (number of mice/experimental group = 6–9) and harvested 1 or 24 h after the last injection

Gene	WT		KO		2-Way ANOVA *P*-values		
	VEH	PTH	VEH	PTH	Genotype	Treatment	Gene × treat
1 h post-injection							
M-csf	1.13 ± 0.72	2.14 ± 0.70	1.19 ± 0.09	2.87 ± 0.53	0.1056	<0.0001	0.1665
Mcp-1	0.79 ± 0.20	2.60 ± 0.90	0.99 ± 0.24	2.61 ± 0.70	0.6657	<0.0001	0.7156
Bcl2	0.96 ± 0.12	1.02 ± 0.14	1.06 ± 0.20	1.03 ± 0.08	0.2997	0.7913	0.4563
Bax	1.02 ± 0.25	0.91 ± 0.14	0.69 ± 0.12	0.71 ± 0.04	0.0005	0.4604	0.3321
Nurr1	0.69 ± 0.22	56.37 ± 6.56	2.06 ± 1.49	58.62 ± 14.05	0.5750	<0.0001	0.8914
Mkp-1	0.83 ± 0.09	2.31 ± 0.90	1.13 ± 0.48	1.95 ± 0.32	0.8708	<0.0001	0.1022
JunD	0.80 ± 0.16	0.94 ± 0.16	0.78 ± 0.19	1.10 ± 0.16	0.3366	0.0036	0.2206
Smad3	0.78 ± 0.12	1.97 ± 0.34	1.05 ± 0.26	2.14 ± 0.63	0.1736	<0.0001	0.7403
Lef1	0.99 ± 0.19	1.52 ± 0.30	1.08 ± 0.21	1.36 ± 0.27	0.7196	0.0006	0.2293
Rage	0.87 ± 0.16	0.74 ± 0.13	1.07 ± 0.35	0.72 ± 0.27	0.3655	0.0261	0.2829
24 h post-injection							
Runx2	0.86 ± 0.21	1.45 ± 0.34	0.59 ± 0.23	1.35 ± 0.84	0.2960	0.0007	0.6482
Osterix	0.63 ± 0.20	1.61 ± 0.48	0.49 ± 0.37	1.67 ± 0.96	0.8385	<0.0001	0.6460
Col1a1	0.92 ± 0.14	2.35 ± 0.65	0.75 ± 0.49	2.70 ± 2.45	0.8424	0.0017	0.5964
Alpl	0.96 ± 0.18	2.95 ± 0.69	0.81 ± 0.47	2.42 ± 1.63	0.3286	<0.0001	0.5814
Mmp13	0.73 ± 0.21	1.05 ± 0.28	0.51 ± 0.22	1.23 ± 0.61	0.3987	0.0007	0.3997
Sost	1.17 ± 0.22	1.79 ± 0.31	1.15 ± 0.38	1.59 ± 0.33	0.3328	<0.0001	0.4419
Bmp2	1.01 ± 0.14	1.41 ± 0.24	0.91 ± 0.26	1.15 ± 0.39	0.0898	0.0036	0.4394
Pthr1	0.86 ± 0.23	1.59 ± 0.40	0.68 ± 0.28	1.38 ± 0.68	0.2223	<0.0001	0.9071
Pthrp	0.75 ± 0.18	1.10 ± 0.44	0.89 ± 0.44	1.00 ± 0.44	0.9024	0.1154	0.4214

P values were determined with a two-factor ANOVA. A Tukey's HSD post hoc test was used to determine differences between treatment groups if a significant genotype × treatment interaction was indicated. Groups not connected by the same letter are significantly different

Table 8 Comparative tibial RNA expression of WT and *Nmp4*-KO mice treated with PTH or vehicle for 3 weeks (number of mice/experimental group = 6) and harvested 1 h after the last injection

Gene	WT		KO		2-Way ANOVA *P*-values		
	VEH	PTH	VEH	PTH	Genotype	Treatment	Gene × treat
c-fos	1.05 ± 0.39	9.05 ± 3.57	1.66 ± 1.19	10.65 ± 3.05	0.2775	<0.0001	0.6243
Fra-2	1.02 ± 0.23	4.62 ± 1.63	1.28 ± 0.31	7.21 ± 3.08	0.0604	<0.0001	0.1178
Nfatc1	1.02 ± 0.20	1.42 ± 0.60	1.36 ± 0.45	2.00 ± 0.53	0.0262	0.0136	0.5470
EphB4	1.02 ± 0.22	1.80 ± 0.75	1.25 ± 0.34	2.07 ± 0.34	0.2372	0.0010	0.9216
EphrinB2	1.08 ± 0.45	5.13 ± 3.31	1.22 ± 0.31	7.40 ± 2.19	0.1551	<0.0001	0.2065
Opg	1.03 ± 0.25	1.4 ± 0.63	1.07 ± 0.23	1.57 ± 0.40	0.5314	0.0181	0.6969
Rankl	1.01 ± 0.18	10.51 ± 3.46	0.79 ± 0.18	11.19 ± 3.61	0.8226	<0.0001	0.6618
Rankl/Opg	1.07 ± 0.49	7.98 ± 1.64	0.76 ± 0.16	7.07 ± 0.75	0.1248	<0.0001	0.4467

P values were determined with a two-factor ANOVA

aspects of this gene program including *Nurr1*, a transcription factor participating in PTH-mediated osteoblast gene induction [24]; *Mkp-1*, a phosphatase implicated in PTH-mediated osteoblast cell cycle arrest [25]; *JunD*, involved in osteoblast differentiation [26]; or *Smad3* and *Lef1*, *trans*-acting proteins involved in coupling the PTH and Wnt signaling pathways in osteoblasts [27].

In addition to its role as a PTH-responsive osteoblast transcription factor, c-Fos is critical to osteoclastogenesis and plays a role in supporting the precursor cell's capacity to undergo differentiation [28]. It fulfills this role in part by mediating the induction of *Nfatc1*, another key transcription factor that supports osteoclastogenesis and osteoblast development [29]; the elevation of *c-fos* mRNA expression

in the nulls may ultimately contribute to the enhanced *Nfatc1* expression in these mice. Additionally, c-Fos has multiple and complex roles in regulating osteoblast-derived signals that regulate osteoclastogenesis and mature osteoclast activity including the RANKL/OPG signaling axis by governing the transcriptional activity of the *Opg* gene in the osteoblast and by activating RANKL target genes in osteoclasts; c-Fos also activates the IFN-γ-driven RANKL negative feedback pathway in the osteoclast [30, 31]. The *Rankl/Opg* ratio was attenuated in the null mice, which achieved significance in the femur by 3 weeks of treatment; perhaps this ultimately contributed some protective effect from the enhanced osteoclast activity. Nmp4/CIZ had a negligible impact on the mRNA expression of other osteoclastogenic cytokines including *Mcp-1*, a cytokine involved in osteoclast recruitment [32], as well as *M-csf* and its receptor *c-fms*, which activate the proliferation and survival of osteoclast precursors [33]. The significantly attenuated expression of the proapoptotic gene *Bax* in the null mice may contribute to a longer-lived osteoblast, critical to the PTH-induced anabolic mechanism [5]; but further studies are required to confirm this possibility.

Recent studies with *c-fos*-null animals indicate that interaction between immature osteoclasts and preosteoblasts may be necessary for an optimal response to intermittent PTH; specifically, the osteoclast precursors support the differentiation of preosteoblasts [34–37]. In one potential scenario this coupling is mediated by the bidirectional interaction between an EphrinB2 ligand on the preosteoclast and the EphB4 receptor on the preosteoblast [34, 35]. Forward signaling from the osteoclast precursor to the preosteoblast enhances differentiation of the latter, whereas reverse signaling suppresses osteoclast differentiation [35]. Therefore, PTH appears to activate both forward and reverse EphrinB–EphB4 signaling, resulting in the enhancement of bone formation and the restraining of resorption [34]. This is consistent with the observed increased expression of EphB4 in *Nmp4*-KO mice and the marginally enhanced EphrinB2 expression in these animals. Future osteoblast–osteoclast coculture studies will be needed to investigate the potential impact of Nmp4/CIZ on the reciprocal regulation of these cells.

We propose that Nmp4/CIZ governs both the osteoblast and osteoclast cellular arms of the PTH-induced anabolic response by controlling the size, activity, and/or PTH responsiveness of these cell populations, in part via the modest suppression of several key transcription factors and receptors critical to the developmental and/or response pathways of both cells. The complex sequence of molecular and cellular events underlying Nmp4/CIZ regulation of bone remodeling remains to be elucidated. Nmp4/CIZ has been previously identified as an attractive potential therapeutic target for treating osteoporosis [38], and the present finding that this protein regulates not only the osteoblast but also the osteoclast underscores this assertion.

Acknowledgments This work was supported by a grant from the National Institute of Diabetes and Digestive and Kidney Diseases (NIDDK, NIH), grant DK053796 (to J. P. B.).

References

1. Stroup J, Kane MP, Abu-Baker AM (2008) Teriparatide in the treatment of osteoporosis. Am J Health Syst Pharm 65:532–539
2. Liu H, Michaud K, Nayak S, Karpf DB, Owens DK, Garber AM (2006) The cost-effectiveness of therapy with teriparatide and alendronate in women with severe osteoporosis. Arch Intern Med 166:1209–1217
3. Childress P, Robling AG, Bidwell JP (2010) Nmp4/CIZ: road block at the intersection of PTH and load. Bone 46:259–266
4. Ahlström M, Lamberg-Allardt C (1997) Rapid protein kinase A—mediated activation of cyclic AMP-phosphodiesterase by parathyroid hormone in UMR-106 osteoblast-like cells. J Bone Miner Res 12:172–178
5. Bellido T, Ali AA, Plotkin LI, Fu Q, Gubrij I, Roberson PK, Weinstein RS, O'Brien CA, Manolagas SC, Jilka RL (2003) Proteasomal degradation of Runx2 shortens parathyroid hormone-induced anti-apoptotic signaling in osteoblasts. A putative explanation for why intermittent administration is needed for bone anabolism. J Biol Chem 278:50259–50272
6. Robling AG, Childress P, Yu J, Cotte J, Heller A, Philip BK, Bidwell JP (2009) Nmp4/CIZ suppresses parathyroid hormone-induced increases in trabecular bone. J Cell Physiol 219:734–743
7. Thunyakitpisal P, Alvarez M, Tokunaga K, Onyia JE, Hock J, Ohashi N, Feister H, Rhodes SJ, Bidwell JP (2001) Cloning and functional analysis of a family of nuclear matrix transcription factors (NP/NMP4) that regulate type I collagen expression in osteoblasts. J Bone Miner Res 16:10–23
8. Shah R, Alvarez M, Jones DR, Torrungruang K, Watt AJ, Selvamurugan N, Partridge NC, Quinn CO, Pavalko FM, Rhodes SJ, Bidwell JP (2004) Nmp4/CIZ regulation of matrix metalloproteinase 13 (MMP-13) response to parathyroid hormone in osteoblasts. Am J Physiol Endocrinol Metab 287:E289–E296
9. Philip BK, Childress PJ, Robling AG, Heller A, Nawroth PP, Bierhaus A, Bidwell JP (2010) RAGE supports parathyroid hormone-induced gains in femoral trabecular bone. Am J Physiol Endocrinol Metab 298:E714–E725
10. Chung DJ, Castro CH, Watkins M, Stains JP, Chung MY, Szejnfeld VL, Willecke K, Theis M, Civitelli R (2006) Low peak bone mass and attenuated anabolic response to parathyroid hormone in mice with an osteoblast-specific deletion of connexin43. J Cell Sci 119:4187–4198
11. Cheng S, Sipilä S, Taaffe DR, Puolakka J, Suominen H (2002) Change in bone mass distribution induced by hormone replacement therapy and high-impact physical exercise in post-menopausal women. Bone 31:126–135
12. Goossens K, Van Poucke M, Van Soom A, Vandesompele J, Van Zeveren A, Peelman LJ (2005) Selection of reference genes for quantitative real-time PCR in bovine preimplantation embryos. BMC Dev Biol 5:27
13. Zhang X, Ding L, Sandford AJ (2005) Selection of reference genes for gene expression studies in human neutrophils by real-time PCR. BMC Mol Biol 6:4
14. Parfitt AM, Drezner MK, Glorieux FH, Kanis JA, Malluche H, Meunier PJ, Ott SM, Recker RR (1987) Bone histomorphometry: standardization of nomenclature, symbols, and units. Report of the

ASBMR Histomorphometry Nomenclature Committee. J Bone Miner Res 2:595–610
15. O'Brien CA, Plotkin LI, Galli C, Goellner JJ, Gortazar AR, Allen MR, Robling AG, Bouxsein M, Schipani E, Turner CH, Jilka RL, Weinstein RS, Manolagas SC, Bellido T (2008) Control of bone mass and remodeling by PTH receptor signaling in osteocytes. PLoS One 3:e2942
16. Tanaka S, Amling M, Neff L, Peyman A, Uhlmann E, Levy JB, Baron R (1996) c-Cbl is downstream of c-Src in a signalling pathway necessary for bone resorption. Nature 383:528–531
17. Iida-Klein A, Zhou H, Lu SS, Levine LR, Ducayen-Knowles M, Dempster DW, Nieves J, Lindsay R (2002) Anabolic action of parathyroid hormone is skeletal site specific at the tissue and cellular levels in mice. J Bone Miner Res 17:808–816
18. Morinobu M, Nakamoto T, Hino K, Tsuji K, Shen ZJ, Nakashima K, Nifuji A, Yamamoto H, Hirai H, Noda M (2005) The nucleocytoplasmic shuttling protein CIZ reduces adult bone mass by inhibiting bone morphogenetic protein-induced bone formation. J Exp Med 201:961–970
19. Karreth F, Hoebertz A, Scheuch H, Eferl R, Wagner EF (2004) The AP1 transcription factor Fra2 is required for efficient cartilage development. Development 131:5717–5725
20. Bozec A, Bakiri L, Hoebertz A, Eferl R, Schilling AF, Komnenovic V, Scheuch H, Priemel M, Stewart CL, Amling M, Wagner EF (2008) Osteoclast size is controlled by Fra-2 through LIF/LIF-receptor signalling and hypoxia. Nature 454:221–225
21. Liang JD, Hock JM, Sandusky GE, Santerre RF, Onyia JE (1999) Immunohistochemical localization of selected early response genes expressed in trabecular bone of young rats given hPTH 1–34. Calcif Tissue Int 65:369–373
22. Qin L, Raggatt LJ, Partridge NC (2004) Parathyroid hormone: a double-edged sword for bone metabolism. Trends Endocrinol Metab 15:60–65
23. D'Alonzo RC, Selvamurugan N, Karsenty G, Partridge NC (2002) Physical interaction of the activator protein-1 factors c-Fos and c-Jun with Cbfa1 for collagenase-3 promoter activation. J Biol Chem 277:816–822
24. Nervina JM, Magyar CE, Pirih FQ, Tetradis S (2006) PGC-1alpha is induced by parathyroid hormone and coactivates Nurr1-mediated promoter activity in osteoblasts. Bone 39:1018–1025
25. Qin L, Li X, Ko JK, Partridge NC (2005) Parathyroid hormone uses multiple mechanisms to arrest the cell cycle progression of osteoblastic cells from G_1 to S phase. J Biol Chem 280:3104–3111
26. Wagner EF (2010) Bone development and inflammatory disease is regulated by AP-1 (Fos/Jun). Ann Rheum Dis 69(Suppl 1):i86–i88
27. Tobimatsu T, Kaji H, Sowa H, Naito J, Canaff L, Hendy GN, Sugimoto T, Chihara K (2006) Parathyroid hormone increases beta-catenin levels through Smad3 in mouse osteoblastic cells. Endocrinology 147(5):2583–2590
28. Boyle WJ, Simonet WS, Lacey DL (2003) Osteoclast differentiation and activation. Nature 423:337–342
29. Takayanagi H (2007) The role of NFAT in osteoclast formation. Ann N Y Acad Sci 1116:227–237
30. Takayanagi H, Kim S, Matsuo K, Suzuki H, Suzuki T, Sato K, Yokochi T, Oda H, Nakamura K, Ida N, Wagner EF, Taniguchi T (2002) RANKL maintains bone homeostasis through c-fos-dependent induction of interferon-beta. Nature 416:744–749
31. Fu Q, Jilka RL, Manolagas SC, O'Brien CA (2002) Parathyroid hormone stimulates receptor activator of NFkappaB ligand and inhibits osteoprotegerin expression via protein kinase A activation of cAMP-response element-binding protein. J Biol Chem 277:48868–48875
32. Li X, Qin L, Bergenstock M, Bevelock LM, Novack DV, Partridge NC (2007) Parathyroid hormone stimulates osteoblastic expression of MCP-1 to recruit and increase the fusion of pre/osteoclasts. J Biol Chem 282:33098–33106
33. Negishi-Koga T, Takayanagi H (2009) Ca^{2+}-NFATc1 signaling is an essential axis of osteoclast differentiation. Immunol Rev 231:241–256
34. Luiz de Freitas PH, Li M, Ninomiya T, Nakamura M, Ubaidus S, Oda K, Udagawa N, Maeda T, Takagi R, Amizuka N (2009) Intermittent PTH administration stimulates pre-osteoblastic proliferation without leading to enhanced bone formation in osteoclast-less c-$fos^{-/-}$ mice. J Bone Miner Res 24:1586–1597
35. Zhao C, Irie N, Takada Y, Shimoda K, Miyamoto T, Nishiwaki T, Suda T, Matsuo K (2006) Bidirectional ephrinB2–EphB4 signaling controls bone homeostasis. Cell Metab 4:111–121
36. Koh AJ, Demiralp B, Neiva KG, Hooten J, Nohutcu RM, Shim H, Datta NS, Taichman RS, McCauley LK (2005) Cells of the osteoclast lineage as mediators of the anabolic actions of parathyroid hormone in bone. Endocrinology 146(11):4584–4596
37. Allen MR, Burr DB (2006) Parathyroid hormone and bone biomechanics. Clin Rev Bone Miner Metab 4:259–268
38. Krane SM (2005) Identifying genes that regulate bone remodeling as potential therapeutic targets. J Exp Med 201:841–843

Human Molecular Genetics, 2006, Vol. 15, No. 19 ***2837–2845***
doi:10.1093/hmg/ddl208
Advance Access published on August 7, 2006

Neurofibromin plays a critical role in modulating osteoblast differentiation of mesenchymal stem/progenitor cells

Xiaohua Wu[1,4], Selina A. Estwick[1,4], Shi Chen[1,4], Menggang Yu[3], Wenyu Ming[1,4], Todd D. Nebesio[1,4], Yan Li[1,4], Jin Yuan[1,4], Reuben Kapur[1,2,4], David Ingram[1,2,4], Mervin C. Yoder[1,2,4] and Feng-Chun Yang[1,4,*]

[1]Department of Pediatrics, [2]Department of Biochemistry and Molecular Biology, [3]Department of Medicine/Biostatistics and [4]Herman B. Wells Center for Pediatric Research and Indiana University School of Medicine, Cancer Research Institute, 1044 W. Walnut Street, R4/427 Indianapolis, IN 46202, USA

Received May 30, 2006; Revised and Accepted July 29, 2006

Mutations in the *NF1* tumor suppressor gene cause neurofibromatosis type 1, a pandemic autosomal dominant genetic disorder with an incidence of 1:3000. Individuals with NF1 have a variety of malignant and non-malignant manifestations, including skeletal manifestations, such as osteoporosis, scoliosis and short statures. However, the mechanism(s) underlying the osseous manifestations in NF1 are poorly understood. In the present study, utilizing *Nf1* haploinsufficient (+/−) mice, we demonstrate that *Nf1*+/− mesenchymal stem/progenitor cells (MSPC) have increased proliferation and colony forming unit-fibroblast (CFU-F) capacity compared with wild-type (WT) MSPC. *Nf1*+/− MSPC also have fewer senescent cells and have a significantly higher telomerase activity compared with WT MSPC. *Nf1*+/− MSPC have impaired osteoblast differentiation as determined by alkaline phosphatase staining, and confirmed by single CFU-F replating assays. The impaired osteoblast differentiation in *Nf1*+/− MSPC is consistent with the reduced expression of osteoblast markers at the mRNA level, including osteocalcin and osteonectin. Importantly, re-expression of the full-length *NF1* GTPase activating related domain (*NF1* GAP-related domain) is sufficient to restore the impaired osteoblast differentiation in *Nf1*+/− MSPC. Taken together, our results suggest that neurofibromin plays a crucial role in modulating MSPC differentiation into osteoblasts, and the defect in osteoblast differentiation may contribute at least in part to the osseous abnormalities seen in individuals with NF1.

INTRODUCTION

Neurofibromatosis type I (NF1) is a common autosomal dominant genetic disorder with a prevalence of 1 in 3000 individuals worldwide (1,2). NF1 occurs as a consequence of mutations in the *NF1* tumor suppressor gene, which encodes the Ras-GTPase activating protein (Ras-GAP), neurofibromin. Neurofibromin functions as a molecular switch that negatively regulates the activation of p21Ras proteins by accelerating intrinsic Ras-guanosine triphosphate (GTP) activity to the inactive Ras-guanosine dephosphate (GDP) state. Ras is at the apex of multiple signaling pathways, including the MEK/ERK and PI3-K pathways, which modulate multiple cellular functions, such as cell proliferation, differentiation and survival (3,4).

NF1 functions as a GTPase in mesothelial-derived tissues including fibroblasts (5,6) and osteoprogenitor cells (7), which are relevant to skeletal development. Individuals with NF1 suffer from a variety of non-malignant, debilitating manifestations, including café-au-lait macules, benign cutaneous neurofibromas and learning disabilities (8,9). In addition, up to 50% of NF1 patients suffer from a variety of skeletal manifestations, including short stature, osteoporosis, pseudoarthrosis of the tibia, kyphoscoliosis and sphenoid wing dysplasia (10–14). Recent clinical studies provide evidence that individuals with NF1 are at significant risk for both

*To whom correspondence should be addressed. Tel: +1 3172744178; Fax: +1 3172748679; Email: fyang@iupui.edu

generalized (13,15–17) and focal skeletal abnormalities (16,18), and suggest that the pathogenesis of the osseous manifestations in NF1 may involve impaired development of the skeletal system and impaired maintenance of bone structure (13). Although precise pathology underlying the localized skeletal abnormalities is incompletely understood, surgical attempts to repair these focal skeletal abnormalities often fail due to non-union and/or pseudoarthrosis of the healing bones. Although clinical observations provide support to suggest that generalized mechanisms regulating the generation and remodeling of bone are impaired.

Functional defects in differentiated bone cells or impairment in the self-renewing osteoprogenitor cells may underlie the cause of abnormal bone development, fragility and lowered fracture threshold in the adult skeleton due to perturbations in key biochemical signaling pathways required to maintain bone competence in NF1 (19). In some human diseases and murine disease models with similar skeletal manifestations as NF1, defects in osteoprogenitor proliferation as well as osteoblast differentiation and function are frequently observed (7,20). Osteoblasts originate from pluripotent mesenchymal stem/progenitor cells (MSPC) of the bone marrow (21,22). MSPC are multipotent stem cells that have the ability to give rise to a variety of mesoderm-derived cells, including osteoblasts, chondrocytes, adipocytes and muscle cells. Studies by Horwitz *et al*. have shown that allogeneic mesenchymal cells offer feasible post-transplantation therapy for osteogenesis imperfecta and likely other disorders originating in mesenchymal precursors (23,24).

Recent insights into the normal physiology of bone formation and remodeling, the development of murine models of NF1 and an increasing understanding of the potential cellular effects of haploinsufficiency of *NF1*, facilitate a detailed evaluation of the pathological mechanisms underlying skeletal disease in NF1. In the present study, utilizing cells derived from *Nf1*+/− mice, we investigated the role of neurofibromin in regulating the differentiation of MSPC into osteoblast and chondrocyte lineages. Our study indicates that haploinsufficiency of *Nf1* in MSPC leads to impaired osteoblast differentiation. The deficiency in osteoblast differentiation reported herein in part is responsible for the osseous abnormalities observed in NF1 patients.

RESULTS

Nf1+/− mice have increased colony forming unit-fibroblast (CFU-F)

To examine whether MSPC express neurofibromin, western blot was performed to check the protein level of neurofibromin. MSPC from WT cultures demonstrate neurofibromin expression (Fig. 1A). In contrast, a significant reduction of neurofibromin expression was observed in *Nf1*+/− MSPC. We next evaluated the frequency of *Nf1*+/− MSPC in bone marrow by CFU-F assays. A 2-fold increase in the frequency and total number of *Nf1*+/− CFU-F was observed compared with WT controls (Fig. 1B and C). Consistently higher numbers of CFU-F were seen over a range of input cells from *Nf1*+/− mice compared with WT controls as shown quantitatively (Fig. 1D) and qualitatively by

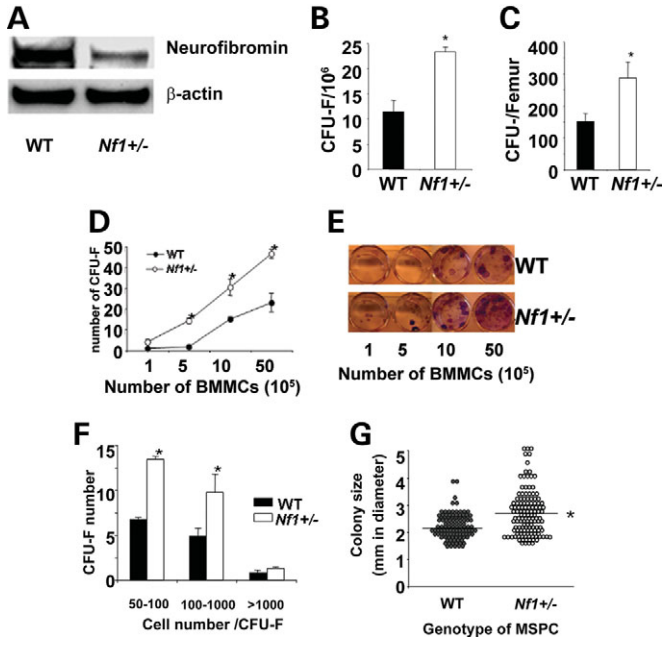

Figure 1. (**A**–**F**). Evaluation of frequency and size of CFU-F. The neurofibromin expression was measured by western blot (A). The frequency of CFU-F in bone marrow from WT and *Nf1* +/− mice was measured and depicted as CFU-F per 10^6 BMMNCs (B) or as total CFU-F per femur (C) ($^*P < 0.01$). (D) Clonogenic efficiency of CFU-F from different concentrations of plated BMMNC from WT and *Nf1* +/− mice ($^*P < 0.01$ for *Nf1*+/− versus WT cells). (E) Qualitative comparison of CFU-F from *Nf1*+/− and WT BMMNC taken with a Fujifilm digital camera (FinePix2400Zoom, Fuji Photo film Co., Japan). (F) Categorical scoring of CFU-F based on number of cells/colony ($^*P < 0.01$ for *Nf1*+/− versus WT cells). (**G**) CFU-F size was quantified in millimeters using a graduated ruler ($^*P < 0.01$ for *Nf1*+/− versus WT cultures using the χ^2 analysis). The results are from one of five representative experiments.

photomicroscopy (Fig. 1E). The size of CFU-F derived from *Nf1*+/− and WT bone marrow was also quantified based on the cell number in each colony, i.e. 50–100 cells/colony, 100–1000 cells/colony as well as over 1000 cells/colony. A significant increase in the number of colonies containing 50–100 cells and 100–1000 cells was detected in *Nf1*+/− cultures compared with cultures containing WT cells (Fig. 1E). The average size of CFU-F was also significantly larger in cultures derived from *Nf1*+/− mice compared with WT controls utilizing a micrometer inside the objective lens of a microscope (Fig. 1F, 2.7 ± 1.2 mm versus 2.1 ± 0.7 mm, respectively, $^*P < 0.01$). These data indicate that *Nf1* haploinsufficient mice have an increased frequency and total number of MSPC, which give rise to larger CFU-F compared with WT controls.

Nf1+/− MSPC display an increased proliferative potential compared with WT MSPC

The phenotype of MSPC derived from WT and *Nf1*+/− mice was evaluated by examining the expression of a range of cell surface markers unique to MSPC (Fig. 2A). Consistent with previous studies (25), both WT and *Nf1*+/− MSPC are negative for the expression of CD45 and CD117, but positive for the expression of CD29, CD105, CD49e, ColIA and CD44.

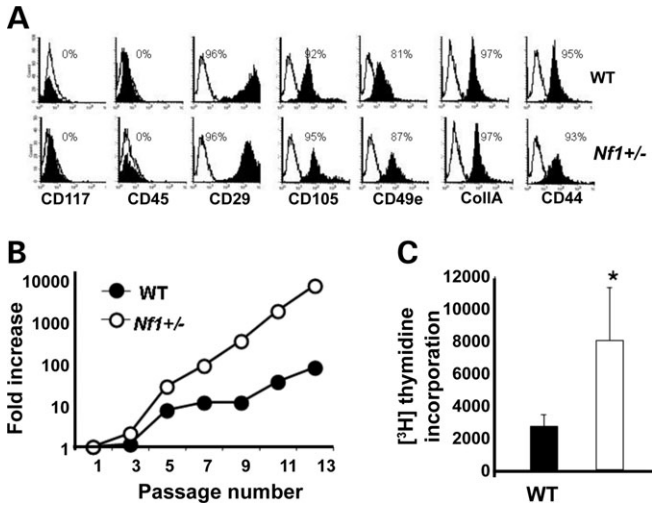

Figure 2. Proliferation of MSPC. (**A**) Expression of cell surface markers for WT and *Nf1*+/− MSPC. Isotype labeled in white and experimental in black. (**B**) WT and *Nf1*+/− MSPC were cultured and expanded for 13 passages and the growth curves of WT and *Nf1*+/− MSPC were plotted. Three independent experiments were performed. (**C**) WT and *Nf1*+/− MSPC were plated in 96-well plates at a concentration of 1×10^4/well. [^{3}H] thymidine incorporation was measured following stimulation with MesenCut containing 10% FBS and data is expressed as mean ± SE from four individual experiments (*$P < 0.001$ for *Nf1*+/− versus WT cells).

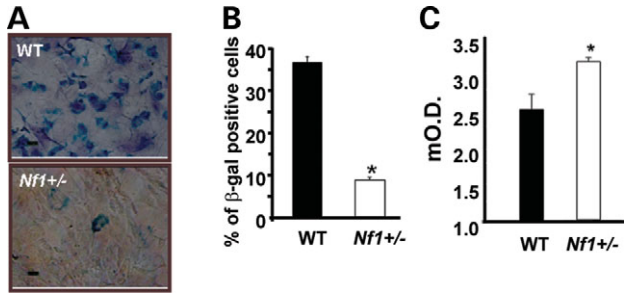

Figure 3. Haploinsufficiency of *Nf1* reduces senescent cells and increases the telomerase activity in MSPC. Senescent cells were scored as cells with light blue cytoplasmic staining from WT (upper photograph) and *Nf1*+/− MSPC (lower photograph) (**A**) Quantitative summary (**B**) revealed *$P < 0.001$ for *Nf1*+/− versus WT senescent cells from four independent experiments. (**C**) Telomerase activity was measured using the TRAPeze ELISA telomerase detection kit (*$P < 0.01$ for *Nf1*+/− cells versus WT cells from four independent experiments).

We next evaluated the impact of loss of neurofibromin on MSPC proliferation. Total number of MSPC were scored by counting viable WT and *Nf1*+/− MSPC cells over a span of 13 continuous passages in the MesenCult complete media (MesenCult basal media + 20% of MesenCult Supplemental) as described in Materials and Methods, and the number of MSPC from each passage was recorded, and a growth curve was generated (Fig. 2B). While a steady increase in the number of MSPC from WT and *Nf1*+/− mice was observed over 13 passages, a significant increase at each time point was observed in *Nf1*+/− MSPC compared with WT MSPC. Consistently, the increased proliferation was also observed in *Nf1*+/− MSPC with [^{3}H] thymidine incorporation assay following the 48 h culture in MesenCult complete media after deprivation of 20% of MesenCult Supplemental (Fig. 2C). Together, these results indicate that haploinsufficiency of *Nf1* promotes the proliferation of MSPC.

Haploinsufficiency of *Nf1* modulates senescence and telomerase activity in MSPC

Cellular senescence is associated with a loss of proliferative ability in response to mitogenic agents (26). To test whether the increase in *Nf1*+/− proliferation was associated with a change in cellular senescence, a senescent assay was performed based upon histochemical staining for β-galactosidase activity (27). A significant reduction in the number of β-galactosidase positive cells was observed in *Nf1*+/− MSPC compared with WT MSPC (Fig. 3A). The quantitative results indicate that nearly 35% of WT MSPC were senescent and β-galactosidase positive. In contrast, only 5% β-galactosidase positive senescent cells were observed in *Nf1*+/− cultures (Fig. 3B). Collectively, these results suggest that the increased proliferation in *Nf1*+/− MSPC is associated with a decrease in the senescent activity of these cells as compared with WT controls.

Telomerase activity has been demonstrated to reflect the proliferation and differentiation status of cells (28). Given that *Nf1*+/− MSPC have increased proliferation, we then measured telomerase activity in WT and *Nf1*+/− MSPC utilizing a sensitive polymerase chain reaction- (PCR) based ELISA detection method (29). Consistently, higher levels of telomerase activity were detected in *Nf1*+/− MSPC as compared with WT MSPC (Fig. 3C). These data indicates that haploinsufficiency of *Nf1* results in down-regulation of the senescent activity and increased telomerase activity, which leads to the increase in *Nf1* +/− MSPC proliferation, indicating an important role of *Nf1* in modulating MSPC proliferation.

Haploinsufficiency of *Nf1* alters MSPC differentiation *in vivo* and *in vitro*

One of the most important features of MSPC is their ability to differentiate into multiple cell types, including osteoblasts and chondrocytes. WT and *Nf1*+/− bone marrow mononuclear cells (BMMNCs) were cultured under conditions that promote the maturation of osteoblasts and chondrocytes. Osteoblasts from WT controls displayed strong alkaline phosphatase (ALP) activity (Fig. 4A, upper panel). In contrast, significantly less ALP expression was observed in *Nf1*+/− cultures [Fig. 4A, lower panel]. The CFU-ALP was calculated on a per femur basis and is shown in Figure 4B. A significant reduction in the number of CFU-ALP was observed in *Nf1*+/− mice as compared with that in WT mice. In addition, the chondrocyte differentiation assay revealed that the CFU-F from both WT and *Nf1*+/− mice expressed Alcian blue positive nodules, and no significant difference was found between the two genotypes (data not shown). Data from the differentiation assay suggests that haploinsufficiency of *Nf1* in MSPC impairs osteogenic differentiation, but not chondrocyte differentiation.

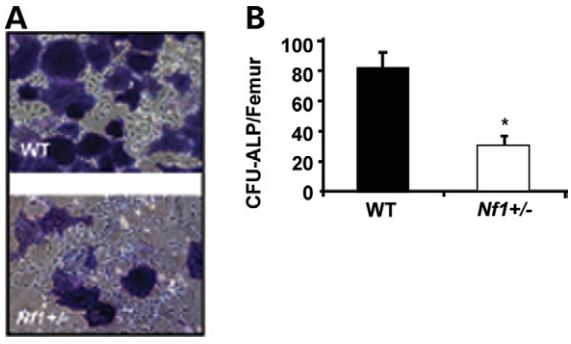

Figure 4. Differentiation of MSPC from WT and *Nf1* +/− mice. (**A**) Differentiation of MSPC from WT and *Nf1* +/− was evaluated *in vitro*. (A) shows the ALP activity measured to define osteoblast differentiation after 14 days of culture. (**B**) Frequency of CFU-ALP/femur was evaluated.

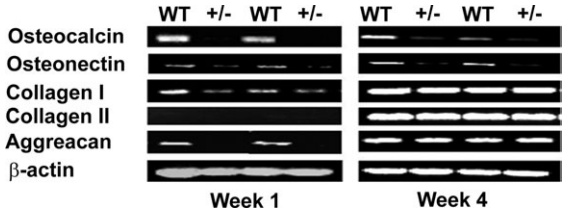

Figure 5. Differential mRNA expression of WT and *Nf1*+/− MSPC in different culture conditions. WT and *Nf1* +/− bone marrow cells were differentiated in osteogenic and chondrogenic differentiation medium for 1 and 4 weeks. Total RNA was extracted and RT–PCR was performed using specific primers for osteoblast and chondrocyte lineage mRNA. One of the representative results from four independent experiments is shown.

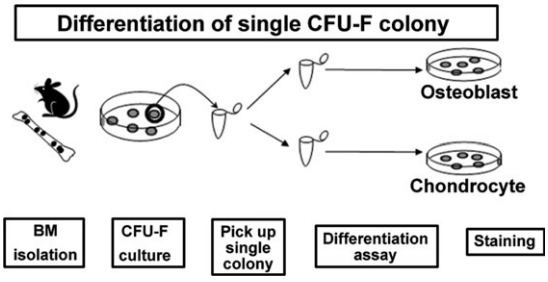

Figure 6. Single CFU-F replating assay. Schematic diagram shows the procedure for the single CFU-F replating assay. CFU-Fs derived from WT and *Nf1*+/− cultures were cloned from WT or *Nf1*+/− cultures from an individual mouse. Cells from individual CFU-F were then divided into two different cultures, and differentiation of MSPC into osteoblasts or chondrocytes was evaluated. Data represents one of three independent experiments.

Table 1. Differentiation of single CFU-F colony

	Total CFU-F number	Cell type	
		Osteoblast	Chondrocyte
WT	24	24	24
Differentiation efficiency (%)		100	100
NF1+/−	24	11	24
Differentiation efficiency (%)		45.8*	100

Differentiation efficiency of CFU-F. The CFU-Fs were picked up from six WT and six *Nf1*+/− cultures from individual mouse, and each CFU-F was divided into two different cultures, and differentiation of osteoblast or chondrocyte was evaluated.
*$P < 0.001$ for *Nf1*+/− versus WT cultures.

Differential mRNA expression of WT and *Nf1*+/− MSPC

To confirm the role of *Nf1* in MSPC differentiation, expression of osteogenic-specific genes, including osteocalcin and osteonectin, was examined in both WT and *Nf1*+/− MSPC (Fig. 5). Osteocalcin mRNA expression was detected at the end of week 1 and week 4 in WT MSPC cultures. Strikingly, no osteocalcin mRNA expression was detected in *Nf1*+/− cells at week 1, and low levels were observed in *Nf1*+/− cultures at week 4. Osteonectin mRNA, another marker for osteogenic differentiation, was consistently reduced in *Nf1*+/− cells compared with WT MSPC. MSPC differentiation into chondrocytes was examined by assessing mRNA expression of collagen I, collagen II and Aggreacan. Despite low expression of Aggreacan mRNA in the *Nf1*+/− cells at week 1, similar expression of Aggreacan mRNA was observed in WT and *Nf1*+/− MSPC at week 4. The expression of collagen I and collagen II was similar in WT and *Nf1*+/− MSPC at weeks 1 and 4. These results support the observation that haploinsufficiency of *Nf1* in MSPC affects osteogenic differentiation, but not the emergence of chondrocytes.

Differentiation of single CFU-F replating assay (SCRA)

Most MSPC studies are based on bulk cell cultures. Smith *et al*. (30) established a single cell colony assay utilizing human bone marrow-derived MSCs, which permitted analysis of the differential clonal potential of small stem-like cells to differentiate into osteoblasts *in vitro*. Similarly, in the present study, we developed a colony-replating assay to understand whether single CFU-F displays the potential to differentiate into multiple lineages (Fig. 6). As shown in Table 1, 24 individual colonies picked from six WT marrow cultures were able to generate osteoblasts or chondrocytes. However, in *Nf1*+/− cultures, 11 out of 24 colonies were able to differentiate into osteoblasts, whereas 24 out of 24 colonies were able to differentiate into chondrocytes. Our study indicates that MSPC from WT mice have the potential to differentiate into osteoblasts as well as chondrocytes. However, haploinsufficiency of *Nf1* in MSPC leads to impairment in osteogenesis.

Expression of *Nf1* GAP-related domains into *Nf1*+/− MSPC increases osteoblast differentiation

Haploinsufficiency of *Nf1* results in Ras hyperactivation in multiple lineages (4–6,31–36). We next assessed the Ras activity by Raf pull down assay in *Nf1*+/− MSPC following 24 h of starvation. Our results show that *Nf1*+/− MSPC have increased Ras activity at baseline as compared with WT MSPC (Fig. 7A). Ras activity also increased after stimulation with 10% fetal bovine serum (FBS). To determine whether reduced osteoblast differentiation in *Nf1*+/− MSPC is directly related to altered p21ras activity, WT and *Nf1*+/− MSPC were transduced with a recombinant retrovirus encoding full

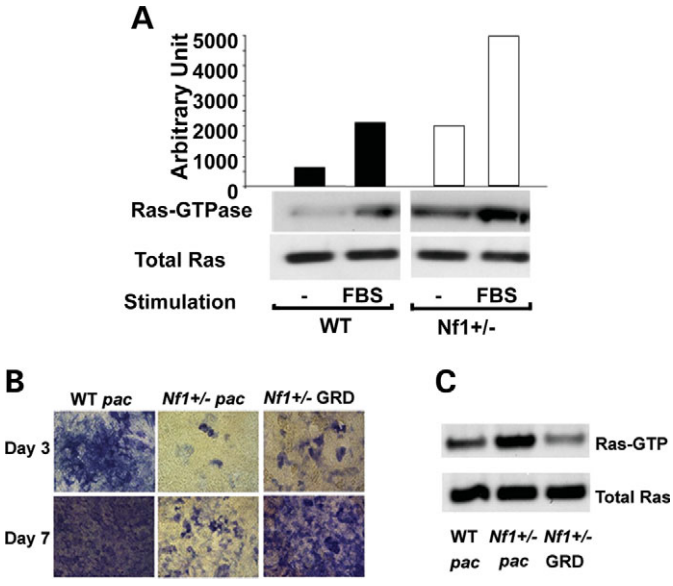

Figure 7. Evaluation of Ras activity and osteoblast differentiation in MSPC. (**A**) Ras activity was measured in WT and *Nf1*+/− MSPC at basal level or in the presence of 10% FBS for 5 min using Raf-pulldown assay. (**B**) Osteoblast differentiation was evaluated by ALP staining after three and seven days of culture in the osteoblast differentiating culture condition using MSPC transduced with *NF1* GRD or MSCV-*pac* control. (**C**) Ras GTPase in the WT MSPC, *Nf1*+/− MSPC transduced with MSCV-*pac* control or *NF1* GRD was measured. Data represents one of three independent results.

length *NF1* GAP-related domain (GRD) and a selectable marker, pac, selected in puromycin, and subjected to culture for further osteoblast differentiation. In contrast to *Nf1*+/− MSPC expressing MSCV-pac alone, expression of *NF1* GRD in *Nf1*+/− MSPC increased osteoblast formation (Fig. 7B). The hyperactivation of Ras in *Nf1*+/− MSPC at baseline was reduced after re-expression of *NF1* GRD (Fig. 7C). The restored osteoblast differentiation is consistent with the normalized Ras GTP activity observed in *Nf1*+/− MSPC following transduction of *NF1* GRD. Thus, increased p21ras activity is directly linked to impaired osteoblast formation in *Nf1*+/− MSPC.

DISCUSSION

The detection of somatic mutations in the residual normal *NF1* allele within the tumors of individuals with NF1 is consistent with *NF1* functioning as a tumor-suppressor gene. However, evidence in selected lineages (4–6,31,37) now indicates that analogous to recent discoveries in *p53* (38) and *p27* (39) gene dosage effects of *NF1* alter cell fates and functions. The majority of recent studies examining *Nf1* haploinsufficiency have focused on the role of *NF1* in modulating the tumor microenvironment of plexiform neurofibromas and optic gliomas (4–6,31–36). However, both clinical data from NF1 patients and experimental studies in *Nf1*+/− mice support the hypothesis that haploinsufficiency of *NF1* (*Nf1*) results in a range of non-malignant phenotypes, including cerebrovascular disease (40), renal vascular hypertension (41–43) and osseous abnormalities (10,13–15,17,44), suggesting that haploinsufficient *NF1* contributes to pathogenesis in multiple lineages. Our present study sought to understand the role of haploinsufficiency of *NF1* (*Nf1*) in disrupting normal MSPC differentiation.

Given that osteoblasts are the progeny of MSPC, we utilized primary MSPC to understand the mechanism underlying the pathological changes in the bone of NF1 patients. The *Nf1*+/− mouse model is a useful tool to understand the role of *Nf1* in modulating the biological functions and differentiation of MSPC. Utilizing *Nf1*+/− mice, MSPC were cultured from BMMNCs followed by evaluation of proliferation and differentiation. We found that haploinsufficiency of *Nf1* promotes MSPC proliferation, but impairs osteoblast differentiation. Given that telomerase activity has been shown to be associated with cellular proliferative potential in cultured cells and is reduced when a variety of cultured cell types are induced to differentiate *in vitro* (28,45), the elevated proliferation observed in *Nf1*+/− MSPC *in vitro* is consistent with the elevated telomerase activity. In addition, the decreased senescence in *Nf1*+/− MSPC is consistent with an increased proliferation and decreased differentiation. Recently, several groups have reported a spontaneous transformation occurring after a long-term *in vitro* culture of human and murine MSPC (46,47). Given that cells proliferate rapidly after passage 5 in WT and *Nf1*+/− MSPC in our study, we performed anchorage-independent soft agar colony assay to check if the MSPC became transformed. No colonies were observed in passage 8 and passage 14 MSPC from WT or *Nf1*+/− cultures (data not shown). Thus, by one assay, MSPC do not appear to transform under our culture condition through 14 cell passages.

Increasing evidence indicates that MSPC have the potential to differentiate into multiple cell lineages, including osteoblasts and chondrocytes (30,48). We report that haploinsufficiency of *Nf1* in MSPC induces an impaired differentiation into osteoblasts compared with WT MSPC. Osteoblastic markers progressively increase at the mRNA level during osteoblastic cell differentiation (49); however, decreased mRNA expression of two osteoblast markers, osteocalcin and osteonectin, was observed in *Nf1*+/− MSPC as compared with WT cells. Yu *et al*. (7) recently reported that *Nf1*+/− mice have less periosteal and endocortical bone formation with significant differences in endocortical percent mineralized bone surface representing active bone forming area and a significantly reduced bone formation rate relative to bone surface area as compared with WT mice. This impaired bone formation *in vivo* may be related to the impaired osteoblast differentiation from MSPC *in vitro* in *Nf1*+/− mice reported herein. Though osteoblasts lineage has impaired differentiation emerging from *Nf1*+/− MSPC, normal differentiation of the chondrocyte lineage, another lineage arising from *Nf1*+/− MSPC, was observed with similar levels of expression for three chondrocyte markers—collagen I, collagen II and Aggreacan, as compared with that in WT cells. These results indicate that haploinsufficiency of *Nf1* regulates osteoblast differentiation from MSPC but not chondrocyte differentiation.

Cycling multipotential progenitor cells from bone marrow have been identified as those cells that undergo 40 or more

population doublings (50). Few studies have examined the clonogenic behavior of MSPC *in vitro*. Here, we utilized SCRA which allowed us to detect the differentiation capacity from a single CFU-F colony. Our results suggest that single CFU-F display multiple lineage differentiation potential. Using this method, we report that loss of a single *Nf1* allele in MSPC diminishes MSPC differentiation into osteoblasts. Precisely how haploinsufficiency of *Nf1* alters MSPC differentiation remains uncertain, but clearly the relative levels of important transcription factors necessary for osteoblast differentiation were altered. A detailed transcriptional comparison of WT and *Nf1*+/− MSPC may be informative.

Neurofibromin, the protein encoded by *NF1*, functions as a GAP for p21Ras by accelerating the hydrolysis of active p21Ras-GTP to inactive p21Ras-GDP (36,51–53). We and others have shown that neurofibromin-deficient mast cells have increased p21ras activity in response to multiple hematopoietic cell growth factors, which is directly linked to increased proliferation (35,52–55). Nose *et al*. (56) has previously shown that overexpression of Ras and MAP kinase was associated with suppression of c-*fos*, whose up-regulation is required for normal osteoblast functions. Consistent with our and other previous studies in different cell lineages, *Nf1*+/− MSPC have increased Ras-GTPase activity. Re-expression of GRD in *Nf1*+/− MSPC restored the impaired osteoblast differentiation defect, indicating that the reduced osteoblast differentiation is directly associated with the hyper Ras activity.

In conclusion, our study indicates that loss of a single allele of *Nf1* in MSPC results in impaired osteoblast differentiation, which is mediated by hyper Ras activity, implying an important role of neurofibromin in regulating osteoblast differentiation. The impaired osteoblast differentiation may be associated with the osseous manifestations found in NF1 patients. Further study of the molecular and biochemical pathway(s) of neurofibromin in modulating MSPC differentiation may help elucidate a better understanding of the pathophysiology underlying the malignant and non-malignant manifestations of this common genetic disorder.

MATERIALS AND METHODS

Animals and materials

Nf1+/− mice were obtained from Dr Tyler Jacks at the Massachusetts Institute of Technology (Cambridge, MA, USA) in a C57BL/6J.129 background and backcrossed for 13 generations into a C57BL/6J strain (57). *Nf1*+/− mice were genotyped by polymerase chain reaction (PCR) as previously described (4). These studies were conducted with a protocol approved by the Indiana University Laboratory Animal Research Center using 4–8-week-old WT and *Nf1*+/− mice. Chemicals were purchased from Sigma (St Louis, MO, USA) unless otherwise stated.

Isolation and expansion of MSPC

Bone marrow cells were collected from 4 to 8-week-old WT and *Nf1*+/− mice by flushing the femurs and tibias with Iscove's MEM (Gibco-Invitrogen, Carsbad, USA) containing 2% FBS using a 21-gauge needle. BMMNCs were then separated by low-density gradient centrifugation (36). Cells were then washed twice with Iscove's MEM and suspended in mouse MesenCult basal medium supplemented with MesenCult Supplemental (Stem Cell Technologies Inc., CA, USA). The cells were diluted to 2×10^6 cells/ml and 10 ml of the single cell suspension was added into a 10 cm tissue culture plate as previously described (58). The cells were plated into a flask at 2×10^6/ml in 10 ml of complete MesenCult medium. Once the culture reached 80–90% confluency, cells were trypsinized and replated at 5×10^5 cells/75 cm^2. MSPC at passage 5 to passage 10 were used for the following experiments.

CFU-F assay

To measure the frequency of MSPC in bone marrow, CFU-F assay was performed as previously reported (58). Briefly, different concentrations of BMMNCs as indicated in Figure 1C and D were plated into six-well tissue culture plates in triplicate for each condition in complete MesenCult medium and incubated at 37°C, 5% CO_2. At day 14 of the culture, media was removed, and each well was washed with PBS and stained with HEMA-3 quick staining kit (Fisher Scientific Company, VA, USA) according to the manufacturer's instruction. The plates were then rinsed in deionized water and air-dried. Colonies with more than 50 cells were counted microscopically at 40X amplification by a phase contract microscope. Colonies whose morphology clearly differed from the MSPC morphology were excluded from the results.

Proliferation assay

To examine the impact of neurofibromin in MSPC proliferation, we performed [^{3}H]thymidine incorporation assays. Briefly, MSPC from WT or *Nf1* +/− mice were deprived of supplement for 24 h and 1×10^4 cells were plated in 96-flat bottom well plates in 200 μl of α-MEM in a 37°C, 5% CO_2, humidified incubator. The cells were then cultured for 48 h, and [^{3}H]thymidine was added to cultures 6 h prior to harvest with an automated cell harvester (96-well harvester, Brandel, Gaithersburg, MD, USA) and β emission was measured with a microplate scintillation counter (Packard Bioscience Company, Shelton, CT, USA). Assays were performed in triplicate. For growth curve, MSPC were plated into a flask at 2×10^6/ml in 10 ml of complete MesenCult medium. Once the culture reached 80–90% confluency, cells were trypsinized and replated at 5×10^5 cells/75 cm^2. Cell numbers were then recorded and plated at the same density each time. The fold increase of cells was calculated for each time point compared with the first point and the growth curve was plotted.

Senescent assay

Histochemical staining for β-galactosidase activity was utilized to measure the senescence of MSPC (27). WT and *Nf1*+/− MSPC were plated in chamber slides at

2×10^4/chamber and incubated at 37°C, 5% CO_2 for 72 h. Cells were then stained with a Senescent Staining Kit (Sigma) according to the manufacturer's instruction. Senescent cells displayed a blue color in the cytoplasma. Four thousand cells were counted for each chamber and the percentage of positive cells/4000 cells was determined.

Telomerase activity assay

Telomerase activity was examined using a telomeric repeat amplification protocol (TRAP) TRAPeze Elisa telomerase detection kit (Chemicon, Temecula, CA, USA) according to the manufacturer's instructions (29). Briefly, cell extracts were incubated with biotinylated telomerase substrate oligonucleotide at 30°C for 30 min. The extended products were amplified by PCR using *Taq* polymerase (Amersham International), reverse primers and a deoxynucleotide mix containing dCTP labeled with dinitrophenyl (DNP). The conditions for the two-step PCR were 33 cycles of 94°C for 30 s, and 55°C for 30 s on a PTC-100™ Programmable Thermal Controller (MJ Research, Inc.). The amplification products were immobilized on streptavidin-coated microtitre plates, and then detected by anti-DNP antibody conjugated to horseradish peroxidase. After addition of the peroxidase substrate (3,3′,5,5′tetramethylbenzidine), the amount of TRAP product was determined by measuring the absorbance at 450 nm and 650 nm via fast kinetic mode for 100 s using an Lmax microplate luminometer and SoftMax Pro software (Molecular Devices, Sunnyvale, CA, USA). For negative controls, lysates were heat-treated by incubating at 85°C for 10 min prior to the TRAP assay to inactivate telomerase. The activity was semi-quantified by ELISA as recommended by the manufacturer.

Analysis of surface markers expression

Antibodies for flow cytometry were purchased from BD PharMingen. MSPC were incubated with fluorescein isothiocyanate (FITC) anti-mouse CD44, R-phycoerythrin (R-PE)-conjugated anti-mouse CD49e, R-PE-conjugated anti-mouse CD29, purified anti-rat CD105 and anti-rat R-PE antibody. After 30 min of incubation at 4°C, cells were washed three times with PBS containing 0.1% BSA and analyzed by fluorescence-activated cytometric analysis (Becton Dickinson, San Jose, CA, USA).

Differentiation assays

Osteogenic differentiation was analyzed by quantitation of mineral deposition. WT and *Nf1*+/− BMMNCs were plated at 2×10^6/ml in osteogenic differentiation medium (MesenCult+Supplemental, 10^{-8}mol/l dexamethasone, 5 μg/ml ascorbic acid 2-phosphate and 10 mmol/l β-glycerophosphate) and maintained for 2 weeks, followed by ALP activity assays. Briefly, cells were fixed in citrate-buffered acetone for 30 s, incubated in alkaline-dye mix for 30 min and counter-stained with Mayer's Hematoxylin for 10 min. Cells were then evaluated microscopically, and the intensity of ALP staining was recorded.

To induce chondrogenic differentiation, BMMNCs were maintained in chondrogenic differentiation medium (MesenCult + Supplemental, 10^{-8}mol/l dexamethasone, 5 μg/ml ascorbic acid 2-phosphate, 10 mmol/l β-glycerophosphate and 10 ng/ml TGFβ3) for 4 weeks. Cells were then fixed in 4% paraformaldehyde in PBS for 30 min at room temperature, washed with PBS and incubated with 1% Alcian Blue in 0.1 M HCl (pH 1.0). Chondrogenic cells were visualized as blue-stained cells under the microscope.

To determine the differentiation potential of WT and *Nf1*+/− MSPC, an SCRA was performed. Briefly, 5×10^5 cells/well in a six-well plate was seeded for CFU-F culture as described earlier. Two weeks after the culture, single CFU-Fs were picked up individually by adding EDTA–trypsin for 5 min and stopped by adding 10% FBS, and transferred into each Eppendrof tube. The cells from the single colony were then divided among two tubes, and plated to two different wells osteogenic and chondrogenic differentiation medium in a 48-well plate. Four weeks later, the cells were stained for specific differentiation markers as described earlier. Twenty-four individual colonies were picked from each genotype for the analysis.

Reverse-transcriptase polymerase chain reaction (RT-PCR)

MSPC were incubated in differentiation medium and total RNA was extracted using the RNeasy mini kit (Qiagen, Valencia, CA, USA) to purify total RNA and 100 ng RNA was used for each reaction. RT-PCR was performed using Qiagen one step RT-PCR kit according to the manufacturer's instruction at week 1 and week 4. The PCR products were resolved on a 1.2% agarose gel. The primers used were GTAGCCATC CAGGCTGTGTTGTC, ACAGCACTGTGTTGGCATAGAG G for β-actin; Osteopontin TCACCATTCGGATGAGTCTG, ACTTGTGGCTCTGATGTTCC 437 bp (59); Osteonectin AGCGCCTGGAGGCTGGAGAC, CTTGATGCCAAAGCA GCCGG 269 bp HM; Osteocalcin TCTGCTCACTCTGCT GAC, GGAGCTGCTGTGACATCC 388 bp (60); Type I collagen GAAGTCAGCTGCATACAC, AGGAAGTCCAGGCT GTCC 313 bp (60); Type II collagen GCCTCGCGGTGAG CCTGATC, CTCCATCTCTGCACGGGGT, IIA: 472 bp (61), IIB: 268 bp; Aggreacan CCAAGTTCCAGGGTCACTG TTACCG, TCCTCTCCGGTGGCAAAGAAGTTG 271 bp (61). All the primers were synthesized by Sigma.

Generation of recombinant retroviral plasmids and retroviral transduction of MSPC

Previously developed recombinant retrovirus constructs were used in these studies (53). The internal sequences of these constructs are under the transcriptional control of the myeloproliferative sarcoma retrovirus promoter. Constructs also contain a puromycin resistance gene, *pac*, which is under the transcriptional control of the phosphoglycerate kinase (PGK) promoter. Two viruses were used in these experiments: a virus expressing the full-length *NF1* GTPase activating related domain (*NF1* GRD) and *pac* (MSCV-*NF1* GRD-pac) and a virus expressing the selectable marker gene alone (MSCV-pac). The transduction protocol has been previously

described and was used here with minor modifications (53). Briefly, MSPC were cultured in liquid cultures of MesenCult + Supplemental and transduced with either MSCV-*NF1*GRD or MSCV-Pac (control), and puromycin-resistant cells were selected after 3 days.

Detection of p21Ras-GTP levels

MSPC were deprived of serum for 24 h and collected with or without 10% FBS stimulation for 5 min. p21Ras activation was subsequently determined using p21Ras activation assay kits (Upstate Biotechnology, Lake Placid, NY, USA) according to the manufacturer's protocol and as described previously (53).

Statistical analysis

Student's *t*-test and χ^2 analysis was used to evaluate statistical differences between WT and *Nf1*+/− MSPC. Statistical significance was defined as $P < 0.05$.

ACKNOWLEDGEMENTS

We thank Dr Wade Clapp for his helpful scientific advice, Dr Brenda R. Grimes for her scientific suggestion, Dr Rebecca J. Chan for her critical reading the manuscript, Marilyn L. Wales and Janice Walls for administrative support. This work was supported by Department of Defense (DOD) NF043032 (FCY).

Conflict of Interest statement. No conflicts declared.

REFERENCES

1. Riccardi, V. (1992) *Neurifbromatosis: Phenotype, Natural History and Pathogenesis*. The Johns Hopkins University Press, Baltimore, MD, USA, p. 479.
2. Friedman, J.M. (1999) Epidemiology of neurofibromatosis type 1. *Am. J. Med. Genet.*, **89**, 1–6.
3. Giehl, K. (2005) Oncogenic Ras in tumour progression and metastasis. *Biol. Chem.*, **386**, 193–205.
4. Ingram, D.A., Yang, F.C., Travers, J.B., Wenning, M.J., Hiatt, K., New, S., Hood, A., Shannon, K., Williams, D.A. and Clapp, D.W. (2000) Genetic and biochemical evidence that haploinsufficiency of the *Nf1* tumor suppressor gene modulates melanocyte and mast cell fates *in vivo*. *J. Exp. Med.*, **191**, 181–188.
5. Atit, R.P., Mitchell, K., Nguyen, L., Warshawsky, D. and Ratner, N. (2000) The neurofibromatosis type 1 (*Nf1*) tumor suppressor is a modifier of carcinogen-induced pigmentation and papilloma formation in C57BL/6 mice. *J. Invest. Dermatol.*, **114**, 1093–1100.
6. Johannessen, C.M., Reczek, E.E., James, M.F., Brems, H., Legius, E. and Cichowski, K. (2005) The NF1 tumor suppressor critically regulates TSC2 and mTOR. *Proc. Natl Acad. Sci. USA*, **102**, 8573–8578.
7. Yu, X., Chen, S., Potter, O.L., Murthy, S.M., Li, J., Pulcini, J.M., Ohashi, N., Winata, T., Everett, E.T., Ingram, D. *et al*. (2005) Neurofibromin and its inactivation of Ras are prerequisites for osteoblast functioning. *Bone*, **36**, 793–802.
8. Riccardi, V.M. (1981) Von Recklinghausen neurofibromatosis. *N. Engl. J. Med.*, **305**, 1617–1627.
9. Friedman, J.M. and Birch, P.H. (1997) Type 1 neurofibromatosis: a descriptive analysis of the disorder in 1728 patients. *Am. J. Med. Genet.*, **70**, 138–143.
10. Crawford, A.H., Jr and Bagamery, N. (1986) Osseous manifestations of neurofibromatosis in childhood. *J. Pediatr. Orthop.*, **6**, 72–88.
11. Crawford, A.H. (1989) Pitfalls of spinal deformities associated with neurofibromatosis in children. *Clin. Orthop. Relat. Res.*, **245**, 29–42.
12. Sbihi, A., Balafrej, A., Iraqui-Hamdouch, N., Hamdouch, M. and Baroudi, A. (1980) Osseous manifestations of Recklinghausen's disease. The role of vertebral scalloping. *Maroc. Med.*, **2**, 393–398.
13. Kuorilehto, T., Poyhonen, M., Bloigu, R., Heikkinen, J., Vaananen, K. and Peltonen, J. (2005) Decreased bone mineral density and content in neurofibromatosis type 1: lowest local values are located in the load-carrying parts of the body. *Osteoporos. Int.*, **16**, 928–936.
14. Kuorilehto, T., Nissinen, M., Koivunen, J., Benson, M.D. and Peltonen, J. (2004) NF1 tumor suppressor protein and mRNA in skeletal tissues of developing and adult normal mouse and NF1-deficient embryos. *J. Bone Miner. Res.*, **19**, 983–989.
15. Lammert, M., Kappler, M., Mautner, V.F., Lammert, K., Storkel, S., Friedman, J.M. and Atkins, D. (2005) Decreased bone mineral density in patients with neurofibromatosis 1. *Osteoporos. Int.*, **16**, 1161–1166.
16. Jacques, C. and Dietemann, J.L. (2005) Imaging features of neurofibromatosis type 1. *J. Neuroradiol.*, **32**, 180–197.
17. Illes, T., Halmai, V., de Jonge, T. and Dubousset, J. (2001) Decreased bone mineral density in neurofibromatosis-1 patients with spinal deformities. *Osteoporos. Int.*, **12**, 823–827.
18. Heuze, Y., Piot, B. and Mercier, J. (2002) Difficult surgical management of facial neurofibromatosis type I or von Recklinghausen disease in children. *Rev. Stomatol. Chir. Maxillofac.*, **103**, 105–113.
19. Bilezekian, J., Raisz, L. and Rodan, G. (2002) *Principles of Bone Biology*, Academic Press, San Diego, CA, USA.
20. Kawaguchi, H., Manabe, N., Miyaura, C., Chikuda, H., Nakamura, K. and Kuro-o, M. (1999) Independent impairment of osteoblast and osteoclast differentiation in klotho mouse exhibiting low-turnover osteopenia. *J. Clin. Invest.*, **104**, 229–237.
21. Malaval, L., Modrowski, D., Gupta, A.K. and Aubin, J.E. (1994) Cellular expression of bone-related proteins during *in vitro* osteogenesis in rat bone marrow stromal cell cultures. *J. Cell. Physiol.*, **158**, 555–572.
22. Olsen, B.R., Reginato, A.M. and Wang, W. (2000) Bone development. *Annu. Rev. Cell. Dev. Biol.*, **16**, 191–220.
23. Horwitz, E.M., Gordon, P.L., Koo, W.K., Marx, J.C., Neel, M.D., McNall, R.Y., Muul, L. and Hofmann, T. (2002) Isolated allogeneic bone marrow-derived mesenchymal cells engraft and stimulate growth in children with osteogenesis imperfecta: implications for cell therapy of bone. *Proc. Natl Acad. Sci. USA*, **99**, 8932–8937.
24. Le Blanc, K., Gotherstrom, C., Ringden, O., Hassan, M., McMahon, R., Horwitz, E., Anneren, G., Axelsson, O., Nunn, J., Ewald, U. *et al*. (2005) Fetal mesenchymal stem-cell engraftment in bone after *in utero* transplantation in a patient with severe osteogenesis imperfecta. *Transplantation*, **79**, 1607–1614.
25. Oswald, J., Boxberger, S., Jorgensen, B., Feldmann, S., Ehninger, G., Bornhauser, M. and Werner, C. (2004) Mesenchymal stem cells can be differentiated into endothelial cells *in vitro*. *Stem Cells*, **22**, 377–384.
26. Ding, W., Gao, S. and Scott, R.E. (2001) Senescence represses the nuclear localization of the serum response factor and differentiation regulates its nuclear localization with lineage specificity. *J. Cell Sci.*, **114**, 1011–1018.
27. Michaloglou, C., Vredeveld, L.C., Soengas, M.S., Denoyelle, C., Kuilman, T., van der Horst, C.M., Majoor, D.M., Shay, J.W., Mooi, W.J. and Peeper, D.S. (2005) BRAFE600-associated senescence-like cell cycle arrest of human naevi. *Nature*, **436**, 720–724.
28. Greider, C.W. (1998) Telomerase activity, cell proliferation, and cancer. *Proc. Natl Acad. Sci. USA*, **95**, 90–92.
29. Parsch, D., Fellenberg, J., Brummendorf, T.H., Eschlbeck, A.M. and Richter, W. (2004) Telomere length and telomerase activity during expansion and differentiation of human mesenchymal stem cells and chondrocytes. *J. Mol. Med.*, **82**, 49–55.
30. Smith, J.R., Pochampally, R., Perry, A., Hsu, S.C. and Prockop, D.J. (2004) Isolation of a highly clonogenic and multipotential subfraction of adult stem cells from bone marrow stroma. *Stem Cells*, **22**, 823–831.
31. Bajenaru, M.L., Hernandez, M.R., Perry, A., Zhu, Y., Parada, L.F., Garbow, J.R. and Gutmann, D.H. (2003) Optic nerve glioma in mice requires astrocyte *Nf1* gene inactivation and *Nf1* brain heterozygosity. *Cancer Res.*, **63**, 8573–8577.
32. Zhu, Y., Ghosh, P., Charnay, P., Burns, D.K. and Parada, L.F. (2002) Neurofibromas in *NF1*: Schwann cell origin and role of tumor environment. *Science*, **296**, 920–922.

33. Atit, R.P., Crowe, M.J., Greenhalgh, D.G., Wenstrup, R.J. and Ratner, N. (1999) The Nf1 tumor suppressor regulates mouse skin wound healing, fibroblast proliferation, and collagen deposited by fibroblasts. *J. Invest. Dermatol.*, **112**, 835–842.
34. Rutkowski, J.L., Wu, K., Gutmann, D.H., Boyer, P.J. and Legius, E. (2000) Genetic and cellular defects contributing to benign tumor formation in neurofibromatosis type 1. *Hum. Mol. Genet.*, **9**, 1059–1066.
35. Ingram, D.A., Hiatt, K., King, A.J., Fisher, L., Shivakumar, R., Derstine, C., Wenning, M.J., Diaz, B., Travers, J.B., Hood, A. *et al*. (2001) Hyperactivation of p21(ras) and the hematopoietic-specific Rho GTPase, Rac2, cooperate to alter the proliferation of neurofibromin-deficient mast cells *in vivo* and *in vitro*. *J. Exp. Med.*, **194**, 57–69.
36. Yang, F.C., Ingram, D.A., Chen, S., Hingtgen, C.M., Ratner, N., Monk, K.R., Clegg, T., White, H., Mead, L., Wenning, M.J. *et al*. (2003) Neurofibromin-deficient Schwann cells secrete a potent migratory stimulus for *Nf1*+/− mast cells. *J. Clin. Invest.*, **112**, 1851–1861.
37. Wu, M., Wallace, M.R. and Muir, D. (2005) Nf1 haploinsufficiency augments angiogenesis. *Oncogene*, **25**, 2297–2303.
38. Venkatachalam, S., Shi, Y.P., Jones, S.N., Vogel, H., Bradley, A., Pinkel, D. and Donehower, L.A. (1998) Retention of wild-type p53 in tumors from p53 heterozygous mice: reduction of p53 dosage can promote cancer formation. *EMBO J.*, **17**, 4657–4667.
39. Fero, M.L., Randel, E., Gurley, K.E., Roberts, J.M. and Kemp, C.J. (1998) The murine gene *p27Kip1* is haplo-insufficient for tumour suppression. *Nature*, **396**, 177–180.
40. Rosser, T.L., Vezina, G. and Packer, R.J. (2005) Cerebrovascular abnormalities in a population of children with neurofibromatosis type 1. *Neurology*, **64**, 553–555.
41. Fossali, E., Signorini, E., Intermite, R.C., Casalini, E., Lovaria, A., Maninetti, M.M. and Rossi, L.N. (2000) Renovascular disease and hypertension in children with neurofibromatosis. *Pediatr. Nephrol.*, **14**, 806–810.
42. Cormier, J.M., Cormier, F., Mayade, F. and Fichelle, J.M. (1999) Arterial complications of neurofibromatosis. *J. Mal. Vasc.*, **24**, 281–286.
43. Kurien, A., John, P.R. and Milford, D.V. (1997) Hypertension secondary to progressive vascular neurofibromatosis. *Arch. Dis. Child.*, **76**, 454–455.
44. Stevenson, D.A., Birch, P.H., Friedman, J.M., Viskochil, D.H., Balestrazzi, P., Boni, S., Buske, A., Korf, B.R., Niimura, M., Pivnick, E.K. *et al*. (1999) Descriptive analysis of tibial pseudarthrosis in patients with neurofibromatosis 1. *Am. J. Med. Genet.*, **84**, 413–419.
45. Till, J.E. (1982) Stem cells in differentiation and neoplasia. *J. Cell. Physiol. Suppl.*, **1**, 3–11.
46. Miura, M., Miura, Y., Padilla-Nash, H.M., Molinolo, A.A., Fu, B., Patel, V., Seo, B.M., Sonoyama, W., Zheng, J.J., Baker, C.C. *et al*. (2006) Accumulated chromosomal instability in murine bone marrow mesenchymal stem cells leads to malignant transformation. *Stem Cells*, **24**, 1095–1103.
47. Rubio, D., Garcia-Castro, J., Martin, M.C., de la Fuente, R., Cigudosa, J.C., Lloyd, A.C. and Bernad, A. (2005) Spontaneous human adult stem cell transformation. *Cancer Res.*, **65**, 3035–3039.
48. Jiang, Y., Jahagirdar, B.N., Reinhardt, R.L., Schwartz, R.E., Keene, C.D., Ortiz-Gonzalez, X.R., Reyes, M., Lenvik, T., Lund, T., Blackstad, M. *et al*. (2002) Pluripotency of mesenchymal stem cells derived from adult marrow. *Nature*, **418**, 41–49.
49. Lian, J.B., Javed, A., Zaidi, S.K., Lengner, C., Montecino, M., van Wijnen, A.J., Stein, J.L. and Stein, G.S. (2004) Regulatory controls for osteoblast growth and differentiation: role of Runx/Cbfa/AML factors. *Crit. Rev. Eukaryot. Gene Expr.*, **14**, 1–41.
50. Reyes, M., Lund, T., Lenvik, T., Aguiar, D., Koodie, L. and Verfaillie, C.M. (2001) Purification and *ex vivo* expansion of postnatal human marrow mesodermal progenitor cells. *Blood*, **98**, 2615–2625.
51. Wallace, M.R., Marchuk, D.A., Andersen, L.B., Letcher, R., Odeh, H.M., Saulino, A.M., Fountain, J.W., Brereton, A., Nicholson, J., Mitchell, A.L. *et al*. (1990) Type 1 neurofibromatosis gene: identification of a large transcript disrupted in three NF1 patients. *Science*, **249**, 181–186.
52. Bollag, G., Clapp, D.W., Shih, S., Adler, F., Zhang, Y.Y., Thompson, P., Lange, B.J., Freedman, M.H., McCormick, F., Jacks, T. *et al*. (1996) Loss of NF1 results in activation of the Ras signaling pathway and leads to aberrant growth in haematopoietic cells. *Nat. Genet.*, **12**, 144–148.
53. Hiatt, K.K., Ingram, D.A., Zhang, Y., Bollag, G. and Clapp, D.W. (2001) Neurofibromin GTPase-activating protein-related domains restore normal growth in *Nf1*−/− cells. *J. Biol. Chem.*, **276**, 7240–7245.
54. Largaespada, D.A., Brannan, C.I., Jenkins, N.A. and Copeland, N.G. (1996) Nf1 deficiency causes Ras-mediated granulocyte/macrophage colony stimulating factor hypersensitivity and chronic myeloid leukaemia. *Nat. Genet.*, **12**, 137–143.
55. Zhang, Y.Y., Vik, T.A., Ryder, J.W., Srour, E.F., Jacks, T., Shannon, K. and Clapp, D.W. (1998) Nf1 regulates hematopoietic progenitor cell growth and ras signaling in response to multiple cytokines. *J. Exp. Med.*, **187**, 1893–1902.
56. Nose, K., Itami, M., Satake, M., Ito, Y. and Kuroki, T. (1989) Abolishment of c-fos inducibility in ras-transformed mouse osteoblast cell lines. *Mol. Carcinog.*, **2**, 208–216.
57. Jacks, T., Shih, T.S., Schmitt, E.M., Bronson, R.T., Bernards, A. and Weinberg, R.A. (1994) Tumour predisposition in mice heterozygous for a targeted mutation in *Nf1*. *Nat. Genet.*, **7**, 353–361.
58. Meirelles Lda, S. and Nardi, N.B. (2003) Murine marrow-derived mesenchymal stem cell: isolation, *in vitro* expansion, and characterization. *Br. J. Haematol.*, **123**, 702–711.
59. Chackalaparampil, I., Peri, A., Nemir, M., McKee, M.D., Lin, P.H., Mukherjee, B.B. and Mukherjee, A.B. (1996) Cells *in vivo* and *in vitro* from osteopetrotic mice homozygous for c-src disruption show suppression of synthesis of osteopontin, a multifunctional extracellular matrix protein. *Oncogene*, **12**, 1457–1467.
60. Windahl, S.H., Vidal, O., Andersson, G., Gustafsson, J.A. and Ohlsson, C. (1999) Increased cortical bone mineral content but unchanged trabecular bone mineral density in female ERbeta(−/−) mice. *J. Clin. Invest.*, **104**, 895–901.
61. Tropel, P., Noel, D., Platet, N., Legrand, P., Benabid, A.L. and Berger, F. (2004) Isolation and characterisation of mesenchymal stem cells from adult mouse bone marrow. *Exp. Cell. Res.*, **295**, 395–406.